ISSN 1000-9620

海洋通报

Marine Science Bulletin

NATIONAL MARINE DATD AND
INFORMATION SERVICE OF CHINA

2013
Volume 15
Number 1

MARINE SCIENCE BULLETIN

Vol. 15 No. 1 May 2013

CONTENTS

Three-dimensional numerical simulation of tides and tidal currents in the Lianzhou Bay and adjacent areas ····· SONG De-hai et al. (01)

Study on the wave extreme parameters of the Bohai Sea with the numerical simulation using SWAN····· SUN Xiao-juan et al. (16)

Distribution characteristics of sea surface temperature along the sourthern coastal region of Zhejiang Province·····HAN Xiao-yan et al. (27)

Screening and identification of an antagonistic bacterium strain LHB02 and the optimization of its fermentation conditions ····· XU Chang-an et al. (39)

Growth and maturity of *Chiromantes dehaani* in the Dazhi River estuary ····· HAN Sha et al. (51)

Effects on the growth and feeding of juvenile Starry flounder (*Platichthys stellatus*) ·····YOU Hong-zheng et al. (66)

Research advances in the biological characteristics of the Crustacean Spermatozoa ····· XU Xing-hong et al. (76)

To establish CMOC China as an important component of marine data and service international cooperation in China·····DU Qiong-wei et al. (91)

LIBRARY
DEC 12 2013
National Oceanic &
Atmospheric Administration
U.S. Dept. of Commerce

Three-dimensional numerical simulation of tides and tidal currents in the Lianzhou Bay and adjacent areas

SONG De-hai [1], BAO Xian-wen [1], ZHANG Shao-feng [2, 3*], ZHANG Chun-hua [2, 3]

1. *Physical Oceanography Laboratory, Ocean University of China, Ministry of Education, Qingdao* 266100, *Shandong province, China;*

2. *Marine Monitoring and Forecasting Center of Guangxi Zhuang Autonomous Region, Beihai* 536000, *Guangxi province, China;*

3. *Beihai Marine Environmental Monitoring Center Station of State Oceanic Administration, Beihai* 536000, *Guangxi province, China*

Abstract: A 3-D unstructured-grid, finite-volume coastal ocean model (FVCOM) was used to study the tides and tidal currents in the Lianzhou Bay and adjacent areas. The simulation results were in good agreement with observations. The co-tidal maps of K_1, O_1, and M_2 indicated that K_1 and O_1 were mostly standing waves outside the Lianzhou Bay, while M_2 had a largely propagating character. However, all three constituents became propagating waves when entering the Lianzhou Bay, due to the shallow waters. The tidal current ellipses showed the characters of K_1, O_1, and M_2 constituents: K_1 and O_1 were rotating outside the bay, but rectilinear along the water channels inside the bay; M_2 was mostly rectilinear over the whole area. The tidal-induced residual current shows the flow was divided into two branches by the Guantouling Peninsula: one turned to flow west; the other was blocked by the southern boundary of the peninsula, creating a clockwise circulation. In Lianzhou Bay, there were two circulation systems, a cyclonic one at the top of the bay and an anti-cyclonic at the mouth.

Keywords: Lianzhou Bay, FVCOM, tide; tidal current, residual tidal current

LIBRARY
Pacific Islands Fisheries Science Center
NOAA Fisheries
Honolulu, Hawai'i

1 Introduction

The Lianzhou Bay is located in the north of the Beibu Gulf, near Beihai City, Guangxi, China. It is a semi-circular bay, facing west and with the width of 17 km at its mouth. The whole area of the Lianzhou Bay is about 190 km^2, of which, tidal flats occupy 100 km^2. Several rivers flow into the Lianzhou Bay, including the largest river in Guangxi, the Nanliu

Received on Jun. 26, 2012

*Corresponding author: unusualcenter@163.com

River, which also brings a large amount of sediments into the bay. Most of the water in the Lianzhou Bay is shallow, but there is a deep channel offshore near Guantouling, Beihai. The Lianzhou Bay has abundant resources, such as tidal flats, harbors, and various biology resources, which attract lots of attention. Since 2006, harbor industries, maritime trades, and coastal tourism in the Lianzhou Bay have developed rapidly, due to the substantial support of the Guangxi Province Government and the Beihai Municipal Government.

In early 2008, the Beibu Gulf Economic Zone Development Plan was approved by the State Council, which led to the start of more projects in the Lianzhou Bay. However, the economic development in this region resulted in some serious problems, such as seawater pollution, eutrophication, red tides, and a decreasing biodiversity, which in turn hindered sustainable economic development and broke the balance between economics, environment, and society. Therefore, it is important to understand, manage, and control pollutants in the coastal ocean for environmental protection and the sustainable use of marine resources. This is also of great importance for healthy economic development around the Lianzhou Bay. Numerical studies of the Lianzhou Bay began in the 1990s. Chen and Shi [1] (1996) simulated the tidal and wind-driven currents using a two-dimensional model based on the equations of motion and continuity. Their results showed that the ebb-current velocity was much greater than the flood-current velocity. To study the tidal flow in the Lianzhou Bay, Bai and Yu [2] (1998) applied a split-step, layered quasi-three-dimensional mathematical model with an unstructured grid. Their simulated results agreed well with the observed tidal elevations and currents. Chen et al. [3] (2001) and Sun and Huang (2001a [4], b [5]) studied the tides and tidal currents along the Guangxi coast, including the Lianzhou Bay. Their results showed a regular diurnal regime for tides along the coast. There are regular or irregular diurnal regimes for tidal currents in most of this region. The strong diurnal tides can be attributed to the resonance between the natural oscillation period of the Beibu Gulf and the periods of the diurnal tides, especially O_1 (Fang et al. [6], 1999). According to these studies, the tidal currents are basically rectilinear in the Lianzhou Bay, due to its topography and morphology. However, a lack of computing capability at that time restricted the model resolution.

As we mentioned above, the tidal flats occupy a large proportion of the Lianzhou Bay, over 50% of the bay area. Therefore, the wet-and-dry process is relatively important in studying the hydrodynamics in the Lianzhou Bay. Previous studies have already showed its importance in the tidal current simulation, due to the change of water volume with or without the wet-and-dry process in the model (Zheng et al. [7], 2003; Lü et al. [8], 2008). Including the wet-and-dry process in the model reproduced the tidal motion and pollutant

transport much better than the result when it was omitted. In this paper, the finite-volume coastal ocean model (FVCOM) was used to study the tides and tidal currents in the Lianzhou Bay and adjacent areas. This finite-volume approach combines the best of finite-element methods for geometric flexibility and finite-difference methods for simple discrete structures and computational efficiency (Chen et al. [9], 2003). The representation of mass, momentum, salt, and heat conservation in coastal and estuarine regions with complex geometry (Chen et al. [10], 2007) makes FVCOM ideally suited for this study and useful for further research on the pollutant transport in the region.

2 Model description

2.1 Model domain

The model covers the region between 108.96°E (Sanniang Bay) and109.38°E (Yingpan Harbor), and between 19.60°N (Weizhou Island) and 21.74°N (Dafeng River Estuary). Construction of the unstructured triangular grid, which consists of 22,941 nodes and 43,235 elements in the horizontal plane, is based on the available bathymetry and shoreline data from the marine chart published by the Maritime Safety Administration of P.R. China. Fig. 1 shows the model mesh for the entire domain; the resolution around the river outlets, tidal flats, and water channels is especially high. The finest resolution in the narrow channels approaches 30m. As the water depth (Fig. 2) is less than 30 m in this domain, we use 6 uniform vertical layers to show the differences in tidal currents between the surface and the bottom.

2.2 Boundary conditions

The open boundary conditions for the water level were specified for 8 tidal constituents (M_2, S_2, N_2, K_2, K_1, O_1, P_1, and Q_1) using the China seas sub-model of the OSU TOPEX/POSEIDON Global Inverse Solution (TPXO, volkov.oce.orst.edu/ tides/global. html), a global model of ocean tides. It best fits, in a least-squares sense, the Laplace Tidal Equation and the along-track averaged data from TOPEX/POSEIDON and Jason (on TOPEX/POSEIDON tracks since 2002). The methods used in the model were described in detail by Egbert et al. [11] (1994) and Egbert and Erofeeva [12] (2002). The China seas sub-model with 1/30° resolution was validated with measurement from 55 coastal tidal gauges in the South China Sea (volkov.oce.orst.edu/tides/YS.html). The root-mean-square error was only 4.16 cm and 1.63 cm for M_2 and K_1, respectively. It indicates that this model is accurate enough to provide the open-boundary water levels for the Lianzhou Bay model.

The averaged discharge in 2008 was only about 163.3 m^3/s for the Nanliu River and

67.4m^3/s for the Dafeng River. As we focused on the tides in this paper, we exclude the river discharge as well as the freshwater-induced baroclinic circulation from the model.

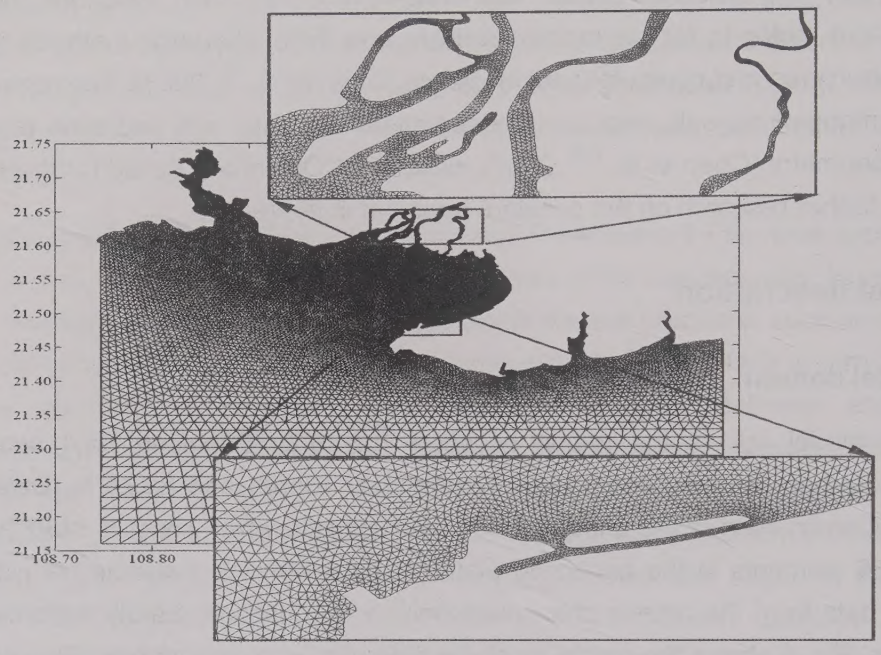

Fig. 1 Unstructured triangular mesh for the 3-D tidal current model of Lianzhou Bay and adjacent areas

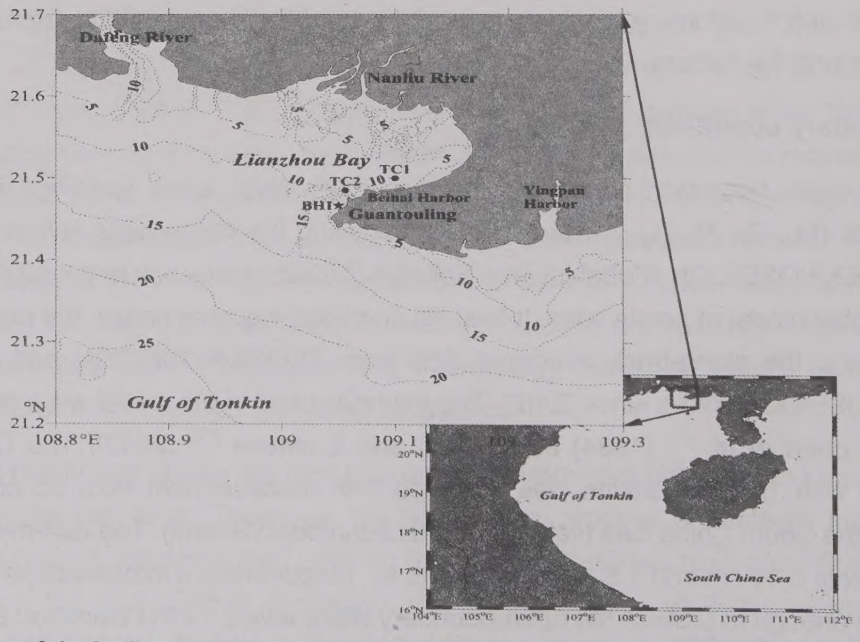

Fig. 2 Map of the bathymetry of Lianzhou Bay and adjacent areas (unit: meter), and the stations for measuring tidal elevation (star, BHI) and tidal current (dots, TC1 and TC2)

3 Model validation

To calibrate the numerical model, we used tidal current data from two stations (TC1 and TC2) measured in July 2007 and tidal elevation data from one tidal gauge station (BHI) measured from July 2007 to June 2008 (see Fig. 2 for the locations of these stations).

Harmonic analysis indicated that the K_1 and O_1 were the dominant diurnal tides, while M_2 was the principal semidiurnal tide. We obtained 8 tidal constituents from the tidal gauge data and compared these with the model results (Tab. 1). There was good agreement between observation and simulation. The root-mean-square of difference for the amplitude was 1.5 cm, with a maximum difference of 4.1 cm for O_1; the root-mean-square of difference for the phase was 7.7°. The large phase errors were for the less important semi-diurnal tides (S_2, N_2, and K_2), which had little impact on the tidal simulation.

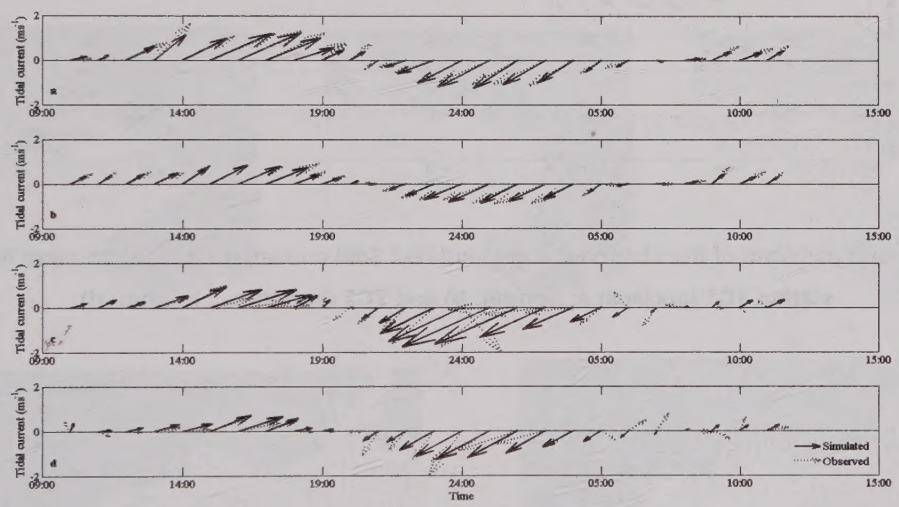

Fig. 3 Comparisons of the observed and simulated tidal current (unit: /ms) on spring tides at station TC1 (surface: a; bottom: b) and TC2 (surface: c; bottom: d)

The current velocity data used here have been measured over a 26-hour period, at 1-hour intervals for both the spring and neap tides, respectively. Fig. 3 and Fig. 4 show the comparison between the simulated tidal current and the observed current. The model accurately represented the tidal current variation, although there were some differences due to the absence of the wind-driven current or baroclinic flow. Simulation at the TC1 station was better than that at the TC2 station, which might be related to the complex geometry near the deep-water channel around Guantouling. The ebb-dominated tidal current was well reproduced by the model, as shown in Fig. 3 and Fig. 4. We plotted the

model results for the tidal current at high slack water and low slack water in Fig. 5a and Fig. 5b, respectively. During high water, the tidal flats are covered by seawater, and the tides go upstream along the river outlets; during low water, the tides recede and the tidal flats are exposed. Compared with previous studies, this model better simulates the wet-and-dry process in the Lianzhou Bay, which provides a more realistic simulation of the actual situation.

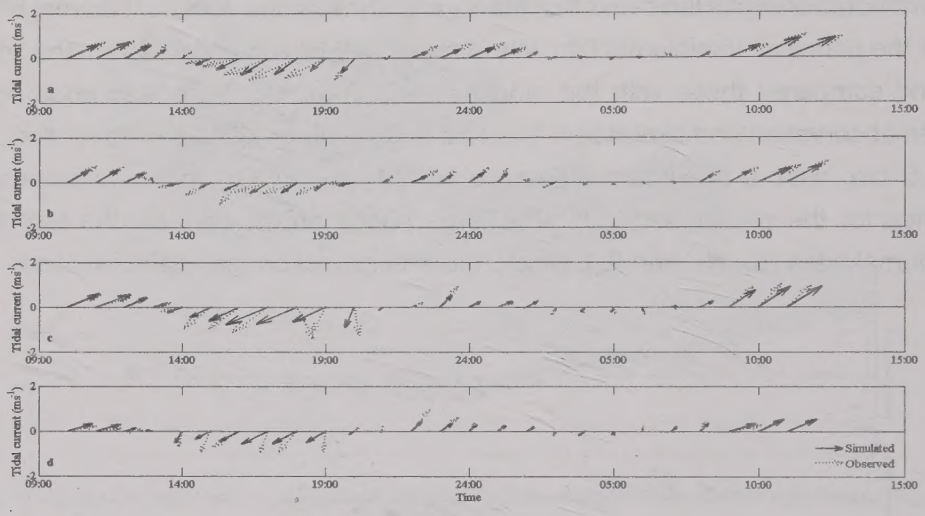

Fig. 4 Comparisons of the observed and simulated tidal current (unit: /ms) on neap tides at station TC1 (surface: a; bottom: b) and TC2 (surface: c; bottom: d)

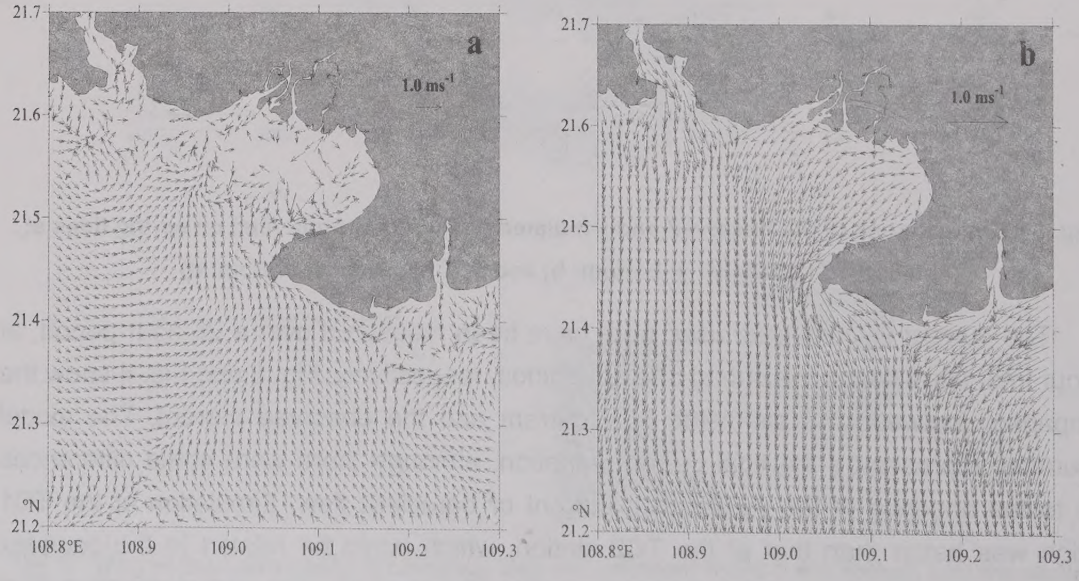

Fig. 5 The tidal current (unit: /ms) in low slack water (a) and high slack water (b) during the spring

tides in Lianzhou Bay and adjacent areas.

4 Model results and discussion

4.1 Tides

The Lianzhou Bay is located at the northeast end of the Beibu Gulf, being considered as a unique basin in the world, where near-resonance of the diurnal components results in a mesotidal diurnal regime (Fang et al. [6], 1999). According to the numerical simulation results of Fang et al. [6] (1999), K_1 and O_1 are mostly standing waves, but with some northward propagation into the Beibu Gulf; M_2 is the largest semidiurnal component and has a largely propagating character. On moving into the Lianzhou Bay, the amplitudes of the diurnal components decrease rapidly, and the tides become propagating waves in the shallow water. The amplitude of M_2 increases dramatically, and its propagating character becomes more evident (Fig. 6).

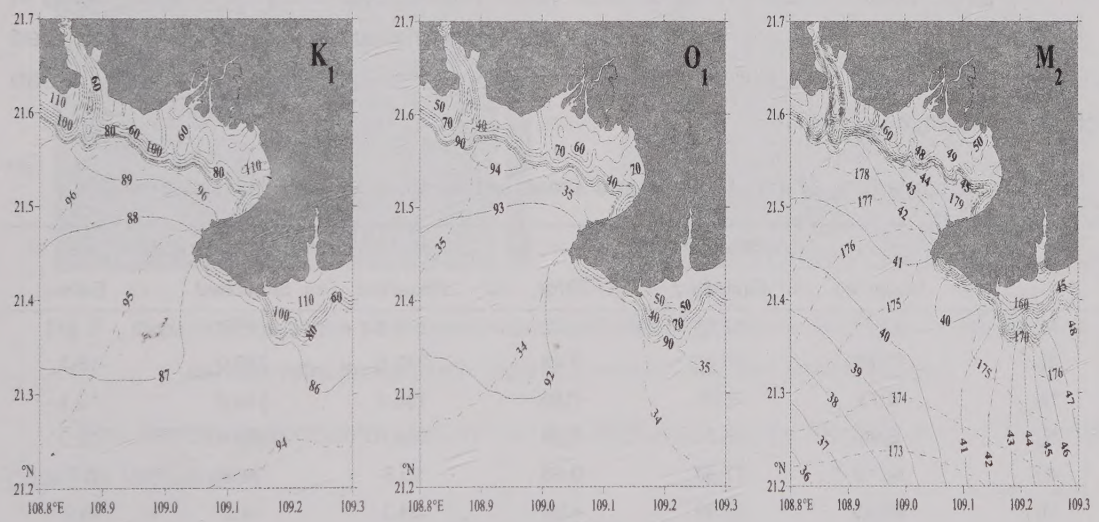

Fig. 6 Co-tidal charts of the K_1, O_1, and M_2 constituents in Lianzhou Bay and adjacent areas. Solid lines: co-amplitudes (unit: cm); dashed lines: co-phases (unit: deg)

In contrast to the semi-diurnal regime, for which the distortion of the tide can be represented by the non-linear growth of shallow-water constituents, the tidal asymmetry in the Beibu Gulf is a combination of the astronomical constituents K_1, O_1, and M_2 (Hoitink et al. [13], 2003). As these three components have the largest amplitudes, the tidal asymmetry in this region is rather strong. According to the *China Embayment Logs* [14] (1993), the average flood duration is 10 hours, much longer than the average ebb duration of 8 hours.

Song et al. [15] (2011) proposed that the tidal asymmetry could be measured via the

skewness

$$\gamma = \frac{\frac{3}{2} a_{K1}\omega_{K1} a_{O1}\omega_{O1} a_{M2}\omega_{M2} \sin(\varphi_{K1} + \varphi_{O1} - \varphi_{M2})}{\left[\frac{1}{2}(a_{K1}^2\omega_{K1}^2 + a_{O1}^2\omega_{O1}^2 + a_{M2}^2\omega_{M2}^2)\right]^{3/2}}$$

where a is the amplitude, ω is the frequency, and φ is the phase of the respective tidal constituent. If a tide spends more time in rising than falling, the skewness will be typically negative ($\gamma < 0$); conversely, a positive skewness ($\gamma > 0$) usually indicates a tide that rises more quickly than it falls (Song et al. [15], 2011). The larger $|\gamma|$, is the stronger the tidal asymmetry is. As shown in Fig. 7a, the contours of tidal asymmetry are basically parallel to the M_2 co-tidal line, which indicates that M_2 plays the most important role in the triplet-induced tidal asymmetry. Tidal asymmetry is strongest in the deep water; it decreases in the tidal flats and estuaries, and the sign of γ can even change. This is mainly due to the large bottom friction in the shallow-water region (Speer et al. [16], 1985; Kang et al. [17], 2003). This tidal asymmetry may cause asymmetric transport of suspended sediment and nutrients, which is significant for environmental protection in a coastal ocean such as the Lianzhou Bay.

Tab. 1 Comparison of the observed and simulated harmonic constants at station BHI

Constituents	Amplitude / cm			Phase / °, UTC +0800		
	Observed	Simulated	Error	Observed	Simulated	Error
M_2	42.71	42.45	0.26	176.8	175.7	1.1
S_2	10.85	10.42	0.43	235.9	248.0	-12.1
N_2	8.13	8.76	-0.63	135.9	149.0	-13.1
K_2	6.98	6.7	0.28	256.8	269.0	-12.2
K_1	88.19	87.84	0.35	95.5	94.8	0.7
O_1	96.45	92.36	4.09	33.3	34.2	-0.9
P_1	26.98	26.87	0.11	87.9	87.3	0.6
Q_1	23.07	22.61	0.46	358.9	359.9	-1.0

4.2 Tidal currents

The model results show the tidal current is rotating outside the Lianzhou Bay, but rectilinear inside the bay. This result is in accordance with previous observations and model simulations (Chen et al. [3], 2001; Sun and Huang, 2001a [4], b [5]). We plotted the surface tidal current ellipses for K_1, O_1, and M_2 in Fig. 8, and the bottom tidal current ellipses in Fig. 9. Of these tidal components, O_1 has the largest rotating character in the open ocean. However, on propagating into the Lianzhou Bay, it becomes rectilinear; its

major axis is parallel to the coastline or the water channel. In some river outlets and the deep-water channel around the Guantouling Peninsula, the tidal current velocity can reach over 0.80/ms. K_1 has similar pattern to O_1, but with smaller ellipticity, and a maximum velocity approaching 0.82/ms. M_2 has an almost rectilinear ellipse with a southwest-northeast orientation, due to its propagating character. Only in Lianzhou Bay, does it show some rotating character in some shallow-water areas with a flat bottom. The M_2 velocity can reach 0.60ms^{-1}. The major difference between the surface and the bottom tidal current ellipses is in the length of the major axis. Due to bottom friction, the tidal current velocity near the bottom is smaller than that on the surface.

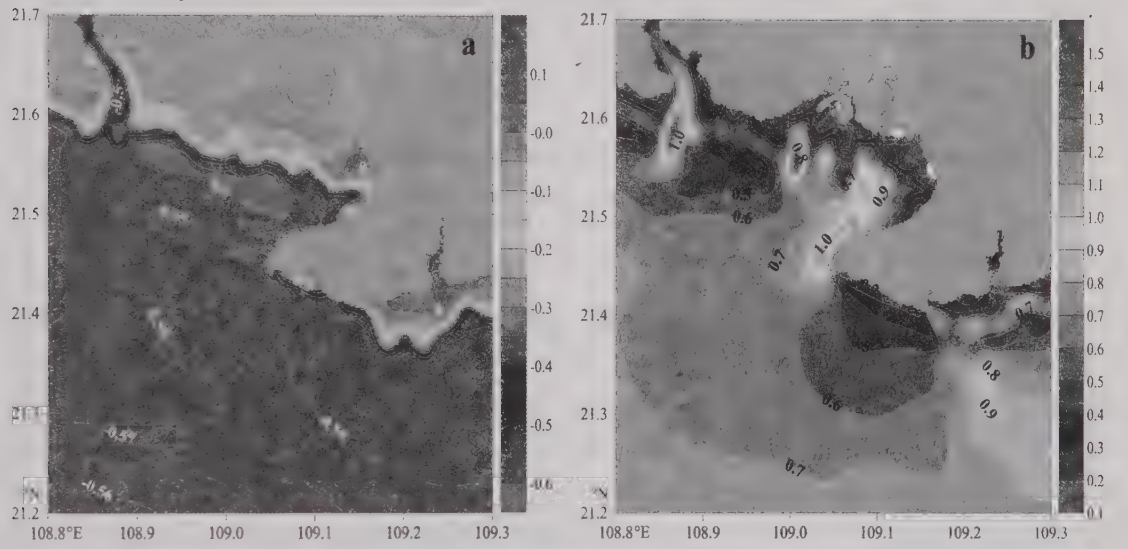

Fig. 7 Distributions of the tidal asymmetry coefficients (a) and the maximum probable tidal current velocities (b, unit: /ms) in Lianzhou Bay and adjacent areas

The maximum probable velocity can be estimated as the large stone of the values given by formulae:

$$v_{max} = 1.29w_{M2} + 1.23w_{S2} + w_{K1} + w_{O1}$$
$$v_{max} = w_{M2} + w_{S2} + 1.68w_{K1} + 1.46w_{O1}$$

where *w* is the length of the major axis of the respective components. As shown in Fig. 7b, the contours of the maximum probable velocity agree well with the isobaths and are parallel to the coastline, which indicates that the maximum probable velocity depends on the bathymetry and morphology in this region. Strong currents appear where there is a large water-depth gradient, such as in the deep-water channel in the Beihai Harbor, as well as in the river outlets, where the maximum probable velocity exceeds 1.0ms^{-1}. These regions have strong tidal-current-induced erosion, and are important passages for sediment transport.

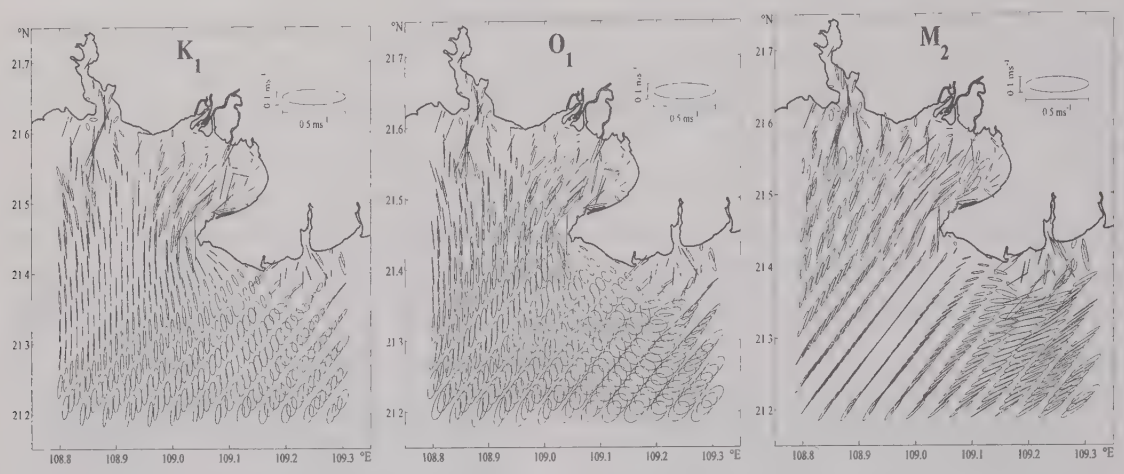

Fig. 8 Distributions of the surface tidal current ellipses (unit: /ms) of the K_1, O_1, and M_2 constituents in Lianzhou Bay and adjacent areas

4.3 Tidal-induced residual current

The tidal-induced residual current shows multi-vortex structures in the Lianzhou Bay (Fig. 10). It has a similar distribution from the surface to the bottom, with a maximum velocity of about 0.11 / ms on the surface and 0.08 / ms near the bottom. The velocity of the tidal-induced residual current is usually related to that of the tidal current, while its direction of tidal-induced residual current is usually the same as that of the maximum tidal current velocity (Chen et al. [18], 2003). As shown in Fig. 10, the residual current flows northward, and is separated into two branches at the Guantouling Peninsula. One turns to the west, the other is blocked by the southern boundary of the Guantouling Peninsula, creating a clockwise eddy. There is also an anti-clockwise eddy at the top of the Lianzhou Bay, and a clockwise eddy northwest of Guantouling. The former moves the fluvial sediment westward to the open ocean, with some deposition on the tidal flats (Jiang et al. [19], 2008). Sediments entering the deep-water channel around Guantouling are taken to the open ocean by the clockwise eddy there, which keeps the channel from silting up. It also accelerates the pollutant advection and diffusion, reducing pollutant concentration in the harbor.

We also found that there was strong ebb-dominant residual current in the Yingpan Harbor, which has not been reported previously. This is due to the large water-depth gradient at the edge of the tidal flats, which favors the ebb current. However, the tidal asymmetry in Fig. 7a is positive value in this region, which means the ebb duration longer than the flood duration. Therefore, in the Yingpan Harbor, there is a significant southward residual flow. This phenomenon only happens on the tidal flats, which also indicates the importance of the wet-and-dry process to the numerical simulation of the tidal currents in

coastal oceans.

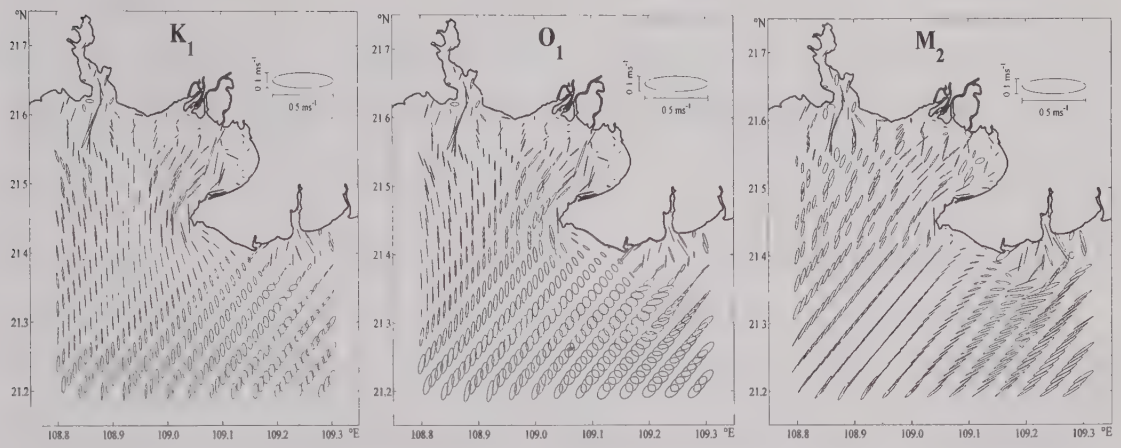

Fig. 9 Distributions of the bottom tidal current ellipses (unit: /ms) of the K_1, O_1, and M_2 constituents in Lianzhou Bay and adjacent areas

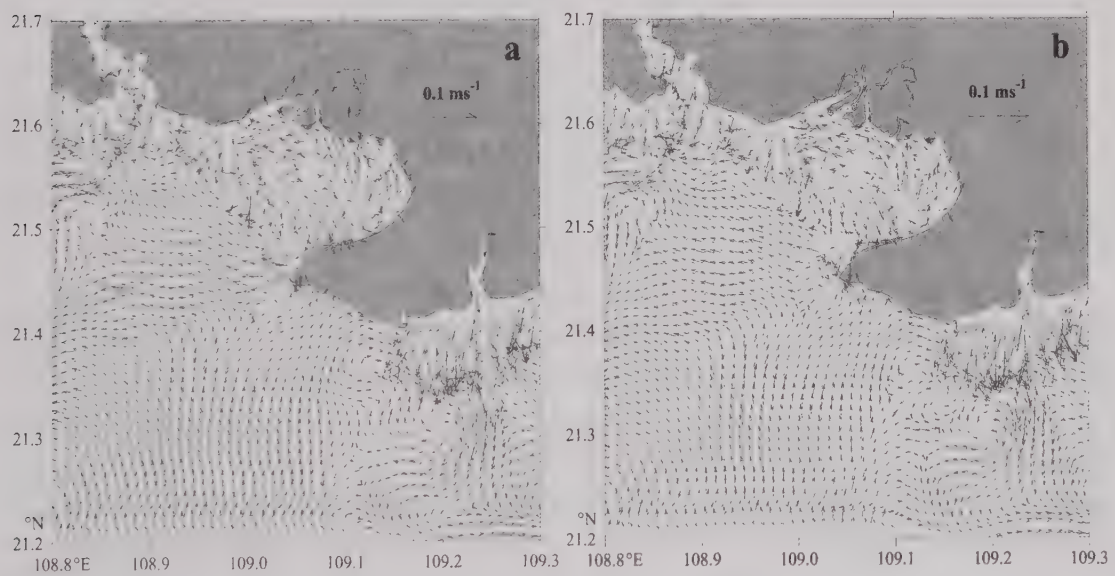

Fig. 10 Distributions of the residual tidal currents (unit: /ms) at the surface (a) and the bottom (b) of Lianzhou Bay and adjacent areas.

5 Conclusions

In this paper, we use a three-dimensional numerical model to study the tides and tidal currents in the Lianzhou Bay, based on an unstructured grid, finite-volume coastal ocean model (FVCOM). The model results are in good agreement with observed tidal elevations

and tidal currents. The tidal characteristics and residual currents also agree well with previous observations and numerical simulations. Nevertheless, our model takes into account the wet-and-dry process, which is of importance to the Lianzhou Bay with its large area of tidal flats. Compared with previous studies, the model more accurately reproduces the tidal motions in the Lianzhou Bay. Furthermore, the model results provide more-accurate hydrodynamics for the study of pollutant and sediment transport in the Lianzhou Bay.

From our model, we concluded as follow:

(a) In the Lianzhou Bay and adjacent areas, K_1 and O_1 are the major diurnal tides and M_2 the most significant semi-diurnal tide. Their combination can generate an asymmetric tidal wave, which leads to flood duration longer than ebb duration. When the predominantly standing waves K_1 and O_1 enter the Lianzhou Bay, their amplitudes decrease rapidly and they acquire a more propagating character. Conversely, the propagating wave M_2 increases in amplitude and gets more propagating character. The tidal asymmetry is strongest in the open ocean, but is reduced on the tidal flats and in the river outlets.

(b) K_1 and O_1 are mostly rotating currents in the open ocean, but rectilinear currents in the Lianzhou Bay. M_2 is rectilinear over the whole region, in accordance with its propagating character. In calculating the maximum probable velocity, we find that the deep channels near the Guantouling, the Dafeng River estuary, and the Nanliu River outlets are important passages for sediment transport, due to the strong tidal currents there.

(c) The tidal-induced residual current has almost the same distribution from the surface to the bottom. The maximum velocity is $0.11ms^{-1}$ on the surface, and 0.08/ms on the bottom. The residual current flowing northward is divided into two branches at the Guantouling Peninsula. One turns to the west, while the other is blocked at the southern boundary of the Guantouling, forming a clockwise eddy. There are two eddies inside the Lianzhou Bay, the cyclone circulation at the top of the bay, and the anti-cyclone circulation at the mouth of the bay.

During this study, we noted that the density-induced residual current might be also of importance in this region, due to the variation in monsoon and river discharges. Based on some numerical experiments, Cai et al. [20] (2003) pointed out that the density-induced residual current might impact on the circulation structure in the Beibu Gulf. In future, we will include the baroclinic process and wind stress in this model, in order to gain a better understanding of the circulation structure in the Lianzhou Bay.

Acknowledgements

The present study was supported by the special fund for the Ocean Public Welfare Scientific Research Project, State Oceanic Administration, People's Republic of China (Grant No. 200805065). We particular thank Dr. Peter McIntyre for proofreading this paper, which has been much improved in English writing.

Reference

[1] Chen B, Shi M. Numerical calculation ábout the tidal current and wind current in the Lianzhou Bay [J]. Guangxi Sciences, 1996, 3(3), 32 - 35.

[2] Bai Y, Yu T. Split step and layered quasi-three-dimensional mathematical model of flow and its application to tide current calculation in the Lianzhou Bay [J]. Acta Oceanologica Sinica, 1998, 20(5), 126 - 135.

[3] Chen B, Qiu S, Ge W, Shi M. Numerical calculation about the tidal currents in the main bays of Guangxi [J]. Guangxi Sciences, 2001, 8(4), 295 - 300.

[4] Sun H, Huang W. Observation, analysis and numerical study of the tide and current in the Guangxi offshore area, Part I: Observation and analysis [J]. Journal of Oceanography of Huanghai and Bohai Seas, 2001, 19(4), 1 - 11.

[5] Sun H, Huang W. Observation, analysis and numerical study of the tide and current in the Guangxi offshore area, Part II: Numerical study [J]. Journal of Oceanography of Huanghai and Bohai Seas, 2001, 19(4), 12 - 21.

[6] Fang G, Kwok Y-K, Yu K, Zhu, Y. Numerical simulation of principal tidal constituents in the South China Sea, Gulf of Tonkin and Gulf of Thailand [J]. Continental Shelf Research, 1999, 19, 845 - 869.

[7] Zheng L, Chen C, Liu H. A modeling study of the Satilla River Estuary, Georgia. I: flooding-drying process and water exchange over the salt marsh-estuary-shelf complex [J]. Estuaries, 2003, 26(3), 651 - 669.

[8] Lü X, Qiao F, Xia C, Numerical simulation of tides and three-dimensional tidal currents in Jiaozhou Bay by a movable land-sea boundary model [J]. Acta Oceanologica Sinica, 2008, 30, 21 - 92.

[9] Chen C, Liu H, Beardsley R C. An unstructured grid, finite volume, three-dimensional, primitive equations ocean model: Application to coastal ocean and estuaries [J]. Journal of Atmospheric and Oceanic Technology, 2003, 20(1), 159 - 186.

[10] Chen C, Huang H, Beardsley R C, Liu H, Xu Q, Cowles G. A finite-volume numerical approach for coastal ocean circulation studies: comparisons with finite difference models

[J]. Journal of Geophysical Research, 2007, 112, C03018, doi:10.1029/2006JC003485.

[11] Egbert G D, Bennett A F, Foreman M G G. Topex/Poseidon tides estimated using a global inverse model [J]. Journal of Geophysical Research, 1994, 99(C12), 24 821 - 24 852.

[12] Egbert G D, Erofeeva S Y. Efficient Inverse Modeling of Barotropic Ocean Tides [J]. Journal of Atmospheric and Oceanic Technology, 2002, 19(2), 183 - 204.

[13] Hoitink A J F, Hoekstra P, and van Maren D S. Flow asymmetry associated with astronomical tides: implications for the residual transport of sediment [J]. Journal of Geophysical Research, 2003, 108(C10), 3315, doi:10.1029/2002JC001539.

[14] China Embayment Logs Editorial Board. China Embayment Logs, 12th Fascicule: Guangxi Province [M]. Beijing: China Ocean Press, 1993, 1 - 335.

[15] Song D, Wang X H, Kiss A, et al. The contribution to tidal duration asymmetry by different combinations of tidal constituents [J]. Journal of Geophysical Research, 2011, 116, C12007, doi: 10.1029/2011JC007270.

[16] Speer P E, Aubrey D E. A study of non-linear tidal propagation in shallow inlet/estuarine systems. Part II: theory [J]. Estuarine, Coastal and Shelf Science, 1985, 21, 207 - 224.

[17] Kang J W, Jun K S. Flood and ebb dominance in estuaries in Korea [J]. Estuarine, Coastal and Shelf Science, 2003, 56(1), 187 - 196.

[18] Chen B, Shi M, Qiu S. Characteristics of residual currents and their influence on the material transportation in five main bays of Guangxi coast [J]. Transactions of Oceanology and Limnology, 2003, (1), 13 - 21.

[19] Jiang L, Chen B, Qiu S. The relationship of silt transportation and ocean dynamical condition in delta of Lianzhou Bay [J]. Journal of Guangxi Academy of Sciences, 2008, 24(1), 1 - 3.

[20] Cai S, Huang Q, Long X. Three-dimensional numerical model study of the residual current in the South China Sea [J]. Oceanologica Acta, 2003, 26(5-6): 597 - 607.

基于 FVCOM 的廉州湾及周边海域三维潮汐潮流数值模拟

宋德海[1]，鲍献文[1]，张少峰[2,3*]，张春华[2,3]

（1. 中国海洋大学 物理海洋实验室，山东 青岛 266100；2. 广西壮族自治区海洋监测预报中心，广西 北海 536000；3. 国家海洋局 北海海洋环境监测中心站，广西 北海 536000）

摘 要：基于采用不规则三角网格和有限体积方法的 FVCOM 模式，建立廉州湾三维潮流数值模型来重现廉州湾及周边海域的潮位和潮流变化状况。根据模拟结果计算得到了较以往更为精细的廉州湾及周边海域 K_1、O_1 和 M_2 分潮的同潮图，并计算了由此三个分潮引起的潮汐不对称的变化情况。K_1 和 O_1 分潮在廉州湾外主要以驻波的形式存在，进入廉州湾后转化为前进波；M_2 分潮在廉州湾外主要以前进波的形式存在，进入廉州湾后前进波特征更为明显。K_1 和 O_1 分潮流在廉州湾外以旋转流为主，在廉州湾内以往复流为上；M_2 分潮流在整个研究海域以往复流为主。由潮余流场的分布特点可以看出自南向北由外海进入廉州湾的潮余流，在冠头岭处分为两支，一支逆时针转向西，另一支被冠头岭阻挡在其南侧形成顺时针封闭环流。在廉州湾内部同时存在两个环流系统，湾顶的气旋式环流和口门处的反气旋式环流。

关键词：廉州湾；FVCOM；潮汐；潮流；余流

Study on the wave extreme parameters of the Bohai Sea with the numerical simulation using SWAN

SUN Xiao-juan[1], ZHOU Liang-ming[1*], WANG Ai-fang[2], WANG Zhi-feng[3], WU Lun-yu[4]

1. Ocean University of China, Qingdao 266100, *Shandong Province, China;*

2. Engineering Reconnaissance & Design Institute, Ocean University of China, Qingdao 266100, *Shandong Province, China;*

3. College of Engineering, Ocean University of China, Qingdao 266100, *Shandong Province, China;*

4. The First Institute of Oceanography, State Oceanic Administration, Qingdao 266100, *Shandong Province, China*

Abstract: Wave fields in Bohai Sea from 1985 to 2004 were simulated using SWAN wave model by inputting high-resolution hindcast wind fields dataset. Comparisons of wave heights between simulation and observation show good agreement in general. According to the annual extreme values of simulation, this paper gives wave extreme parameters with different return-period for all computation grids in Bohai sea.

Keywords: Bohai Sea; SWAN; significant wave height; extreme parameter

1 Introduction

Studying on wave conditions in the Bohai Sea is very important for the economic research, coastal engineering, marine engineering, transportation engineering and oil exploitation et al. According to wave data from observation station, the annual extreme wave parameters and design wave parameters in the Bohai Sea were calculated [1, 2]. Without the limitations associated with measurements, numerical simulation becomes a very important method for wave investigation, because it is a very useful and convenient way to obtain the spatial and temporal distribution of wave fields. Li et al. gave the annual extreme wave heights by making the hindcast with the HISWA model based on 54 historical wind fields of the Bohai Sea from 1972 to 1992 [3, 4]. Recently, considerable improvements have been made in predicting ocean wave fields for shallow waters. The third generation wave action model-SWAN (Simulating Waves Nearshore) was designed to overcome traditional difficulties of applying wave action models in coastal regions [5]. It makes use of the most advanced wave research achievements and has been applied to

Received on Oct. 29, 2012

*Corresponding author: zhou5299@ouc.edu.cn

several theoretical and field conditions successfully [6-10].

In this study, SWAN was implemented in the Bohai Sea to investigate the wave fields. Wind field data, current and tide elevation as the inputs were described in section II. The wave model was given in section III. Comparisons of the simulated results with observations were also given in this section. Wave extreme parameters for different return-period were discussed in section IV, and summary and conclusions were given in the last section.

2 Model input

2.1 Wind field data

The wind field dataset used in this paper was 20-year long (from 1985 to 2004), which was hindcasted by RAMS wind model with NCEP-DOE Reanalysis wind data as inputs. The wind input interval was 1 h, so all wind processes including tropical cyclones and cold fronts were covered, and the horizontal resolution was 0.1°×0.1°.

Wind observation for twenty-three passages of wind process at six oil platform stations were selected to compare with the wind hindcast, where the mean correlative coefficient and relative error for wind speed were 0.91 and 8.9%, respectively. Fig. 1 gives the comparison of wind speed between simulation hindcast and observation at platform SZ36 when Typhoon Winnie passed over the Bohai Sea from Aug. 16 to Aug. 24, 1997, which showed good agreement between observation and simulation for wind speed.

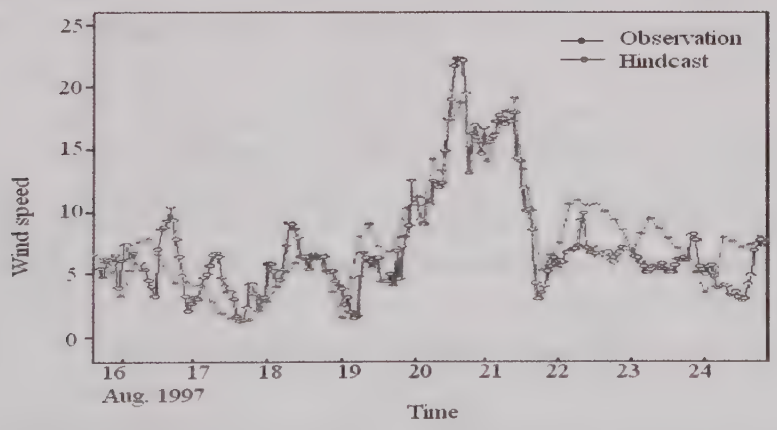

Fig. 1 Comparisons of wind speed between observation (dot-line) and hindcast value (circle-line) by RAMS wind model at oil platform SZ36 from Aug. 16 to Aug. 24, 1997 when Typhoon Winnie passed, where the wind speed was 10-min averaged and 10 m height above the sea surface.

(unit: m/s)

2.2 Current and water elevation

The current and water elevation used as inputs in this study were simulated by POM model, with the same spatial grid and interval as wind field data. Also, many comparisons were carried out between observation and simulation of currents and tide elevation, and results indicated that the simulation data could describe the current and tide characteristics of the Bohai Sea well.

3 Wave model and validation

SWAN is a numerical wave model for obtaining realistic estimates of wave parameters in coastal areas, lakes and estuaries from given wind, bottom and current conditions. The following wave propagation processes are represented in SWAN: a) propagation through geographic space, b) refraction due to spatial variations in bottom and current, c) shoaling due to spatial variations in bottom and current, d) blocking and reflections by opposing currents, and e) transmission through blockage, reflection by or against obstacles.

The model is based on the wave action balance equation with sources and sinks, and the waves are described with the two-dimensional wave action density spectrum, even when nonlinear phenomenon dominates in the surf zone. The spectrum is the action density spectrum $N(\sigma,\theta)$ rather than the energy density spectrum $E(\sigma,\theta)$, since in the presence of currents, action density is conserved whereas energy density is not[11]. The action density is equal to the energy density divided by relative frequency

$$N(\sigma,\theta) = E(\sigma,\theta)/\sigma \tag{1}$$

where σ is the relative frequency and θ is the wave direction.

The evolution of the wave spectrum is described by the spectral action balance equation which for Cartesian coordinates is (Hasselmann et al. 1973) as follow,

$$\frac{\partial N}{\partial t}+\frac{\partial}{\partial x}c_x N+\frac{\partial}{\partial y}c_y N+\frac{\partial}{\partial \sigma}c_\sigma N+\frac{\partial}{\partial \theta}c_\theta N=\frac{S}{\sigma} \tag{2}$$

The first term in the left-hand side of this equation represents the local rate of change of action density in time, and the second and third term represent propagation of action in geographical space with propagation velocities c_x and c_y in x and y space, respectively. The fourth term represents shifting of the relative frequency due to variations

in depths and currents with propagation velocity c_σ. The fifth term represents depth-induced and current-induced refraction with propagation velocity c_θ. The expressions for these propagation speeds are taken from linear wave theory [12, 13]. S is the source term representing the effects of wind generation, dissipation and nonlinear wave-wave interactions, where dissipation mainly includes whitecapping, bottom friction and depth-induced wave breaking.

Tab. 1 Comparison results for significant wave height between observation and simulations at different stations

Oil station	Time	Longitude / N	Latitude / E	Average error / m	RMS / m
BZ28	From 25 to 29 Nov, 1995	119°37′	38°20′	0.21	0.35
BZ28	From 1 to 10 Jan, 1996	119°37′	38°20′	0.09	0.27
BZ28	From 10 to 14 Jun, 1996	119°37′	38°20′	0.19	0.31
BZ28	From 1 to 12 Sec,, 1996	119°37′	38°20′	-0.18	0.27
QK18	From 15 to 19 Nov, 1998	117°57′	38°39′	0.20	0.21
QK18	From 20 to 25 Nov, 1998	117°57′	38°39′	-0.15	0.32
SZ36	From 18 to 22 Jun, 1997	120°48′	40°02′	0.18	0.29
SZ36	From 15 to 20 Aug, 1997	120°48′	40°02′	-0.15	0.23
SZ36	From 1 to 3 Sec, 1997	120°48′	40°02′	0.22	0.23
SZ36	From 11 to 15 Jul, 1997	120°48′	40°02′	-0.08	0.22
SZ36	From 12 to 19 Nov, 1997	120°48′	40°02′	-0.12	0.34
SZ36	From 5 to 7 Dec, 1997	120°48′	40°02′	0.10	0.19
SZ36	From 19 to 22 Dec, 1997	120°48′	40°02′	-0.11	0.18

The grid in this study was regularly spaced by longitude-latitude grid, extending from 37° to 41° N, 117° to 123° E, and the spatial grid was 1/18° ×1/18°. The wave model used in this study used time step of 3600s, wind input interval of 1h, calculating time from 1985 to 2004. The model inputs mainly included wind, current and water level (described in section III). Considering the water depth of the Bohai Sea was shallow in generally, the boundary spectra shape in this study was defined as JONSWAP with the power of high frequency tail of 4.

Wave fields in the Bohai Sea from 1985 to 2004 were simulated with SWAN. Comparisons between observations from oil platform BZ28, QK18, JZ09, LD16 and SZ36 and model hindcast were carried out, and the wave processes for comparison included typhoon and cold fronts passages. Fig. 2 compares significant wave heights between the model hindcast and the observation from oil platforms, and shows good agreement between hindcast and observation in generally. Tab. 1 gives the comparison results at different oil platforms for 13 wave processes. And the maxixum average error and the RMS(Root Mean square error) between simulation and observation for significant wave

height were about ± 0.22 m and 0.35 m, respectively.

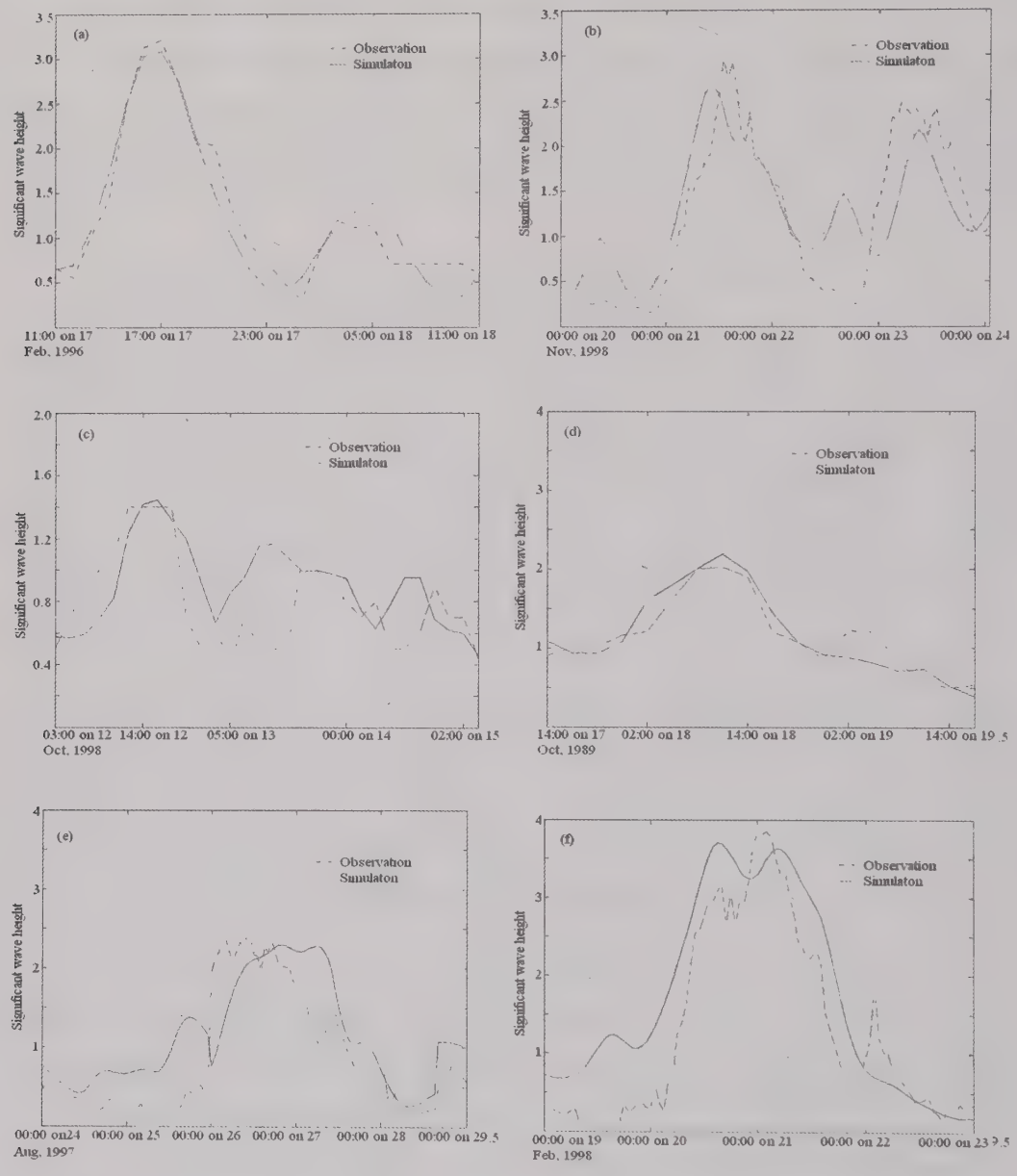

Fig. 2 Comparisons of significant wave heights between hindcast (real line) and observations (dashed line) at oil platform

a) BZ28 (from Feb. 17 to Feb. 18, 1996), b) QK18 (from Nov. 20 to Nov. 24, 1998), c) JZ09 (from Oct. 12 to Oct. 15, 1998), d) Ld16 (from Oct. 17 to Oct. 19, 1989), e) SZ36 (from Aug. 24 to Aug. 29, 1997) and f) SZ36 (from Feb. 19 to Feb. 23, 1998), unit: m.

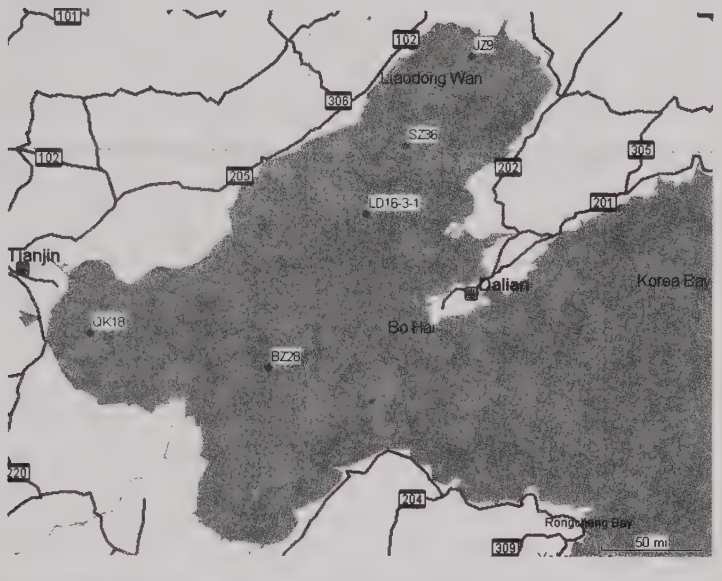

Fig. 3 Distribution of stations for comparing the significant wave heights

Tab. 2 Water depth of stations

Oil station	Longitude / E	Latitude / N	Water depth / m
BZ28	119°37′	38°20′	22.5
QK18	117°57′	38°39′	10.0
JZ9	121°30′	40°40′	7.8
LD16	120°31′	39°31′	26.5
SZ36	120°54′	40°2′	31.0

4 Results

4.1 Annual wave extreme values

From wave model simulation data, the annual extreme values of wave parameters such as wave height, wave period and wave length for all calculation grids (1028) were got. By convenience of discussion, four points marked A, B, C and D were selected which were located in Bohai Bay, Laizhou Bay, Liaodong Bay and the middle sea area of the Bohai Sea, respectively. Figure 4 gives the locations of four points. Tab. 3 gives the annual extreme significant wave heights with occurring time and wave directions at four points. From the table, we can find that for point A (in the Bohai Bay), the annual extreme significant wave height mainly occurs in autumn and winter, and the main wave direction is northeast, that is, the annual maximum wave height generated by NE wind with the longest wind fetch of NE direction. For point B (in the Laizhou Bay), the annual extreme values all occurs from

September to February in the next year, and the corresponding wave directions are all north direction. However, in the Liaodong Bay (point C), the main wave direction for annual maximum wave height is south direction, and the occuring time is mainly in March and April. In the middle sea area of the Bohai Sea (point D), the annual extreme value mainly occurs in October to February (in the next year), and it is influenced by north wind, where NE direction accounts for 45%.

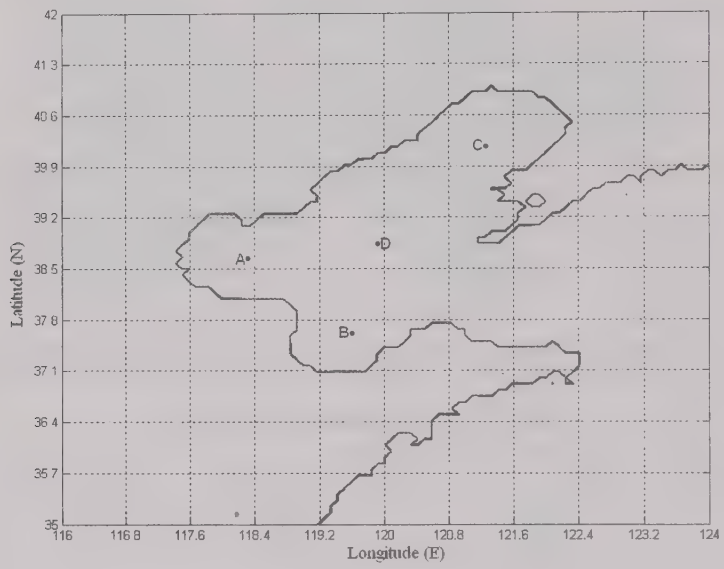

Fig. 4 Locations of point A, B, C and D

4.2 Extreme parameters for different return period

Through analytical calculation of observed wave data from marine meteorological stations along the coast of China, Wang proved that, for long-term distribution, it was appropriate to use Weibull function to fit the distribution of the maximum wave height and wave period [2]. Comparisons between the well-known extreme value distributions such as Pearson III distribution, Gumbel distribution and Weibull distribution were carried out, and results showed the Weibull distribution was more suitable for long-term inference of extreme values. In this study, we adopted the Weibull distribution as the extrapolation method to calculate the wave extreme parameters for different return-periods.

Tab. 4 gives the extreme values of significant wave height and mean wave period with 5-year, 10-year, 25-year, 50-year and 100-year return-periods for point A, B, C and D. For 100-year return period, extreme values for significant wave height and mean wave period of point D are the most, which are 5.38 m and 5.86 s, respectively. Then the values of point B and point D are medium, and values of point A are the least, respectively.

Fig. 5 gives the spatial distribution of 100-year return period extreme values for significant wave height and mean wave period. From this figure, we may find that wave heights and wave periods decrease gradually from the middle sea area of the Bohai Sea to coastal sea areas, where the maximum of wave height is more than 6.0 m, which is located in the range of 120° - 120.5° E, 38.0° - 38.5° N. Different from wave height in some sort, the maximum wave period (more than 6 s) of sea area moves to southwest and located in the north of Laizhou Bay, with the large range of 119.3°~120.6° E, 37.8°~38.5° N.

Tab. 3 Annual extreme values of significant wave heights / m for point A, B, C and D

Point	A			B			C			D		
Location	118°10′0″E, 38°40′0″N			119°30′0″E, 37°40′0″N			121°10′0″E, 40°00′0″N			119°50′0″E, 38°40′0″N		
Depth	15.0m			14.7 m			29.2 m			26.0 m		
Year	Annual extreme value	Occuring time /month	Wave direction	Annual extreme value	Occuring time /month	Wave direction	Annual extreme value	Occuring time /month	Wave direction	Annual extreme value	Occuring time /month	Wave direction
1985	2.15	01	W	2.85	10	N	4.15	04	SW	3.35	01	W
1986	2.48	01	NW	3.93	12	N	3.99	04	N	4.23	12	N
1987	3.21	11	NE	4.49	11	NE	4.25	11	NE	5.05	11	NE
1988	2.53	01	NW	3.11	01	NW	3.21	04	SW	3.53	01	NW
1989	2.33	06	SE	3.67	10	N	3.93	10	N	3.92	10	N
1990	2.96	12	N	4.02	02	N	4.39	04	N	4.59	02	NE
1991	2.87	12	NE	3.29	12	N	3.38	12	NE	3.97	12	NE
1992	2.53	09	NE	3.34	09	N	3.34	09	S	3.55	09	N
1993	2.51	11	NE	3.53	11	N	3.59	04	SW	3.81	11	NW
1994	2.26	02	N	3.22	10	N	3.58	05	SW	3.33	02	N
1995	2.44	11	NW	3.49	11	NW	3.78	04	S	3.74	11	NW
1996	2.53	10	E	3.80	11	N	4.62	10	S	3.80	11	NE
1997	2.63	01	NW	3.32	11	NE	3.72	11	NW	3.94	01	NW
1998	2.77	12	NE	3.97	12	NE	3.23	03	SW	4.17	12	NE
1999	2.35	09	NE	3.94	09	N	3.81	03	N	4.38	09	NE
2000	2.13	11	NW	2.94	02	N	4.91	04	SW	3.19	02	N
2001	2.44	02	NE	3.07	02	NE	3.90	03	N	3.34	02	NE
2002	2.89	10	NE	3.63	10	NE	3.79	04	SW	3.93	10	NE
2003	3.17	10	NE	4.18	10	NE	4.59	04	S	4.63	10	NE
2004	2.30	11	NE	3.13	11	NE	3.96	04	SW	3.71	11	W

Tab. 4 Extreme values of significant wave heights / m and mean wave periods / s with 5-year, 10-year, 25-year, 50-year and 100-year return-periods for point A, B, C and D

Sea area		Bohai Bay	Laizhou Bay	Liaodong Bay	Middle sea area
point		A	B	C	D
Significant	5a	3.08	4.21	4.43	4.70
Wave	10a	3.18	4.39	4.60	4.86
Height	25a	3.30	4.62	4.81	5.07
/ m	50a	3.40	4.79	4.97	5.23
	100a	3.49	5.06	5.12	5.38
Mean	5a	4.12	4.93	4.87	5.12
Wave	10a	4.26	5.12	4.99	5.30
Period	25a	4.44	5.35	5.14	5.52
/ s	50a	4.57	5.53	5.25	5.69
	100a	4.70	5.70	5.36	5.86

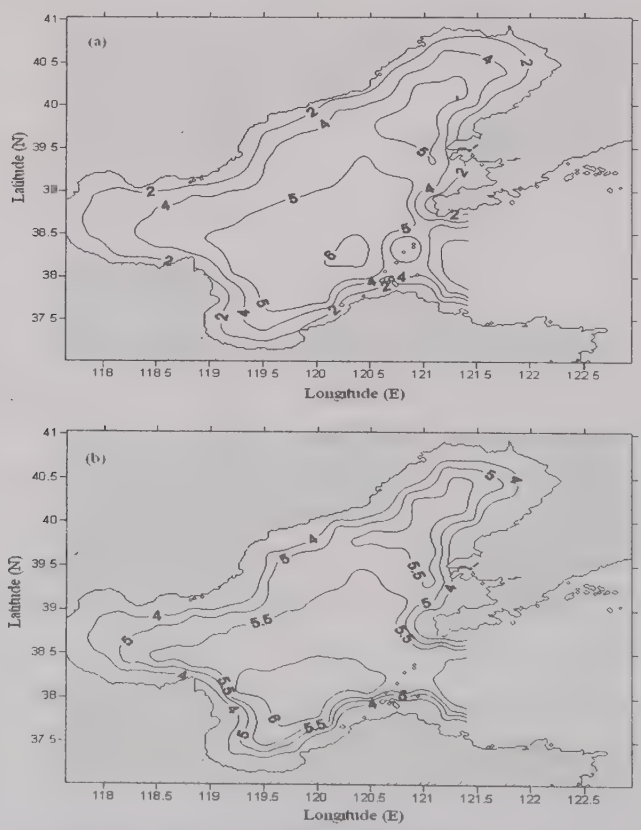

Fig. 5 Spatial distribution (contours) of 100-year return-period extreme values of a) significant wave height (m) and b) mean wave period (s) in the Bohai Sea

5 Summary and conclusion

In this study, wave fields in Bohai Sea from 1985 to 2004 were simulated by SWAN wave model. Comparisons between observations and hindcast showed good agreement. By statistical analysis, we found that, for annual extreme wave height in the Bohai Bay, it was mainly generated by northeast wind and occurred in autumn and winter. In the Laizhou Bay, it mainly occurred in winter, with the north direction. Different form that in the Laizhou Bay, the maximum wave height in the Liaodong Bay was mainly formed by the south wind in spring. In the middle sea area of the Bohai Sea, the annual extreme value mainly occurred in October to February of the next year, and it was influenced by northeast wind generally.

Using the Weibull function, the extreme parameters for significant wave height and mean wave period with different return-periods were calculated. For 100-year return-period significant wave height, the maximum value exceeded 6.0 m, which located in the southeast of the middle sea area of the Bohai Sea.

This study could increases our understanding of the wave conditions of the whole Bohai Sea and provide basic data for ocean environmental research and engineering design.

Acknowledgments

This work was supported by National Nature Science Foundation of China, China National Basic Research Program (Grant No. 2009CB421201). The authors wish to thank Professor Fu Gang and Associate Professor Lin Xiao-pei for providing the wind field data, current and water elevation data, respectively.

References

[1] Yao Guoquan, Ding Bingcan, Wang jianyi, et al. Statistic analysis of the annual extreme wave parameters for the coastal of China [J]. China Ocean Engineering, 1993, 7(1): 109 - 116.

[2] Wang Yanying. Investigation of design wave parameters for Chinese coastal areas [J]. China Ocean Engineering, 1988, 2(4): 71 - 78.

[3] LI Luping, HUANG Peiji, CHEN Xueying. Estimation of design wave heights for coastal sea areas [J]. China Ocean Engineering, 2000, 14(4): 517 - 524.

[4] Holthuijsen L H, Booij N, Herbers T H. A prediction model for stationary, short-crested waves in

shallow water with ambient currents [J]. Coastal Engineering, 1989,13: 23 - 54.

[5] Booij N, Ris R C, Holthuijsen L H. A third-generation wave model for coastal regions 1: Model description and validation [J]. Geophys. Res., 1999, 104(C4): 7 649 - 7 666.

[6] Rogers W E, Kaihatu J M, Petit H A H, et al. Diffusion reduction in an aritrary scale third generation wind wave model [J]. Ocean Eng., 2002, 29: 1 357 - 1 390.

[7] Rogers W E, Hwang P A, Wang D W. Investigation of wave growth and decay in the SWAN model: Three regional-scale application [J]. J. Phys. Oceanogr., 2003, 33: 366 - 389.

[8] Rogers W E, James M K, Larry Hsu, et al. Forcasting and hindcasting waves with the SWAN model in the Southern California Bight [J]. Coastal Engineering, 2007, 54, (1): 1 - 15.

[9] SWAN Team. SWAN User & Tecnical Manual（40.72）[M]. Delft：Delft University of Technology, 2008.

[10] Zijlema M, Westhuysen A J V. On convergence behaviour and numerical accuracy in stationary SWAN simulations of nearshore wind wave spectra [J]. Coast. Eng., 2005, 52: 237 - 256.

[11] Whitham G B. Linear and nonlinear waves [M]. New York: Wiley, 1974.

[12] Dingemans M W. Water wave propagation over uneven bottoms. Part I -linear wave propagation. Advanced Series on Ocean Engineering-Volume 13 [M]. Singapore: World Scientific, 1997.

[13] Mei C C. The applied dynamics of ocean surface waves [M]. Singapore: World Scientific, 1989.

运用 SWAN 数值模拟对渤海波浪极值参数的研究

孙晓娟[1]，周良明[1]，王爱方[2]，王智峰[3]，吴伦宇[4]

（1. 中国海洋大学 海洋环境学院，山东 青岛 266100；2. 中国海洋大学 工程勘察设计开发院，山东 青岛 266100；3. 中国海洋大学 工程学院，山东 青岛 266100；4. 国家海洋局第一研究所，山东 青岛 266100）

摘 要：本文以高分辨率后报风场资料为输入，采用 SWAN 波浪模式，模拟了渤海海域 1985 年至 2004 年共 20 年间的波浪场。通过有效波高数据的比较，可看出波浪数值结果与实测资料符合较好，可以用数值结果分析渤海海域的波浪特征。利用计算的年极值波要素，本文给出并分析了渤海海域不同重现期下的极值参数分布情况。

关键词：渤海；SWAN；有效波高；极值参数

Distribution characteristics of sea surface temperature along the southern coastal region of Zhejiang Province

HAN Xiao-yan, PAN Xiao-dong, MA Lin-fang

Wenzhou Oceanic Situation Monitoring Station, Wenzhou 325013, *Zhejiang province, China*

Abstract: The SST temporal and spatial distribution in the southern coast of Zhejiang is presented as the result of statistical analysis based on the observation data of 51 years from Dachen, kanmen and Nanji gauge stations. It shows that the overall SST along the coast is higher in the southern part and lower in the northern part, and the discrepancy between south and north parts becomes smallest in winter and largest in summer. Along the southern coast of Zhejiang, SST as a whole generally has a uptrend at rising the rate of 0.017 ℃/a in last 51 years. In addition, there are oscillation periods of 3.5 a, 5 - 6 a and 11 a stay with SST changes. Mainly, the annual cyclical variation determines SST with a good match of harmonic fitting effect.

Keywords: the southern coastal region of Zhejiang; SST; homogeneous; power spectrum; harmonic

1 Overview

Sea temperature, especially the sea surface temperature is the important physical oceanography factor. It is one of the rare elements of timing observations, which is included in the national meteorological observation network, and it is also the most referenced marine element to the research of physical oceanography and global climate anomalies. It is closely linked with the phenomenon of El Nino, La Nina and sea level rising. To the ocean development, the SST observation and research directly serve the aquaculture, the marine fisheries and the disaster prevention and reduction of the red tide and sea ice. The southern water of Zhejiang eastly boarding the Northeast Pacific Ocean, is often suffered from marine disasters, such as Typhoon, the red tide, sea water intrusion and et al. Especially, with the increasing of ocean development activities, the effects are more and more serious. Therefore the study of SST variation along the southern coastal region of Zhejiang is very necessary. It has practical significance for disaster prevention and reduction to promote and safeguard the development of marine fishing better.

Received on Nov. 29, 2012

Corresponding author: xiaoyong0728@163.com

2 Data collection and pretreatment

In order to comprehensively descript the general characteristics of SST along the southern coastal region of Zhejiang, from north to south, the SST data were collected from Dachen, Kanmen and Nanji, 3 ocean observation stations, to do the research. The data picked the monthly and annual average value of month and year, with the length 46a of Dachen (1960 - 2001, 2007 - 2010), 50 a of Kanmen (1960 - 2001, 2003 - 2010) and 46a of Nanji (1960 - 2001, 2007 - 2010). All the observation data were collected and sorted according to " The Specification for Offshore Observations". The station locations are shown in Tab. 1.

Tab. 1 Latitude and longitude of stations

Station	latitude	longitude
Dachen	28°27′	121°14′
Kanmen	28°05′	121°17′
Nanji	27°28′	121°04′

Because of the long datum length, the site changed, observation instruments replaced, observation specification corrected and et al., there is a probability of discontinuity in observation data. This paper used the U-inspection method [1, 2] to do the homogeneity test of SST data, and then to simply distinguish whether there is notable difference of SST observation data or not.

The statistics value $U=\frac{\bar{Y}-\bar{X}}{S_X/\sqrt{m}}$ was selected. By testing it and it was found that the numerical value of U in every stage were all less than the critical value 1.96(when reliability a=0.05, $U_{0.05}$=1.96). It was shown that there was not essence difference in SST data.

During the process of SST data collected, because of the instruments, some data were lost. In the view of the continuity of SST variation, this paper used the method of cubic spline interpolation to revise those data. This method is not only good in the convergence and stability but also simple and useful, and has an advantage of small amount of calculation. This method is: supposing to choose (n+1) nodes in space [a, b], cubic spline function s(x) exists and m_i is the derivative of s(x) in spot x_i, so in every space $[x_i, x_{i+1}]$ that

$$s(x)=\left(1+2\frac{x-x_i}{x_{i+1}-x_i}\right)\left(\frac{x-x_{i+1}}{x_x-x_{x+1}}\right)^2 y_i$$

$$+\left(1+2\frac{x-x_{i+1}}{x_i-x_{i+1}}\right)\left(\frac{x-x_i}{x_{i+1}-x_i}\right)^2 y_{i+1}$$

$$+(x-x_i)\left(\frac{x-x_{i+1}}{x_i-x_{i+1}}\right)^2 m_i$$

$$+(x-x_{i+1})\left(\frac{x-x_i}{x_{i+1}-x_i}\right)^2 m_{i+1}$$

Calculation conditions are:

$$s(x_i)=y_i, s(x_{i+1})=y_{i+1}, s'(x_i)=m_i, s'(x_{i+1})=m_{i+1}$$

Because the datum series of Kanmen station was longer, they were used to revise the lost data of Dachen and Nanji stations by the SST correlation between Kanmen and 2 stations. Used correlation coefficient is as $r=\frac{\sum_{i=1}^{n}(x_i-\bar{x})(y_i-\bar{y})}{\sqrt{\sum_{i=1}^{n}(x_i-\bar{x})^2}\sqrt{\sum_{i=1}^{n}(y_i-\bar{y})^2}}$, whose value is between -1.0 and +1.0. When r is much closer to +1.0, the positive correlation of two series is much more significant; in turn, when r is much closer to -1.0, the negative correlation of two series is much more significant. The results of r were $R_{N\text{-}K}$=0.89, $R_{D\text{-}K}$=0.95, which shows that correlations between Kanmen and Dachen, Nanji, were both significant. Then we rejected the SST data which were affected by severe weather systems and revised the interpolation values according to the SST D-value of hourly, dayly, monthly and yearly between Kanmen and Dachen, Nanji. At last, the complete SST time series values were derived.

3 The distribution characteristics of SST along the southern coastal region of Zhejiang Province

3.1 Space distribution characteristics of SST

Southern coastal region of Zhejiang is close to the East China Sea, which is the epicontinental sea of Northwest Pacific Ocean. The SST distribution characteristics mainly depend on the influences of solar radiation, warm current, air-sea heat transfer, runoff, precipitation and etc. And also because of the effect of the sea geographic environment, coast morphology and et al., the spatial distribution characteristics of SST along the southern coastal region of Zhejiang are much more complicated.

The annual mean SST distribution of 3 stations mainly showed high in the south and low in the north; SST in Nanji was the maximum, indicating around 19.0 ℃; that in Kanmen was the next, indicating around 18.5 ℃; that in Dachen was the minimum, indicating

around 17.9 ℃. The spatial distribution of SST had the difference not only in the yearly variation but also in seasonal variation. According to the marine season division [3], from January to March, it is winter, from April to June, it is spring, from July to September, it is summer and October to December, it is autumn. The SST annual average of opposite month was used to analyze the space distribution characteristics of SST (Tab. 2).

Tab. 2 Statistics of seasonal and annual average

station	spring	summer	autumn	winter	annual mean
Dachen	18.0	25.9	18.1	9.6	17.9
Kanmen	19.3	27.7	17.3	9.4	18.5
Nanji	19.1	27.1	19.0	10.6	19.0

Winter is the season when SST along the southern coastal region of Zhejiang is the lowest, because solar radiation in winter is the weakest and SST is affectedmainly by the cold air moving from north to south, at the same time by Kuroshio and Taiwan Warm Current [4] also. Different to the variation of annual mean SST in winter, the maximum SST was in Nanji, indicating around 10.6 ℃ and the minimum SST was in Kanmen, indicating around 9.4 ℃.The highest difference of mean SST in winter among 3 stations was 1.2 ℃ and winter was the season which showed the minimum difference of SST between south and north in a year along the southern coastal region of Zhejiang.

Spring is the season shifting from winter to summer. Following the north-east monsoon winds diminishing and the solar radiation reinforcing, SST is rising step by step. Due to the effect of bedrock and hydrodynamic environment, SST rose much faster in Kanmen that the rising rate was 9.9 ℃. SST rose slower in Dachen and Nanji and the rates kept balance basically, respectively indicating around 8.4 ℃ and 8.5 ℃. The maximum mean SST in spring was in Kanmen, indicating around 19.3 ℃ and the minimum was in Dachen, indicating around 18.0 ℃. The highest difference among 3 stations was 1.3 ℃.

Summer is the season when solar radiation is the strongest in a year, which makes a further significant increase in SST. The rising rate in Kanmen was 8.4 ℃ and in Dachen and Nanji, the rates kept balance bacically, respectively indicating around 7.9 ℃ and 8.0 ℃. The spatial distribution was similar with spring, and the maximum was in Kanmen, indicating around 27.7 ℃ and the minimum was in Dachen, indicating around 25.9 ℃. The highest difference of mean SST among 3 stations in summer was 1.8 ℃. Summer was the season that showed the maximum difference of SST between south and north along the southern coastal region of Zhejiang in a year.

Autumn is the season when the distribution characteristics of SST shifts from summer to winter. Some hydrological phenomena in summer basically disappeared [5], at

the same time with the solar radiation dying down and the strengthening effect of cold air, SST presented the falling trend. The maximum falling rate was in Kanmen, indicating around 10.4 ℃ and the minimum was in Dachen, indicating around 7.8 ℃. The spatial distribution characteristics were similar with those in winter, and the maximum of SST was in Nanji, indicating around 19.0 ℃ and the minimum was in Kanmen, indicating around 17.3 ℃. The highest difference among 3 stations was 1.7 ℃.

3.2 Variation characteristics of annual mean SST

The long-term variation of annual mean SST along the southern coastal region of Zhejiang are affected not only by upper-air climate system (such as the area and intensity of WPSH and the East Asia Trough) but by the phenomena of El Nino and La Nina. From the analysis of annual mean SST variation trends in Dachen, Kanmen, and Nanji, it presented upward trend in 50 years as the rate of rise was 0.017 ℃/a in 3 stations (Tab. 3).

Tab. 3 Statistics of annual mean SST variation rate

station	1960 - 2010
Dachen	0.019
Kanmen	0.017
Nanji	0.014

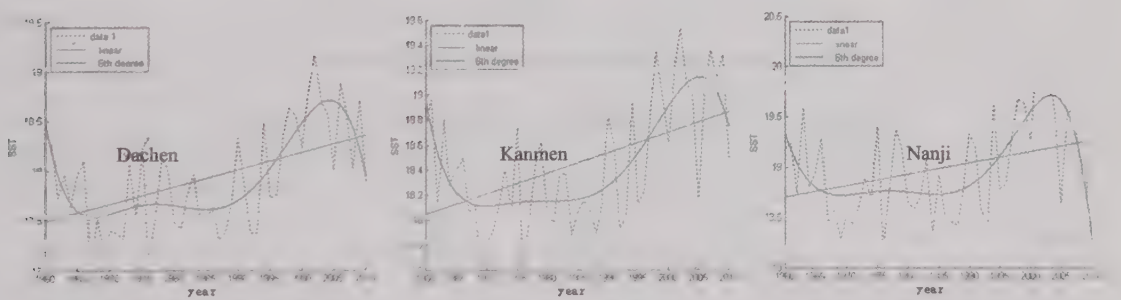

Dachen Kanmen Nanji

Fig. 1 Variation curve of annual mean SST

Besides the significant long-term variation trend, annual mean SST also had the characteristics of phase variation. This paper used six-order polynomial to fit the variation trend as Fig. 1. It showed that variation trends of 3 stations were similar basically; SST had presented downward trend before the late of the mid-1960s and risen slowly from the late of the mid-1960s to the mid-1970s and had begun another falling process from the mid-1970s to the mid-1980s and been rising until to 2005 as the rate of rise was obviously greater than the rising process former. From 2005 to 2010, annual mean SST had presented falling trend.

It was different that the variation trends of Kanmen and Nanji stations from the late of mid-1960s to the mid-1980s were obviously slower than that in Dachen and the curvature of fitted line of the rising event beginning from the mid-1980s in Kanmen was smaller than those in Dachen and Nanji. Because of the SST rising slowly, the following falling trend was postponed a little in Kanmen. Through the understanding of geographic location and using observation instruments in 3 stations, all phenomena above may relate with the difference of observation instruments using time and the marine area openness of launching instruments.

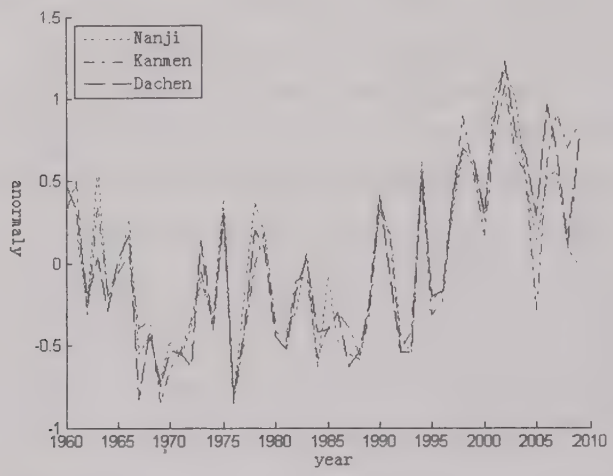

Fig. 2 Anomaly variation curve of annual mean SST

Tab. 4 Anomaly probability statistics of annual mean SST

station	year	normal $\triangle T \leq \lvert \pm 0.2\ ℃ \rvert$	appreciably warm $0.5\ ℃ < \triangle T < 0.2\ ℃$	warmer $\triangle T \geq 0.5\ ℃$	appreciably cold $-0.5\ ℃ < \triangle T < -0.2\ ℃$	colder $\triangle T \leq -0.5\ ℃$
Dachen	1960 - 2010	20%	18%	20%	22%	22%
	1960 - 1989	23%	13%	-	34%	30%
Kanmen	1960 - 2010	20%	12%	22%	32%	16%
	1960 - 1989	27%	10%	3%	40%	20%
Nanji	1960 - 2010	24%	16%	20%	26%	16%
	1960 - 1989	23%	13%	3%	37%	24%

Fig. 2 presents the anomaly variation curve of annual mean SST. It shows that before the late 1980s, variation of SST remained normal ($\triangle T \leq \lvert \pm 0.2\ ℃ \rvert$) or appreciably cold ($-0.5\ ℃ < \triangle T < -0.2\ ℃$) or colder ($\triangle T \leq -0.5\ ℃$). The anomaly probability statistics of annual mean SST is listed in Tab. 4.

Beginning from the late 1980s, the anomaly of SST along the southern coastal region

of Zhejiang had risen gradually and the warmer year (△T≥0.5 ℃) had increased obviously. During 2000 to 2010, the number of warmer year of Nanji, Kanmen and Dachen were 6a, 8a and 7a. By analyzing the correlation of annual mean SST and annual mean air temperature of 3 stations, it was discovered that the variation trends of both above were very similar and had high relevance. The correlation coefficients were 0.77 (Dachen), 0.92 (Kanmen), 0.81 (Nanji) and all pasted the significance test. So normally people usually take it for granted that global warming is the main reason for long sequence SST rising linearly.

3.3 Analysis of annual mean SST variation cycles

To find out the cycle distribution characteristics of SST in detail, this paper used the analytical method of power spectrum [6] to analyze the main cycle of vibration of SST. Firstly, considering that SST contains many time scale variations, then used the 9-order recursive filter was used to do 5 years of filter processing of SST. Secondly, coefficient *R(i)* was calculated considering the truth of power spectrum used 51/3 as maximum leg length m. Thirdly, Hanning coefficient was used to smooth estimated power spectrum values and the continuous spectrum values were derived. At last, the significance test of spectrum estimation was made. Because correlation coefficient *R(1)* was a greater positive value, indicating that the sequence of spectrum estimates was continuity, red noise spectrum was used to do the significance test and the spectrum estimate significance cycles was got by the red noise spectrum limit value under the significance level 0.05(Tab. 5). There were such time scale variation cycles as 15a, 6a, 5a, 4.3a and 3.8a in 3 stations at the same time. Besides this, Dachen and Nanji had the time scale variation as 30a, and Kanmen and Nanji had the variation as 7.5a and Nanji had the variation as 10a.

Tab. 5 Statistics of remarkable cycles

station	cycle							
	30a	15a	10a	7.5a	6a	5a	4.3a	3.8a
Dachen	+	+			+	+	+	+
Kanmen		+		+	+	+	+	+
Nanji	+	+	+	+	+	+	+	+

All of above showed that the periodic variations of 3 stations were similar with the analysis results of SST of the East China Sea by Guo Wei-qi [7], Tang Ming-yi [8], Yan Jun-yue [9] and Ding fei [10], indicating that the periodic variation of SST was related closely with El Nino, South Oscillation and solar activities.

The 30a's periodic variation in Dachen and Nanji was uniformed with the 30a's time scale variation in Nino region by Huang Hai-ren [11]. It might be associated with the weak

effect of land because Dachen and Nanji stations were both located in sea island and much closer to offshore than Kanmen.

The 10a's periodic variation in Nanji and 7.5a in Kanmen and Nanji were similar to the analysis results by Tang Ming-yi [8] that there were 10a - 11a and 6a - 7a periodic variations in the region Kuroshio flowing through. That can be inferred that it might be associated with Kuroshio.

3.4 Distribution characteristic of monthly mean SST of multi-year

The variation trend of SST along the southern coastal region of Zhejiang in a year was near to cosine curve (Fig. 3) for being affected by solar radiation, Taiwan Warm Current, coastal stream of Zhejiang and property differences between ocean and land. It indicated the annual distribution characteristics of a peak and a valley. In summer, monthly mean SST performed Kanmen > Nanji > Dachen and it might be associated with the difference circumstance of underlying surface of every station. In February, monthly mean SST indicated a valley and at that time SST of the southern coastal region of Zhejiang was the lowest in a year and with the change of latitude, it performed high in the south and low in the north. The SST in Nanji was 9.8 ℃ and because station launching was affected by the land climate and the difference of seawater capacity, SST in Kanmen was lower than that in Dachen, indicating around 8.4 ℃. The greatest SST difference among 3 stations was 1.4 ℃. Monthly mean SST began to enter the period of rapid warming from March to August, SST achieved the highest. At this period, the maximum monthly mean SST was in Kanmen, indicating around 28.8 ℃ and the minimum was in Dachen, indicating around 26.7 ℃. The highest difference among 3 stations was 2.1 ℃.

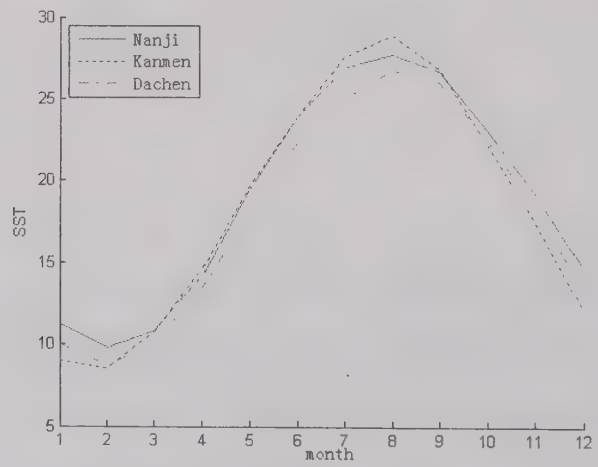

Fig. 3 Curve of monthly mean SST

By doing the harmonic analysis of monthly mean SST of 3 stations, the remarkable annual and semi-annual cycles were derived. Those amplitudes and initial phases were listed in Tab. 6, in which A_1, φ_1 represented the amplitude and phase of annual cycle, and A_2, φ_2 represented the amplitude and phase of semi-annual cycle. In harmonic analysis, amplitude and phase determined size and time. From Tab. 6, we could see that the maximum amplitude of annual cycle A_1 was in Kanmen, and the maximum amplitude of semi-annual cycle A_2 was in Nanji. The variation of SST along the southern coastal region of Zhejiang was determined by the component of annual cycle.

Tab. 6 Statistics of SST major harmonic analysis

station	annual cycle		semi- annual cycle	
	amplitude (A_1)	phase (φ_1)	amplitude (A_1)	phase (φ_1)
Dachen	8.96	241	0.65	262
Kanmen	10.06	233	0.6	182
Nanji	9.04	240	0.7	351

Because the phase determined the appearing time of the extreme value of SST and φ_1 changed from 233° - 241°, we preliminarily judged that the extreme value of SST in a year appeared about mid-Aug (the maximum) and mid-February (the minimum), and the appearing time difference of 3 stations was about 7 days. All these indicated the analysis results were in accordance with the observation data.

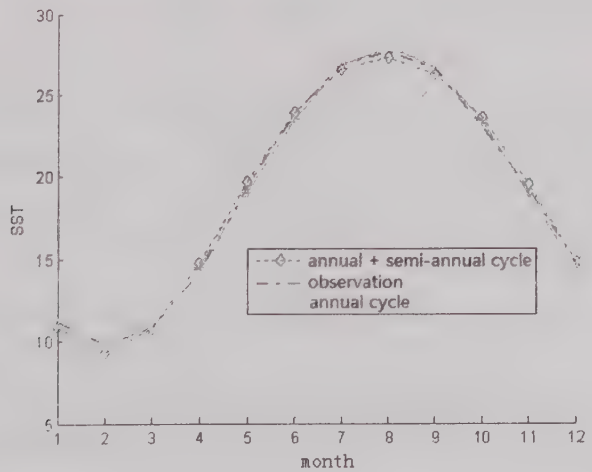

Fig. 4 Harmonic fitting curve of Nanji station

A case study of Nanji, taking the harmonic analysis results of annual cycle, annual and semi-annual cycle to fit with the observation datum, it showed that three lines fitted

well. But because the phase difference between semi-annual and annual cycle was 111° and it weakened the effect of annual cycle amplitude and made the extreme value of fitting line of annual and semi-annual cycle minishing.

4 summary

(a) SST along the southern coastal region of Zhejiang is generally affected by the solar radiation and presents the space distribution characteristics of high in the south and low in the north. And because of the influence of launching geographical conditions, thermal capacity of seawater, different currents and et al., the distribution of SST presents different characteristics.

(b) SST along the southern coastal region of Zhejiang generally presents rising trend and the rising rate is 0.017 ℃/a and the rising rate in the north is greater than that in the south. The variation trends of 3 stations are similar basically that it has presented downward trend before the late of the mid-1960s and risen slowly from the late of the mid-1960s to the mid-1970s and begun the another falling process from the mid-1970s to the mid-1980s and been rising until to 2005 as the rising rate was obviously greater than the rising process former. From 2005 to 2010, annual mean SST had presented falling trend.

(c) Former 30 years, SST basically remained in the colder period and from the north to the south, the percent of cold year was 64%,60% and 61%. From 2000 to 2010 the warmer years rised substantially indicating around 7a,8a and 6a.

(d) The result of power spectrum showed that SST had the time scale variations of 15a, 6a, 5a, 4.3a and 3.8a and it was close related with El Nino, South Oscillation and solar activities. Dachen and Nanji had the time scale variation as 30a, Kanmen and Nanji had the variation as 7.5a and Nanji had the variation as 10a. These may be related with the launching of station and the region which Kuroshio flows through.

(e) The annual variation trend of SST is near to the cosine curve and the variation is mainly determined by the annual cycle. The maximum amplitude of annual cycleis in Kanmen, and the maximum amplitude of semi-annual cycle is in Nanji. The fitting results of annual cycle and semi-annual cycle are better and in Nanji, the semi-annual cycle has the role of minishing the annual cycle.

Acknowledgments

Thanks for the strong guidance to this paper of Sha Wei, the Professor from The East China Sea Branch of State Oceanic Administration.

References

[1] Yu Jian-min. The homogeneity test of the meteorological data series before and after the weather station moved of Cixi City [J]. Zhejiang Meteorological Science and Technology, 1999, 20(1): 54 - 55.

[2] Li Qing-xiang, Lliu Xiao-ning, Zhang Hong-zheng, et al. The homogeneity test of the climate data series of the fixed-point observation [J]. Meteorological Science and Technology, 2003, 30(1): 3 - 22.

[3] Chen Shang-ji, He Wei-huan, Yao Shi-yu, et al. the hydro-climatic seasons division of Chinese offshore marine [J]. Acta Oceanologica Sinica, 1992, 14(6): 1 - 11.

[4] Bao Xian-wen, Wan Xiu-quan, Gao Guo-ping, et al. The characteristics of the seasonal variability of the sea surface temperature field in the Bohai sea, the Huang Sea and the East China Sea from AVHRR data [J]. ACTA Oceanologica Sinica, 2002, 24(5): 125 - 133.

[5] Tang Ming-yi, Liu Yu-zhong, Li Hong-hai, et al. Preliminary analysis of the characteristics and causes of the seasonal variation of the average surface temperature field in the Bohai Sea, Yellow Sea and northern East China Sea [J]. Acta Oceanologica Sinica, 1989, 11(5): 544 - 553.

[6] Wei Feng-ying. Modern climate statistics diagnosis and forecasting techniques [M]. Beijing: Meteorological Press, 2007.

[7] Guo Wei-qi, Sha Wei, Shen Hong-mei, et al. Statistic analysis of sea surface temperature along East China Sea coast [J]. Acta Oceanologica Sinica, 2005, 27(5): 1 - 8.

[8] Tang Ming-yi, Yin Jie, Qu Ru-mei, et al. The annual and inter-annual variation characteristics of the island station surface sea temperature field to the waters of the Kuroshio [J]. Acta Oceanologica Sinica, 1994, 16(3): 12 - 20.

[9] Yan Jun-yue, Li Jiang-long. Change in temperature in East China Sea and adjacent areas for centuries [J]. Acta Oceanologica Sinica, 1997, 19(6): 121 - 126.

[10] Yu Fei, Xu Yi. Long-term trend studies of the East China Sea surface temperature [J]. Advances in Marine Science, 2003, 21(4): 477 - 481.

[11] Huang Hai-ren, Sun Wei-guo, Cheng Bing-yan. The time-frequency structural features of SSTA in Nino Sea [J]. Meteorological Science and Technology, 2005, 33(3): 218 - 226.

浙南沿岸海表面温度分布特征

韩小燕，潘晓东，马林芳

（温州海洋环境监测中心站，浙江 温州 325013）

摘 要：文章根据浙南沿岸3个海洋观测站大陈、坎门、南麂站 51a（1960 ～ 2010年）SST观测资料，进行统计分析，得出SST时空分布特征。结果表明，浙南沿岸的SST总体呈现北低南高的趋势，冬季南北差异最小，夏季南北差异最大；51 a年浙南沿岸SST总体呈现上升趋势，上升速率为0.017 °C/a；SST变化存在3.5 a、5a ～ 6 a、2 a ～ 7 a及11 a左右的振荡周期；SST主要由年循环分量决定，谐波拟合效果良好。

关键词：浙南沿岸；SST；均一性；功率谱；谐波

Screening and identification of an antagonistic bacterium strain LHB02 and the optimization of its fermentation conditions

XU Chang-an[1], TANG Xu[1], HE Jian-lin[1], LIN Ling[1], LIU Yuan-sen[1], FANG Wei-dong[2]

1. *Third Institute of Oceanography, State Oceanic Administration, Xiamen* 361005, *Fujian province, China;*
2. *Fishery Department, Jimei University, Xiamen* 361015, *Fujian province, China;*

Abstract: A strain LHB02 with strong antibacterial activity against some aquatic pathogens was screened from the coastal marine sediment in Fujian province, China. LHB02 was identified as Bacillus subtilis, based on its 16S rRNA sequence, together with the morphological, physiological and biochemical characteristics. The antagonistic activity of strain LHB02 and its optimal fermentation conditions were also investigated. The results showed that LHB02 had strong antagonistic activity against 3 species of vibrios: Vibrio harveyi,Vibrio alginolyticus and Vibrio anguillarum, and the optimum fermentation conditions for the strain LHB02 were as follows: KB culture medium (peptone 20 g, glycerol 10 mL, K_2HPO_4 1.5 g, $MgSO_4.7H_2O$ 1.5 g, H_2O 1 000 mL); temperature, 28 ℃; pH ,7.0; culture time, 36 h; and inoculation amount, 1.5% (v/v).

Keywords: screening; identification; bacillus subtilis; antagonistic activity; optimization

Introduction

Diseases caused by vibrio bacteria are responsible for the mass mortality of cultured fish in the south of China [6]. Antibiotics provides an important measure to fight against those pathogens to some extent. However, it causes a lot of problems, including decreased efficacy, resistance of pathogens to antibiotics, potential adverse health effect on consumer's health of antibiotic residues in aquatic foods, environmental hazards, etc.[10] Therefore, effective alternatives against aquatic pathogens, is needed urgently[11].

Numerous studies have shown that biological control with beneficial microorganisms was an effective method to control aquaculture diseases. Among microorganisms, bacillus species have been used to treat bacterial infections of fish experimentally, and satisfactory results have been obtained in those trials [17, 4,16].

Received on Mar. 4, 2013

Corresponding author: changan_xu@yahoo.com.cn

Bacillus is a gram-positive, aerobic or facultative anaerobic, spore-forming rod shaped bacteria. It is widely distributed in nature. More importantly, it has antagonistic effect on other icroorganisms [8].The aims of this study were to screen and isolate a bacillus strain LHB02 with strong antagonistic activity from the coastal marine sediment, and to optimize its fermentation conditions.

1 Materials and methods

1.1 Soil sample

Soil samples for strain screening were collected in sterile containers from the surface of the coastal mud near Zhangpu aquaculture base, Fujian province, China.

1.2 Medium

LB medium: peptone 10 g, yeast extract 5 g, NaCl 10 g, agar 20 g, H_2O 1000 mL.

KB medium: peptone 20 g, glycerol 10 mL, K_2HPO_4 1.5 g, $MgSO_4.7H_2O$ 1.5 g, H_2O 1 000 mL.

1.3 Test bacterium

Vibrio anguillarum was used as a test microorganism. And this pathogenic bacterium was obtained from the Biological Department of Fujian Normal University, China.

1.4 Bacterial isolation and screening

10 g of soil sample was added to 90 mL sterilized water. Then, a serial dilution of 10^{-2} - 10^{-6} was conducted in each case. For each dilution, 0.1 mL liquid was inoculated onto the LB screening medium and 3 replicates were performed. The plates were incubated at 37 °C for 24 - 48 hours. Colonies with similar morphological appearance to that of *Bacillus* species were picked up as the candidates and were streaked in another screening medium for further purification.

1.5 Antibacterial activity test and determination of target bacteria

The antibacterial activity was conducted using an agar diffusion technique [12]. For each test, three replicates were performed. Each isolated bacterium (candidate) was cultured under aerobic condition in KB medium at 37 °C and 180 rpm for 36 h. After centrifugation, 20 uL of cell free supernatant was added to the hole of agar plate seeded with the test bacterium stated above and the plates were incubated at 37 °C for 36 h. As control, the plates were added with 20 uL KB medium and were incubated at 37 °C for

36 h. The candidates with inhibition zones were regarded as the target bacteria strains. The inhibition zones were recorded and measured.

1.6 Morphologic characteristics and physiological and biochemical tests

The target strain was inoculated in LB solid medium (at 37 °C) and KB 1iquid medium (at 37 °C and 180 rpm) for 36 h, respectively. The morphologic characteristics were observed and recorded. Besides, some physiological and biochemical experiments were conducted on the strain according to Dong, et al.[2], including gram staining, catalase, starch hydrolysis, voges proskauer (vp), citrate utilizations tests and so on.

1.7 Sequence analysis of 16S rDNA gene

Bacteria1 cells of exponential growth phase were harvested by centrifugation at 10 000 rpm for 10 mins and washed with sterile water. The genome DNA of the strain was extracted using the method introduced by Ren et al. [9] and the 16S rDNA fragment was amplified by PCR using a pair of universa1 16S rDNA primers (A: 5, -AGA GTT TGA TCC TGG CTC AG3, and B: 5, -ACG GCT ACC TTG TTA CGA CTT-3). PCR products were purified with a Ge1 Extraction Kit and sent to Sangon biotech. (Shanghai, China) Co., Ltd. for sequencing.

The 16 S rDNA sequence was submitted to the database of GenBank, BLAST algorithm was used to search for homologous sequences in the GenBank. Multiple alignment of the 16S rDNA sequences were carried out using the ClustalX program [14] and the phylogenetic tree was constructed by the MEGA3 software [7].

1.8 The antagonistic activity of target bacterium against aquatic pathogens

7 aquatic pathogens including *Vibrio alginolyticus*, *Aeromonas hydrophila*, *Aeromonas. Sobria, Pseudomonas fluorescens*, *Vibrio Parahaemolyticus*, *Vibrio harveyi* and *Vibrio anguillarum* were selected as test microorganisms, which were obtained from the Biological Department of Fujian Normal University, China. The antagonistic tests of target strain against microorganisms were performed by the method of agar diffusion technique as described above for 3 times. The inhibitory zone was observed and recorded, respectively.

1.9 Optimization of fermentation conditions

The fermentation experiment of target strain was carried out in 250 mL bottles under different conditions including: different mediums, temperature, pH, culture time and inoculation amount. The antagonistic activity test of the cell free supernatant against the pathogen (here the *Vibrio anguillarum* was selected as the test pathogen) in each condition

was conducted. All experiments were performed in triplicate, and the conditions were optimized, based on antagonistic activity.

Different conditions selection:

medium:

KB medium: peptone 20 g, glycerol 10 mL, K_2HPO_4 1.5 g, $MgSO_4.7H_2O$ 1.5 g, H_2O 1 000 mL

LB medium: peptone 10 g, yeast extract 5 g, NaCl 10 g, H_2O 1 000 mL

PPM medium: peptone 20 g, glucose 18 g, KNO_3 5 g, NaCl 1 g, H_2O 1 000 mL

YPG medium: peptone 5 g, glucose 5 g, yeast extract 5 g, H_2O 1 000 mL

NA medium: peptone 5 g, beef extract 1 g, yeast extract 2 g, NaCl 5 g, H_2O 1 000 mL

NYBD medium: glucose 10 g, beef extract 8 g, yeast extract 5 g, H_2O 1 000 mL

CM medium: peptone 10 g, beef extract 3 g, H_2O 1 000 mL

Temperature(°C): 20, 24, 28, 32, 37

pH value: 3.0, 4.0, 5.0, 6.0, 7.0, 8.0, 9.0

culture time (h): 12, 18, 24, 30, 36, 42, 48, 54, 60, 66, 72

inoculation amount: 0.5%, 1.0%, 1.5%, 2.0%, 2.5%, 3.0%, 3.5%, 4.0%, 4.5%, 5.0%

2 Results and analysis

2.1 Strain isolation and screening

There were 7 target bacteria with antagonistic activity harvested from the isolation process, namely, LHB01, LHB02, LHB03……and LHB07. The results of their antagonistic activity test were listed in Tab. 1. Among those target bacteria, LHB02 showed the highest antagonistic activity, so LHB02 was selected for further study.

Tab. 1 Antagonistic activity of target strains against selected aquatic pathogen

Strain	Inhibitory zone/mm
LHB01	13.60 ± 1.14
LHB02	26.75 ± 1.59
LHB03	12.13 ± 1.41
LHB04	19.23 ± 0.3
LHB05	13.22 ± 1.42
LHB06	20.53 ± 1.6
LHB07	15.67 ± 1.55

2.2 Identification of the strain LHB02

The strain LHB02 was aerobic and grew quickly in KB medium. The cell observed under microscope was rod-shaped, gram-positive. Besides, the colony on solid medium was round and convex, pale yellow in color. The physiological-biochemical characteristics of the strain LHB02 were listed in Tab. 2. The strain could hydrolyze starch, gelatin and utilized D-glucose, D-Arabinose, D-Xylose, D-Mannose, propionate and citrate. All these showed the strain was closed to *Bacillus subtilis*. In addition, the phylogenetic analysis based on the partial 16S rDNA sequence data indicated that LHB02 was closely related to the genus *Bacillus* (Fig. 1) and was most closely related to *Bacillus subtilis* strain BL02 with the sequences accession No. EF488974.

Based upon the results of morphologic characteristics, physiological and biochemica1 characteristics and 16S rDNA sequence analysis, the strain LHB02 was identified as *Bacillus subtilis*.

2.3 The antagonistic activity of LHB02 against aquatic pathogens

The results of antagonistic test were shown in Tab. 3. It indicated that except for *Pseudomonas fluorescens*, LHB02 had inhibitory effect on the growth of the other 6 aquatic pathogens. Specially, it presented a strong antagonistic activity against three kinds of vibrios: *V. harveyi*, *V. alginolyticus* and *V. anguillarum* especially.

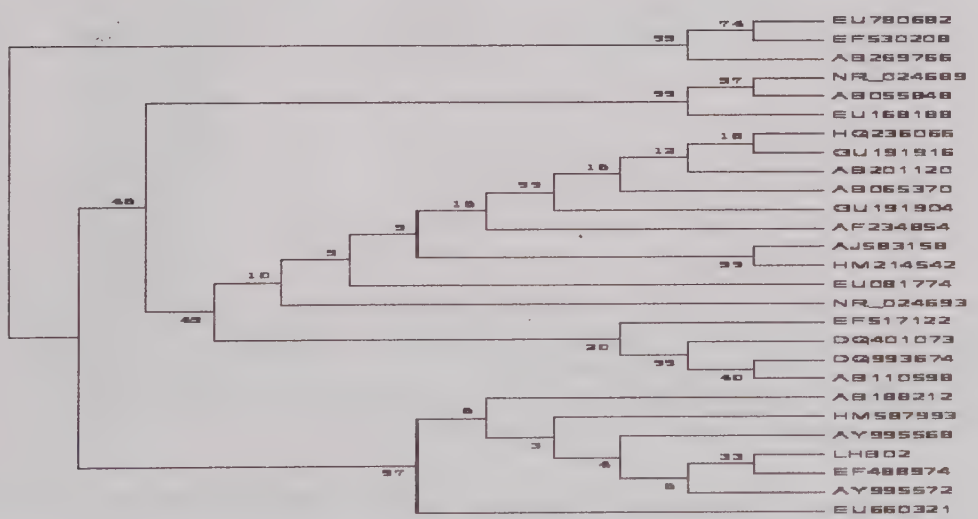

Fig. 1 Phylogenetic tree based on 16S rDNA sequence

Tab. 2 Physiological-biochemical characteristics of the strain LHB02 and *B. subtilis*

Characteristic	Strain LHB02	Ref. *Bacillus subtilis*
Carbohydrate utilization		
D-glucose	+	+
L- arabinose	+	+
D-Xylose	+	+
D- Mannose	+	+
Hydrolysis of		
Starch	+	+
Gelatin	+	+
Reaction with		
PheDH	+	+
Peroxidase	+	+
Catalase	+	+
V- P	+	+
Indole	-	-
Methyl red	+	+
Utilization of		
Propionate	-	-
Citrate	+	+
Growth in NaCl (w/v)		
0%	-	+
2%	+	ND
3%	+	ND
5%	+	+
7%	-	+

Tab. 3 Inhibitory effect of strain LHB02 to selected aquatic pathogens

Pathogen	Diameter of inhibitory zone / mm
Vibrio alginolyticus	24.525±1.21
Aeromonas hydrophila	17.375±0.59
Aeromonas sobria	12.53±0.61
Pseudomonas fluorescens	10.64±0.5
Vibrio parahaemolyticus	16.312±1.12
Vibrio harveyi	22.73±0.6
Vibrio anguillarum	25.57±0.5

2.4 Optimization for fermentation conditions

2.4.1 Effect of medium

Seven kinds of mediums were chosen to investigate the effect of nutrient sources on antagonistic activity. The cultivations were performed at an initial pH of 7, 37 °C and 200 rpm for 36 h with 2%(v/v) inoculation amount in each medium. The results were shown in Fig. 2, indicating that KB medium gave the highest antagonistic activity.

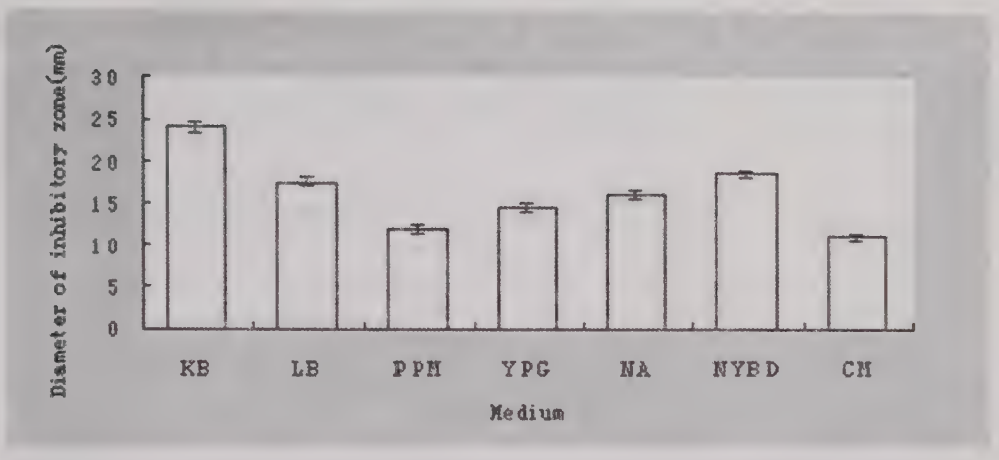

Fig. 2 Effect of medium on antagonistic activity

2.4.2 Effect of fermentation temperature

The cultivations were performed at an initial pH of 7.0 and 200 rpm for 36 h with 2% (v/v) inoculation amount in KB medium at different temperature. The effects of fermentation temperature on antagonistic activity were shown in Fig. 3. It indicated that the antagonistic activity of the cell free supernatant increased when temperature rose from 20 °C and reached its highest point at 28 °C. After that, the antagonistic activity decreased gradually. Therefore, the optimum temperature was 28 °C.

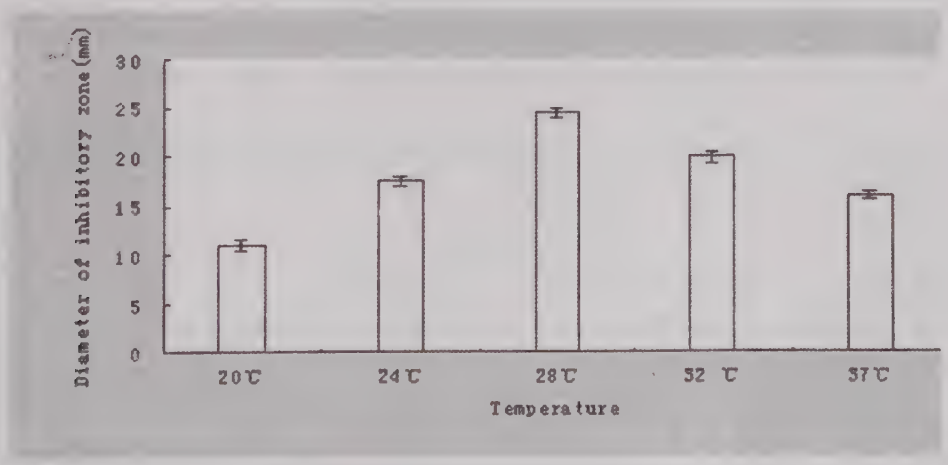

Fig. 3 Effect of fermentation temperature on antagonistic activity

2.4.3 Effect of pH value

The cultivations were performed with 2% (v/v) inoculation amount in KB medium,

28 °C and 200 rpm for 36 h at different initial pH value. The effects of pH values on antagonistic activity were shown in Fig. 4. It indicated that there was no antagonistic activity in the cell free supernatant when pH value was lower than 3.0, and the optimum pH value was 7.0 at which the antagonistic activity of the supernatant reached its highest point.

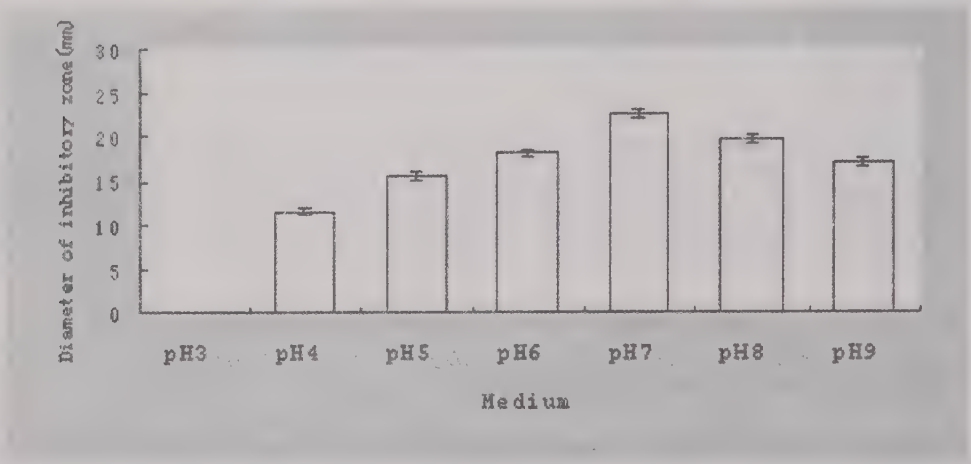

Fig. 4 Effect of pH value on antagonistic activity

2.4.4 Effect of culture time

The cultivations were performed at an initial pH of 7.0, 28 °C and 200 rpm with 2% (v/v) inoculation amount in KB medium for different culture time. The antagonistic activity increased when the culture time extended. As is shown, the optimal culture time was 36 h (Fig. 5), since after this period, the antagonistic activity decreased gradually.

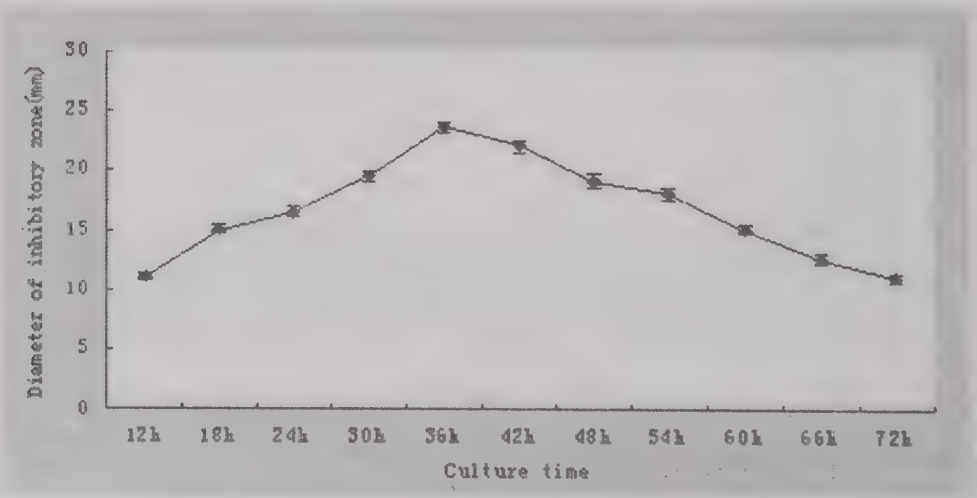

Fig. 5 Effect of culture time on antagonistic activity

2.4.5 Effect of inoculation amount

The cultivations were performed at an initial pH of 7.0, 28 °C and 200 rpm for 36 h in KB medium with different inoculation amount. The results of antagonistic activity test were shown in Fig. 6. It indicated that the inoculation amount of 1.5% (v/v) was optimal for antagonistic substance production.

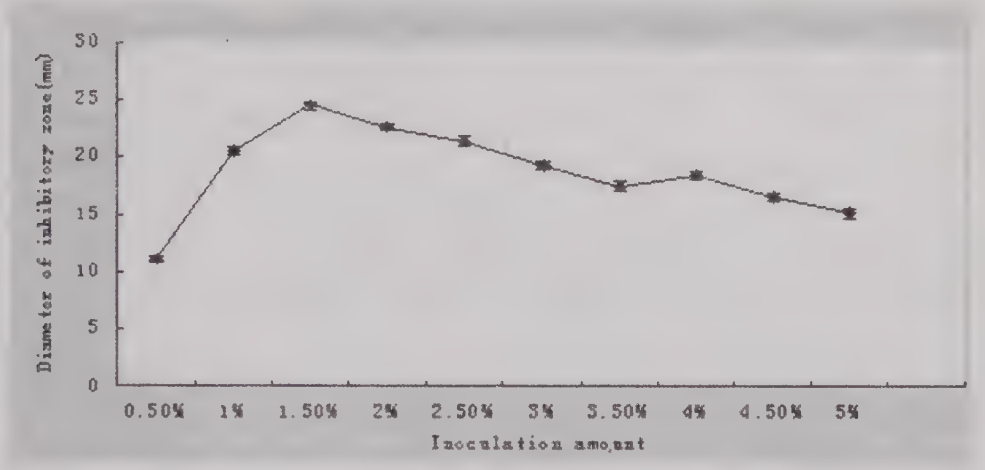

Fig. 6 Effect of inoculation amount on antagonistic activity

3 Discussion

Generally, *Bacillus* species are widely distributed in nature and most previous study of *Bacillus sp.* screening focused on the land area as screening source [4]. In particular, the diversity of marine environment, including high salinity, high hydraulic pressure, low temperature, darkness, et al., endows *bacillus sp.* with more unique characteristics, including antagonistic activity [15]. In this study, we screened a strain LHB02 from marine sediment and it was identified as *Bacillus subtilus*, based on the 16S rDNA sequence and its morphological, physiological and biochemical characteristics. Furthermore, the antagonistic activity of the strain was investigated, showing that the strain had strong antagonistic activity against 3 kinds of vibrios: *Vibrio harveyi*, *Vibrio alginolyticus* and *Vibrio anguillarum*.

At present, about 30 kinds of vibrios have been identified and more than half of them are pathogenic to farmed fish, shell fish and shrimp [1]. Among those, *Vibrio harveyi* and *Vibrio alginolyticus* are the top 2 pathogenic vibrios, causing heavy mortality in yellow

croaker(*Pseudosciaena crocea*)[5], an important commercial fish farmed in net cage in the south of China. Thus, it's urgent to search for the methods to prevent or control the diseases caused by the vibrios. Importantly, it was showed that LHB02 had strong ability to inhibit the growth of these two vibrio pathogens in laboratory experiment, revealing the prospect of LHB02 being used as highly effective biocontrol bacterium in the prevention and control of vibrio pathogen disease in farmed fish. However, it has to be noted that this potential needs to be further examined in field conditions.

Bacillus subtilus can produce several kinds of antibacterial substances during fermentation [13] including protein, peptide, polysaccharose, aliphatic acid, et al. Those antibacterial substances can be intracellular or secretive, and the yield of those depends on the conditions of fermentation. In this study, we have optimized fermentation conditions under which the strain LHB02 showed its strongest antagonism effect. Fortunately, the antibacterial substance produced by LHB02 in this study is secretive, and it's convenient to collect and purify the antibacterial substance from the fermentation broth. So, in further study, we will conduct some research work on the purification and identification of this antibacterial substance, as well as the mechanism of LHB02'S antagonistic activity against pathogens so as to support the application of LHB02 in the prevention and control of farmed fish diseases.

Acknowledgements

This work was supported by the Scientific Research Foundation of Xiamen Marine Research and Development Institute (No. K10102 (1)).

References

[1] Austin B, Austin D A. Bacterial fish pathogens: Disease in farmed and wild fish. [M]. 2nd ed. Chichester, UK: Ellis Horwood Ltd., 1993, 265 - 314.

[2] Dong X Z, Cai M Y. Manual of common determinative bacteriology. Beijing: Science Press, 2001.

[3] Huang J H, Li J, Liu L, et al. Screening, Identification and Antibiotic Effect of a Strain of Bacillus [J]. J. Anhui Agri. Sci., 2008, 36(6): 2 321 - 2 326.

[4] Huang X, Xu L L, Huang R S, et al. Research Advance in Controlling Plant Diseases By *Bacillus subtilis*. Biotechnol. BuLletin, 2010, 1: 24 - 29.

[5] Hong J N, Mao Y, Su Y Q, et al. Effects of *Vibrio harveyi* and *V. anguillarum* on Enzymes Activities in Different Organs of Large Yellow Croaker(*Pseudosciaena crocea)* [J]. J. Xiamen Uni., 2009, 48(3): 418 - 422.

[6] Jin S, Wang G L, Zhao Q S, et al. Epidemiology of Vibriosis in Large Yellow Croaker *Pseudosciaena*

crocea in Marine Cage Culture [J]. Fish. Sci., 2005, 24(1): 17 - 19.

[7] Kumar S, Tamura K, Nei M. Mega3: integrated software for Molecular evolutionary genetics analysis and sequence alignment [J]. Brief. Bioinform., 2004, 5(2): 150 - 163.

[8] Kuta F A. Antifungal effects of Calotropis Procera stem bank extract against Trichoplyton gypseun and Epiderinoplyton Flocosum [J]. AFR. J. Biotechnol., 2008, 7(13): 2 116 - 2 118.

[9] Ren S Y, Wang Z F, Xiao T, et al. Isolation and Identification of a Marine Polyphosphate-accumuLating Bacterium YSR-3 [J]. Oceanologia et Limnologia Sinica, 2006, 5: 55 - 61.

[10] Sambasivam S, Chandran R, Khan S A. Role of probiotics on the environment of shrimp pond [J]. J. Environ. Biol., 2003, 24(1): 103 - I06.

[11] Song J H. What's new on the antimicrobial horizon? [J]. Int. J. Antimicrob. Agents., 2008, 32(Suppl4): S207 - S213.

[12] Tagg J R, McGiven A R. Assay systems for bacteriocins [J]. Appl. Microbio., 1971: I21 - 125.

[13] Tamehiro N, Okamoto Y, Okamoto S. Bacilysocin, a novel phospholipid antibiotic produced by Bacillus subtilis168 [J]. Antimicrob. Agent. Chemother., 2002, 46(2): 315 - 320.

[14] Thompson J D, Gibson TJ, Plewniak F, et al. The ClustalX windows interface: flexible strategies for muLtiple sequence alignment aided by quality analysis tools [J]. Nucleic. Acids. Res., 1997, 25(24): 4 876 - 4882.

[15] Wang X M, Hu J C, Wang S J. Identification of the Protease-Producing Strain B1394 and Characterization of the Protease [J]. J. Jilin Agr. Uni., 2009, 31(2): 143 - 147.

[16] Xu C A, Luo X Z, Zhang Y P.; Lu, Y, et al. Study on the Isolation of a Marine Bacillus B09 and the Optimization of its fermentation Conditions. Mar Sci B. 2009, 28(5):74 - 78.

[17] Zheng G. Isolation partial purification and characterization of a baeteriocin produced by a newly isolated Bacillus subtilis strain [J]. Lett. Appl. Microbiol., 1999, 28(5): 363 - 367.

一株生防细菌LHB02的筛选、鉴定及其发酵条件优化

徐长安[1]，唐 旭[1]，何建林[1]，林 凌[1]，刘源森[1]，方卫东[2]

（1. 国家海洋局第三海洋研究所，福建 厦门 361005；2. 集美大学水产学院，福建 厦门 361015）

摘 要：从中国福建沿海某一污染滩涂的沉积物中筛选到一株具有较强拮抗水产病原菌的生防细菌LHB02。采用通用引物，对LHB02的16S rRNA片段进行扩增，获得1511 bp的DNA系列，基于该DNA系列，结合细菌形态学、生理生化特征，鉴定LHB02为一株枯草芽孢杆菌。对LHB02进行了抗菌试验、抗菌谱检测和发酵条件优化研究，结果表明，LHB02对哈维氏弧菌、溶藻弧菌、鳗弧菌等有很强的拮抗作用，其优化后的发酵条件为：KB培养基（蛋白胨20 g，丙三醇10 mL，K_2HPO_4 1.5 g，$MgSO_4.7H_2O$ 1.5 g，H_2O 1 000 mL）；温度28 °C，pH值7.0，培养时间36 h，接种量1.5%。

关键词：筛选；鉴定；枯草芽孢杆菌；抗菌活性；优化

Growth and maturity of *Chiromantes dehaani* in the Dazhi River estuary

HAN Sha[1], GUAN Wei-bing [2]

1. *Sea Aquiculture Research Institution of Shandong Province, Qingdao* 266300, *Shandong province, China;*

2. *College of Marine Sciences, Shanghai Ocean University, Shanghai* 201306, *China*

Abstract: *Chiromantes dehaani,* as one of the dominant species in intertidal regions of the Yangtze estuary, plays an important role in the ecosystem. To study allometry and maturity in different phases, morphological data had been collected from October in 2009 to September in 2010. Morphologic data such as carapace, cheliped and abdomen were processed by cluster and piecewise linear regression analyses. Discriminat function and logistic curves were built to determine different phases and sizes at 50% maturity, respectively. The results showed that the cheliped width in males and abdomen width in females both presented obvious allometry. The sizes of 50% morphometric maturity occurred at 16.36 mm and 18.22 mm carapace width in males and females, respectively. The life history of males could be divided into three phases while that of females only had two phases according to different growth rates. A significant change in allometry of juvenile males with a break point was detected at 11.78 mm carapace width; carapace width of juvenile and adult females overlapped in a range of 13.04 - 18.64 mm. The crabs attained 50% physiological maturity at the size of 17.50 mm and 17.20 mm for females and males, respectively. For male, the size of morphological maturity was larger than that of physiological maturity, which was opposite to that of female.

Keywords: *Chiromantes dehaani*; cheliped; abdomen; allometric growth; morphological maturity; physiological maturity

Introduction

The mudflat crab *Chiromantes dehaan*, Grapsoidea, Sesarminae, is one of the most abundant zoobenthos in the intertidal and/or supratidal zone of the Yangtze estuary [1], with characters of large quantity, wide distribution and strong reproduction. Moreover, it plays an ecological role in nutrition circulation and energy flow in the process of feeding,

Received on Jan. 21, 2013

Corresponding author: shahan_2012@163.com

burrowing, inhabiting and moving, commonly known as ecological engineer [2]. However, compared with local economic species, for example, Chinese mitten crab *Eriocheir sinensis*, *C. dehaan* is paid little attention and correspondingly few publications have been reported. Study on the basic biology of the crab inland has merely involved molecular phylogenetics, population genetics [3, 4], and larval development [5, 6], and population biology is poorly understood. While for Sesarminae, study on other species abroad has been in relation to the morphology of larval development [7, 8], population dynamic [9] and gonad annual development [10], and little information for morphological maturity is directly examined in the population dynamic study [11-13].

Sexual maturity is an important aspect of population dynamic research for species [9], and the size of maturity is also a key parameter in the whole crustacean life history [14]. The purpose of this work was to determine the allometric growth phases of *C. dehaan* using the linear regression analysis, cluster analysis and discriminant analysis. At last, the size of 50% maturity was obtained through logistic regression. This study was thought to provide useful information concerning the foundational biology and life history strategy of this crab; most importantly, it also benefited for evaluation, government, protection and reasonable exploitation to the natural population resources in the Yangtze estuary.

1 Materials and methods

1.1 Samplings and variable measure

The crabs were caught monthly from the Dazhi River of Pudong in shanghai from October 2009 to September 2010, which was carried out by two people over 30 mins periods each time(N=399 males and 361 females). The following variables were measured accurately to the extent of 0.1 mm using a digital caliper: carapace width (CW), carapace length (CL), cheliped length (CHL), cheliped width (CHW), cheliped height (CHH), second pereiopod merus length (2PML), abdominal width (AW), abdominal length (AL).(Fig. 1)

1.2 Statistical analysis

1.2.1 Sexual dimorphism analysis

For males, taking the CW as a reference variable, the allometric relationship was established by a simple linear regression between different morphometric variables (CHL, CHW, CHH, 2PML, and CW for males) and different morphometric ratio variables(AW/CW, AW/CL, AW/AL for females), which aimed to remove the effect of body measurement on the abdomen variables. Analysis of covariance was performed to determine whether the slope and intercepts differed within each allometric relationship. Hierarchical cluster

analysis was made for all the variables to verify the indication variables which best exemplified the species sexual dimorphism for males [15].

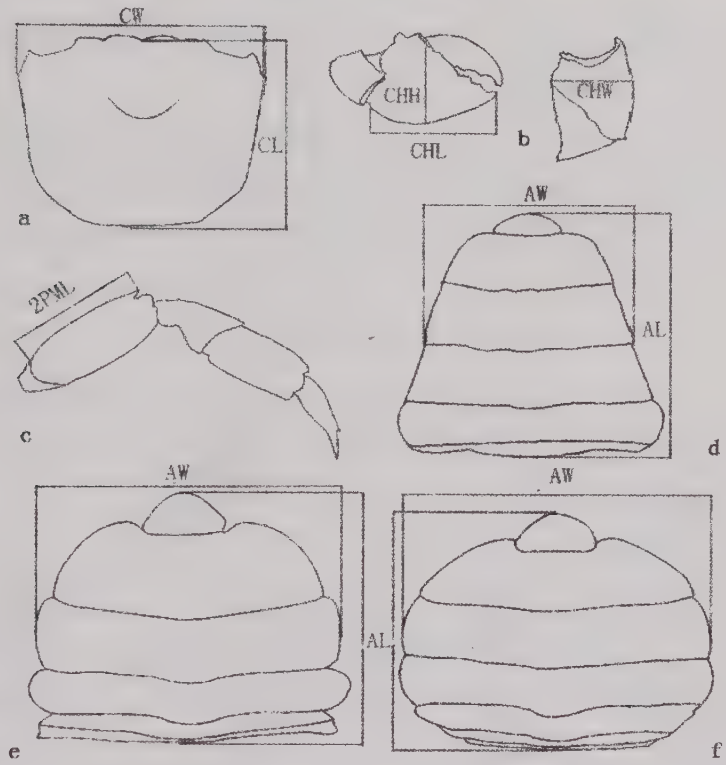

Fig. 1 Position of basic morphometric data of *Chiromantes dehaan*

carapace width(CW), carapace length(CL), cheliped lengh(CHL), cheliped width(CHW), cheliped height(CHH), second pereiopod merus length(2PML), abdominal width(AW), abdominal length(AL)

(Note: d, male's abdomen; e, immature female's abdomen; f, mature female's abdomen)

1.2.2 Determination of growth phase

A non-hierarchical classification procedure (K-means) was carried out on the log-transformed morphometric variables for males to divide into two groups (corresponding to juveniles and adults). The Akaike Information Criterion was calculated to define the rationality of the model as AIC=nlog (SSE/n) + 2k (SSE is the sum of squared deviations, and k is the number of parameters plus 1).The smallest value for AIC was accepted as the closest representation of the allometric relationship [16].

The morphological change in female abdomen took place at the terminal molt, and juvenile grew into adult along with the flat abdomen into domed abdomen [17], which provided the direct identification between morphological maturity and immaturity.

The allometric equation was as $Y=aX^b$, and linear version was as follows:

$$\log_{10}Y=\log_{10}a+b*\log_{10}X$$

where b>1 represented positive allometric; b=1 represented Isometric and b<1 represented negative allometric.

In order to analyze if there were allometric changes in the immaturity, two allometric equations were fitted for each phase using linear regression. The two phases were compared by means of F-statistic and the break point of the two equations [14] was calculated.

$$F= [(SSR_1-SSR_2)/2]/[(SSR_2/(N-P))]$$

where SSR1 and SSR2 were the sum of the squared residuals of the two phase models respectively, N was the number of the individuals, and P was the number of parameters (4 in this case)

1.2.3 Establish discriminant function

In order to specify a crab as a juvenile or an adult, a discriminant analysis was conducted to obtain a discriminating function based on the group by classification analysis. The discriminate equation was $Y=a\log_{10}CW+b\log_{10}X+c$, where Y>0 was maturity and Y<0 was immaturity [14].

1.2.4 Estimation of the size at 50% maturity (CL50)

The relationship between carapace width (CW) and the probability of maturity were analyzed by logistic regression, for estimating the size at 50% maturity [18]. The logistic regression equation was as follows: P=1/1+exp (-a*(CW-b), where b was the 50% maturity point. According to the status of the vasa deferentia of males and the ovary of females by means of histological observation to analyze gonad maturity stage, the 50% size of gonad maturity was determined for both sexes, and this method was exactly the same as the determination of mophometric size.

All the morphometric data were analyzed by SPSS, and a statistic significance of 5% was adopted in all cases. The figure was drawn by Simplot.

2 Results

2.1 Sexual dimorphism variable analysis for males

First, given the morphological changes between the left and right cheliped, the result

from comparing the morphometric data of both cheliped was not statistically significant (P>0.05), so we took the morphometric data of the right cheliped for the analysis. Taking the CW as a reference variable, simple linear regression was carried out for the variables CHL, CHW, CHH and 2PML against CW. There were remarkable differences in variables CHL, CHW and CHH between sexes(COANCOVA, P<0.001) except variable 2PML (COANCOVA, P>0.05). The hierarchical classification analysis for the male variables CHL, CHW, CHH and 2PML revealed clear dissimilarity between the 2PML and the rest variables. In general, the variables CHW and CHL were in the first group, then variables CHW and CHH were in the second group, finally the third one was the independent 2PML group (Fig. 3). Therefore, the CHW promoted an evident allometric growth indication of sexual dimorphism in males.

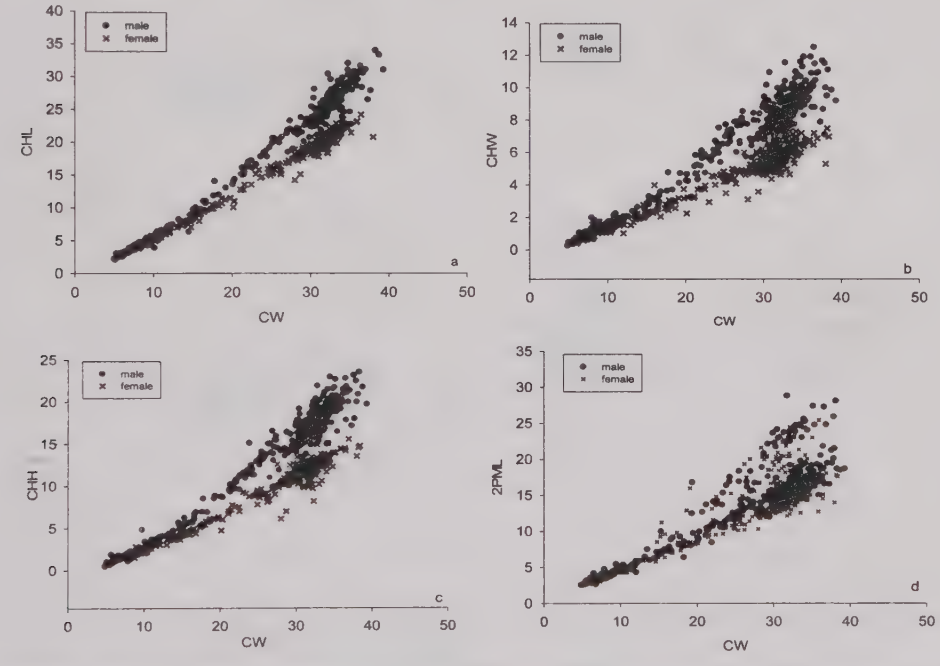

Fig. 2 Relationship between carapace width and cheliped or pereiopod size by the sex of *C. dehaan*

a. relationship between cheliped length and carapace width; b. relationship between cheliped width and carapace width; c. relationship between cheliped height and carapace width; d. relationship between second pereiopod merus length and carapace width

2.2 Sexual dimorphism variable analysis for females

Taking the CW as the independent variable, scatter plots were made of the ratio variables AW/CW, AW/CL and AW/AL against CW for both sexes to determine the correlation between the variables (fig 4). The results showed the variables AW/CW, AW/CL and AW/AL had no allometric growth against the variety of variable CW but kept flat for

males(P>0.05), while for females, the variables AW/CW, AW/CL and AW/AL appeared significant allometric growth increasing in size (P<0.001). We made a conclusion that the variable AW was more fit than AL for allometric growth indication of sexual dimorphism in females.

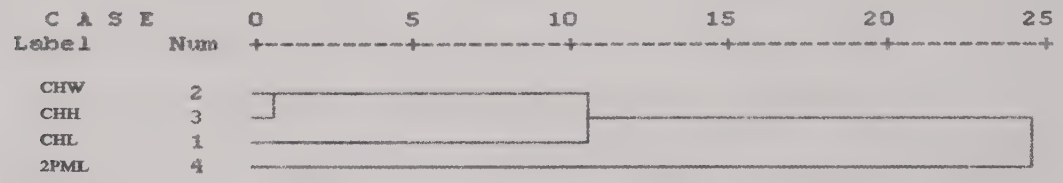

Fig. 3 Dendrogram using hierarchical classification analysis of variables in males of *C. dehaan*

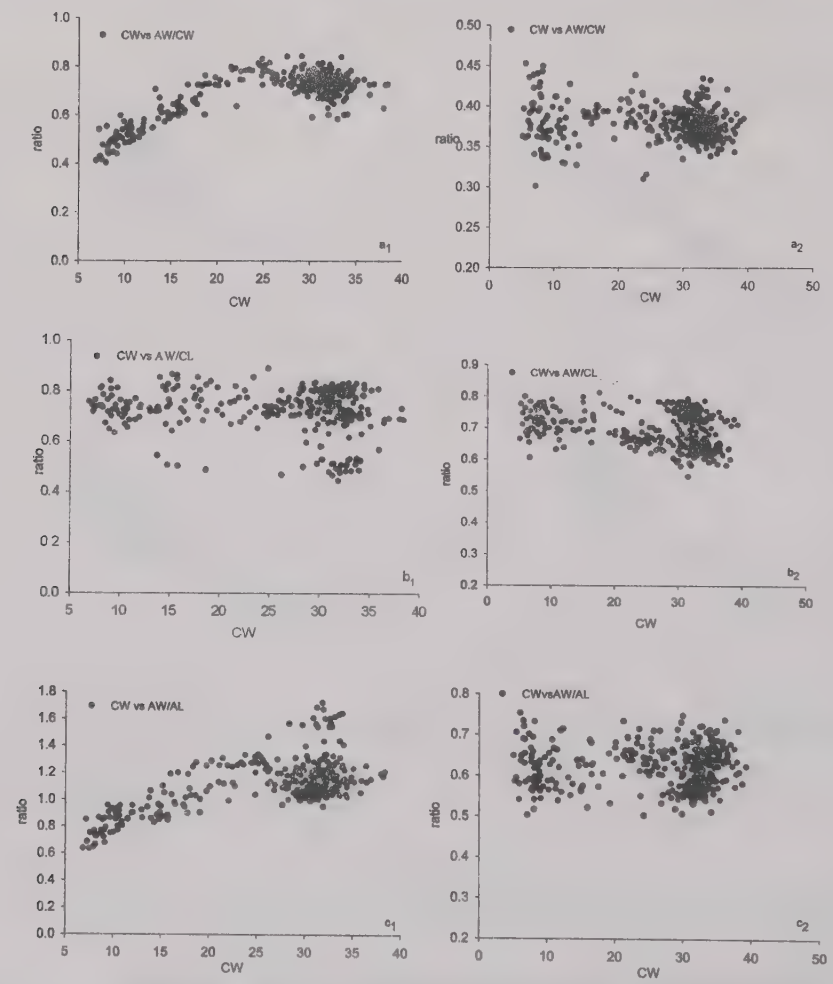

Fig. 4 Relationship between the abdominal width vs abdominal length, abdominal length vs carapace length and abdominal width vs carapace width and carapace by the sex of *C. dehaan*

Note: ($a_1b_1c_1$: female; $a_2b_2c_2$: male)

2.3 Morphological maturity and allometric growth of cheliped for males

Crabs were classified into two groups using K-means classification analysis with the log-transformed morphometric variables CHW and CW data. According to the classification, the immaturity group ranged from 6.89 to 16.38 mm CW; the other maturity group crabs ranged from 15.31 to 39.33 mm CW (Fig. 5).The values of AIC were calculated through an information-theoretic approach for each model, where AIC was the smallest value determined for the set of the candidate model, 1-stage growth model (-2096.86) and 2-stage growth model (-2137.07). There was extreme support for 2-stage growth model that assumed that morphological changes could be described. The growth of immature and mature phase both showed positive allometric, whose rate was 1.944 and 1.197 respectively. The degree of the allometry was different, stronger in the immature phase than the mature phase. The parameters of the allometric equation for each growth phase were as follows (Tab.1).

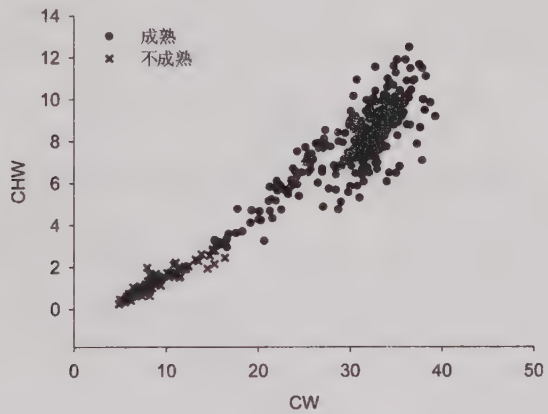

Fig. 5 Relationship between the right cheliped width and carapace width for males of *C. dehaan*

Tab. 1 Allometric equations for each category of males of *C. dehaan*

Phase	$\log_{10}CHW=\log_{10}a+b*\log_{10}CW$	CW/mm	R^2	number
Immature	$\log_{10}$ CHW = -1.745+1.944*$\log_{10}$CW	6.89 - 16.38	0.835	148
Mature	$\log_{10}$ CHW =-0.833+1.197*$\log_{10}$CW	15.31 - 39.33	0.635	251

Based on the group that was classified by k-means method, discriminant analysis was carried out on the variables CW and CHW, which allowed for correct classification of 100% (100% of immature, 99% of mature). With respect to the character of CW and CHW,

the discriminant function was established to estimate the probability of mature corresponding to Y>0 or Y<0 (Y>0 for mature, Y<0 for immature). The discriminant function was as follows:

$$Y=51.909\log_{10}CW+7.481\log_{10}ChW-66.255 \text{ (Y>0 for mature, Y<0 for immature)}$$

In order to analyze whether allometric changes were existing in the immature phase or not, two equations were obtained by using a piecewise linear regression, with the break point occurred at 11.78 mm CW (Fig. 6). Two-stage growth model was more fit than single-stage growth model in the immature phase (F=102.94, P<0.001).We defined the first stage as juvenile phase, and the second stage as adolescent phase. The adolescents had CHW relative to CW with a lower allometric growth level than the juveniles (the value of b was smaller) (Tab. 2).

Immature and mature crabs were both present with CW range in size from 15.31 - 16.38 mm, and the proportion of morphological mature individuals (15.31 - 16.38 mm CW) in each 1 mm size class was calculated. Size at 50% morphological mature of the males was estimated by means of logistic regression at 16.36 mm, and the individuals were absolutely mature when CW>16.38 mm. The logistic regression function was as follows:

$$P=1/1+\exp(-2.625*(CW-16.36))$$

and the crab attained physiological mature at 17.20 mm CW for males (n=111).

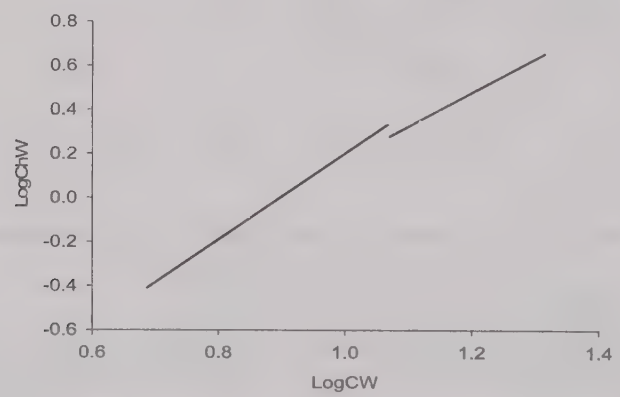

Fig. 6 Relationship between cheliped width and carapace width in logarithmic scale for males of *C. dehaan*

Tab. 2 Allometric equations for each category of immature males of *C. dehaan*

Phase	$\log_{10}CHW=\log_{10}a+b*\log_{10}CW$	CW/mm	number
Juvenile	$\log_{10}CHW=1.327+1.599*\log_{10}CW$	4.87 - 11.78	76
Adolescent	$\log_{10}CHW=1.29+1.458*\log_{10}CW$	11.78 - 16.38	72

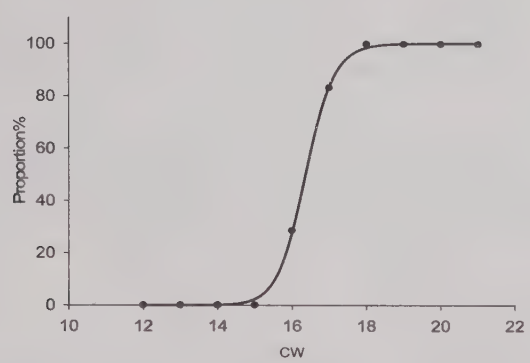

Fig. 7 Estimated sizes at 50% morphological maturity for males *C. dehaan*

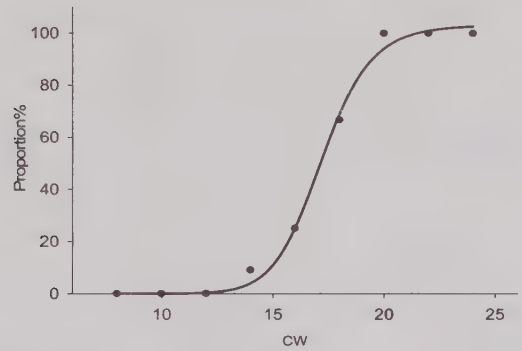

Fig. 8 Estimated sizes at 50% physiological maturity for males *C. dehaan*

2.4 Morphological mature and allometric growth of abdomen for females

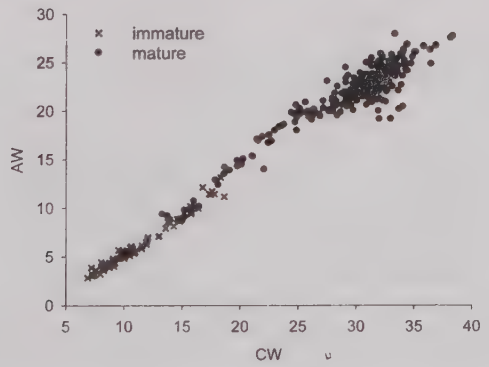

Fig. 9 Relationship between abdomen width and carapace width for females *C.dehaan*

Female crabs could be categorized into immature and mature categories based on the shape of the abdomen directly. The sizes of immature crabs ranged from 6.89 to 18.64 mm, and from 13.04 to 18.64 mm for mature crabs. There were coexistent immature and

mature crabs with CW ranging from 13.04 to 18.64 mm, which we defined as intermediate phase. The growth of immature phase showed positive allometric, while isometry for mature phase. The allometric growth rates were 1.42 and 1.029, respectively.

Tab. 3 Allometric equations for each category of females of *C. dehaan*

Phase	$\log_{10}AW=\log_{10}a+b*\log_{10}CW$	CW/mm	R^2	number
Immature	$\log_{10}AW=-0.717+1.42*\log_{10}CW$	6.89 - 18.64	0.972	124
Mature	$\log_{10}AW=-0.179+1.029*\log_{10}CW$	13.04 - 38.4	0.876	237

The proportion of morphological mature individuals was calculated in each 3 mm size class. Sizes of 50% morphological mature of the females was estimated by means of logistic regression reaching at 18.22 mm CW, and the individuals attaining 18.64 mm CW were absolute mature crabs. The regression function was as follows:

$$P=1/1+\exp(-0.503*(CW-18.22))$$

and the crab attained physiological mature at 17.50 mm CW for females (n=106).

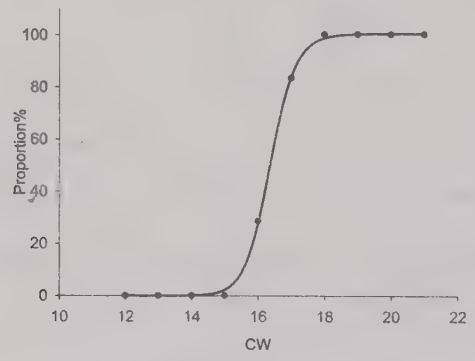

Fig. 10 Estimated sizes at 50% morphological maturity for females *C. dehaan*

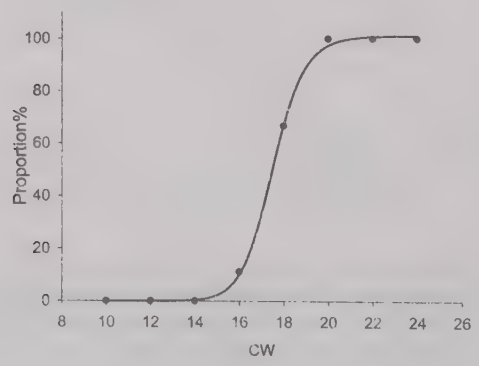

Fig. 11 Estimated sizes at 50% physiological maturity for females *C. dehaan*

Piecewise linear regression was used for individuals with CW<18.64 mm, and two equations were obtained. We defined the first stage as juvenile phase, and the second stage as intermediate phase. The juvenile and intermediate growth phase partially overlapped in which the individuals with CW ranged from 10.28 to 18.64 mm, and the break point of the two stages occurred at 10.28 mm CW. There was no difference in the allometric level in the two growth phases (F=1.96, P>0.05). A conclusion was made that there were only two allometric growth phases for females in life history.

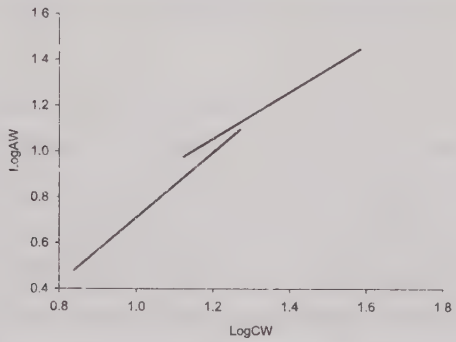

Fig. 12 Relationship between abdomen width and carapace width in logarithmic scale for females of *C. dehaan*

Tab. 4 Allometric equations for each category of immature females of *C. dehaan*

Phase	$\log_{10}AW=\log_{10}a+b*\log_{10}CW$	CW/mm	number
Juvenile	$\log_{10}AW=-0.954+1.68*\log_{10}CW$	6.89 - 10.28	54
Intermediate	$\log_{10}AW=0.725+1.486*\log_{10}CW$	10.28 - 18.64	70

3 Conclusions

Based on the morphometric data, the characters of allometric growth of *C. dehaani* were analyzed and the sizes of morphological and physiological maturities were both estimated finally. In brachyurans, the relative growth through molt was known as the changes in the growth rate of the secondary sexual characters, such as cheliped for males, the abdomen for females, and they obviously differed. The allometric growth differed not only between sexes, but also in different growth phases, when the differentiation in sexes preceded [19]. The transition was related to the puberty molt or terminal molt. The allometric growth pattern indicated the reproductive strategy and the energy investment demand of this specie in years with carapace grew [20, 21].

The cheliped for males was advantageous in feeding, competing, mating, and protecting after copulating in reproductive season [19]. But cheliped was not always useful

in estimating allometric growth. For example, there were the parallels for cheliped growth of *Sesarma rectum* between the sexes, with the analogical function for cheliped between sexes [11]. In this paper for this crab, there was differentiation for the three cheliped variables, CHL, CHH, CHW, respectively, except for 2PML. The cheliped could be chosen for estimating the allometric growth. Based on the hierarchical cluster analysis, compared with the obvious three differentiation variables for cheliped, the cheliped width was the most representative of allometric growth, which was different in choosing the cheliped length for *S. rectum* [11] and the cheliped length, cheliped width for *Perisesarma guttatum* [12].

There were three different growth phases separated by the pre-puberty molt and puberty molt, and there were the juvenile and the adolescent with a break point in size 11.78 mm CW for pre-puberty molt. The growth slowed down for this crab coming into adolescent, while for the others, it was opposite. It seemed that the growth and reproduction were not consistent at the same time [20]. The individuals would put more energy into gonad development instead of growth after pre-puberty molt, which was the reproductive strategy prepared for reproduction.

The characteristics of female abdomen provided an extra space, available for hatching and protecting [21]. The abdomen of females was usually chosen for the allometric growth variables. The females were divided into two phases, the mature and immature, whereas the relative growth of the immature showed allometric, and the mature was isometric. The mature crab in smaller size and the immature crab in larger size coexist in the size ranging from 13.04 to 18.64 mm CW, which was close to the result of the *S. rectum* with 13.2 - 18.5 mm CW [11]. There was no obviously different growth rate compared with the juveniles. It made a conclusion that there were two different allometric phases separated by the puberty molt. The crab attaining morphological maturity could mate with females, and the abdomen growed wider for the extra space for laying eggs. The size of morphological maturity was different, such as the *S. rectum* ranging from 15 to 18 mm CW, which was close to the 50% size 18.22 mm CW for *C. dehaani*. The relative growth of *S. rectum* showed allometric for immature and mature, whereas *C. dehaani* turned allometric into isometric as being mature. The specialties were that abdominal development for the crab showed continuous and overlap between immature and mature, with no abrupt or gradual development [11, 19]. Conclusion was made that females could breed during the intermolt period [13].

The 50% size of physiological mature was 17.50 and 17.20 mm CW for females and males, respectively. The species in spiders attained the physiological mature before the terminal molt, which was before being morphological mature [14, 22]. There were also species

with the physiological mature and morphological synchronize [23]. In some sense, the individuals became mature authentically when attained morphological mature [14]. But the result in this study was that the size of physiological mature for female was smaller than morphological mature, and the abdomen grew wider to lay eggs for available. In contrast, the male was opposite, which revealed the energy distribution differences. The females accumulate energy for gonad development first, then for morphological change, while the males competed for copulating through morphological advantage then for gonad development. Whether or not it was a particular case in sexual mature for shore crab to adapt to the survival and reproduction in the intertidal zone, needs further study.

The sexual mature for crabs consisted of physiological mature, morphological mature and function mature. Individuals with gonad development before terminal molt attained authentically maturity after morphological mature allowing for copulation and incubation, which was available for reproduction [14]. We prefered to determine the sexual mature for crabs considering all aspects instead of the single method. The dynamic of the intertidal ecosystem had an influence on the population dynamic of intertidal fishery resources. The study of growth and mature for *C. dehaani* was not only the supplement for population biology, but also for understanding the key role playing the salt marsh ecosystem [24]. In addition, *C. dehaani* could be used for baiting aboard, which had effects in the resource exploitation. The size of morphological mature was a foundation to confine economic species exploitation and a reference to exploitative evolution and government in order to make sure the mature copulation once before the exploitation [14]. The human should exploit the fishery resource in a continuous way to protect the reproduction ability of the parents to preserve the population resource, indirectly making contribution to the protection to salt marsh.

References

[1] Xiong L H, Lu J J. Different vegetations in salt marsh of Yangtze estuary [J].Chinese Journal of Zoology, 2009, 44(6):1 - 9.

[2] Gutierrez J L, Jones C G, Groffman P M, et al. The contribution of crab burrow excavation to carbon availabitity in surficial salt-marsh sediments [J]. Ecosystems, 2006, 9: 647 - 658.

[3] Xu J M, Fang H H, Gao T X. Sequence comparison of the mitochondrial CO1 gene between two *Sesarma* species [J]. Marine Science Bulletin, 2007, 26(6): 26 - 31.

[4] Xu J M, Zhang L J, Fang H H. Sequence comparison of mitochondrial 16rRNA gene between two *Sesarma* species [J]. Fisheries Science, 2009, 11(2): 65 - 71.

[5] Wang L Q. The complete larval development of *Sesarma dehaani* [J]. Journal of Shanghai Fisheries University, 2001, 3: 199 - 206.

[6] Li L S. Difference between Chinese Mitten Crab and *Sesarma* in megalopal stage development [J]. Fisheries Science & Technology Information, 1995, 06: 278.

[7] Anger K. The early life history of *Sesarma fossarum*, an endemic freshwater crab from Jamaica [J]. Invertebrate Reproduction & Development, 2005, 47(1): 63 - 72.

[8] Cuesta J A, Garcia-Guerrero M U. Larval morphology of the Sesarmid crab, *Aratus pisonii* (H.Milne Edwards, 1837) (Decapoda, Brachyura, Grapsoidea) from laboratory-reared material [J]. Crustaceana, 2006, 79: 175 - 196.

[9] Silva S, Hirose G. Population dynamic of *Sesarma rectum* (Crustacea, Brachyura, Sesarmidae) from a muddy flat under human impact. Paraty, Rio de Janeiro, Brazil, Iheringia [J]. Srie Zoologia, 2007, 97: 207 - 214.

[10] Santos C, Lima G. Histological and histochemical analysis of the gonadal development of males and females of *Armases rubripes* (Rathbun 1897)(Crustacea, Brachyura, Sesarmidae) [J] . Brazilian Journal of Biology, 2009, 69: 161 - 169.

[11] Augusto A V. Flores, João Saraiva, José Paula. Sexual maturity, Reproductive cycles, and juvenile recruitment of *Perisesarma guttatum* (Brachyura, Sesarmidae) at Ponta Rasa Mangrove Swamp, Inhaca Island, Mozambique [J]. Journal of Crustacean Biology, 2002, 22(1): 143 - 156.

[12] Seiple W H, Salmon M. Reproductive, growth and life-history contrasts between two species of grapsid crabs, *Sesarma cinereum* and *S. reticulatum* [J]. Marine Biology, 1987, 94: 1 - 6.

[13] Maria H. Leme de A. Size at sexual maturity of female crabs *Sesarma rectum Randall* (Crustacea, Brachyura) and ontogenetic variations in the abdomen relative growth [J]. Revista Brasileira De Zoologia, 2005, 22(2): 433 - 437.

[14] Corgos A, Freire J. Morphometric and gonad maturity in the spider crab *Maja brachydactyla*: a comparison of methods for estimating size at maturity in species with determinate growth [J]. ICES Journal of Marine Science, 2006, 63(5): 851.

[15] Fernandez-Vergaz V, Abellan L, Balguerias E. Morphometric, functional and sexual maturity of the deep-sea red crab Chaceon affinis inhabiting Canary Island waters: chronology of maturation [J]. Marine Ecology Progress Series, 2000, 204: 169 - 178.

[16] Hall N, Smith K. Does the largest chela of the males of three crab species undergo an allometric change that can be used to determine morphometric maturity? [J]. ICES Journal of Marine Science, 2006, 63(1): 140 - 150.

[17] Alunno-Bruscia M, Sainte-Marie B. Abdomen allometry, ovary development, and growth of female snow crab, *Chionoecetes opilio* (Brachyura, Majidae), in the northwestern Gulf of St Lawrence [J]. Canadian Journal of Fisheries and Aquatic Sciences, 1998, 55(2): 459 - 477.

[18] Moriyasu M, Benhalima K. Reproductive biology of male jonah crab, *Cancer borealis Stimpson*, 1859 (Decapoda, Cancridae) on the Scotian shelf, Northwestern Atlantic [J]. Crustaceana, 2002: 891 - 913.

[19] Hartnoll R G. Variation in growth pattern between some secondary sexual characters in crabs Decapoda Brachyura [J]. Crustaceana, 1974: 131 - 136.

[20] Hartnoll R G. Growth, sexual matutity and reproductive output [J]. Factors in Adult Growth, 1985, 3: 101 - 128.

[21] Charnov E L, Turner T F, Winemiller K O. Reproductive constraints and the evolution of life histories with indeterminate growth. Proceedings of the national academy of sciences of the United States of America [J]. Washington, 2001, 98: 9 460 - 9 464.

[22] Sampedro M P, González-Gurriarán E. Morphometry and Sexual Maturity in the Spider Crab Maja squinado (Decapoda: Majidea) in Galicia, Spain [J]. Journal of Crustacean Biology, 1999, 19(3): 578 - 592.

[23] Marco mura, Flavio orrù, Angelo Cau. Size at sexual maturity of the spider crab *Anamathia Rissoana* (Decapoda:Majiodea) from the sardinian sea [J]. Journal of Crustacean Biology, 2005, 25(1): 110 - 115.

[24] Lee S Y, Kwok P W. The importance of mangrove species association to the population biology of the sesarmine crabs *Parasesarma affinis* and *Perisesarma bidens* [J].Wetlands Ecology and Management, 2002, 10: 215 - 226.

大治河河口无齿螳臂相手蟹生长和成熟的研究

韩 莎[1]，管卫兵[2]

（1. 山东省海水养殖研究所，山东 青岛 266300；2. 上海海洋大学 海洋科学学院，上海 201306）

摘 要：无齿螳臂相手蟹是长江口潮间带和潮上带的优势种之一，具有重要的生态功能。为探求无齿螳臂相手蟹不同阶段的异速生长和成熟状况，于 2009 年 10 月至 2010 年 9 月期间采集样本，通过聚类和分段线性回归等分析方法对雌雄蟹头胸甲、螯、腹部等形态数据进行分析，建立区别不同生长阶段的判别函数并用逻辑斯蒂回归估计其 50% 形态成熟点。结果如下：雌雄蟹 50% 形态成熟点分别为头胸甲宽 18.22 mm 和 16.36 mm。雄蟹的螯宽和雌蟹的腹宽均表现出明显的异速生长；根据相对生长率的不同，雄蟹异速生长可分为三个阶段，雌蟹分为两个阶段；不成熟的雄蟹异速生长拐点发生在壳宽 11.78 mm，不成熟和成熟雌蟹腹部在壳宽 13.04～18.64 mm 范围内重叠。同时研究了 50% 的生理成熟大小，雌雄成熟大小分别为 17.50 mm，17.20 mm。雄性形态成熟大小小于生理成熟大小，而雌性则相反。

关键词：无齿螳臂相手蟹；螯；腹部；异速生长；形态成熟；生理成熟；

Effects of salinity on growth and feeding of juvenile Starry flounder (*Platichthys stellatus*)

YOU Hong-zheng[1], ZHANG Sheng-li[2], GUO Zhong-bao[3], JIANG Zhi-qiang[4*]

1. *Tianjin Fisheries Technology Promotion Station, Tianjin* 300221, *China;*

2. *Beijing Fisheries Research Institute, Beijing* 100068, *China;*

3. *Guangxi Institute of Fisheries, Nanning* 530021, *Guangxi province, China;*

4. *Key Laboratory of Mariculture and Stock Enhancement in North China's Sea, Ministry of Agriculture, Dalian Ocean University, Dalian* 116023, *Liaoning province, China*

Abstract: The survival rate, feeding, growth of juvenile Starry flounder were studied at different salinities. The results showed that when the fish was directly translated from salinity of 32 to 0 and more than 0, the survival rate was 100% in 96 hours. If the fish was acclimatized, it was still 100% in 42 days. The fish at the salinity of 0 - 16 grew faster than others; feeding rate varied as salinity changed, and the highest one was at salinity of 32 and the lowest one was at the salinity of 16. As to feed conversion efficiency, the highest one was at the salinity of 16, and the lowest one was at the salinity of 24. There were no significant differences among the treatments ($P>0.05$). It was found that low salinity benefited for recovering albinism.

Keywords: Starry flounder; salinity; survival rate; feeding; growth

1 Introduction

Salinity is one of the most important non-biological factors that affect the growth and survival of the hydrobios, and also the main factor that directly affects fish growth and development. The sea water is mainly composed of Chlorides while the fresh water is carbonate. Variety of salts that dissolved in water primarily affect the fish by the osmotic pressure of the water. All kinds of fish in different developmental stages have their own appropriate growth, survival and salt intake ranges. Therefore, determination of the optimal salinity level is very important to the fish fed at the salinity could be changed [1].

Starry flounder (*Platichthys stellatus*) is commonly known as Pearl flounder which has the large scale in flatfishes. It becomes a very strong competitive farmed fish with highly commercial development value abroad. Since the fishing in China has been shifted into the "raise" direction, the marine fish farming develops in an unprecedented rapid. To

Received on Nov. 28, 2012

*Corresponding author: yy_8245@163.com

select the regional suitable fingerling becomes one of the most concerned things by the regional producers. For its fecundity, feeding miscellaneous, docile temperaments, suitable for intensive culture and a wide scope of temperature and salinity, especially low-temperature tolerance and resistance, strong ability of tolerance to low oxygen, low oxygen consumption rate, high survival rate of culture, naturally live through the winter, and many other advantages, Starry flounder attracts the interest from the market. After many years of research and development by the north Pacific coastal states, they proved Starry flounder had a great potential of high-grade fishes to breed [2].

Although there are many studies on the artificial breeding of the Starry flounder at home and abroad, but the study of the impact of the salinity is very little, especially for the low salinity, and that is more common in the foreign reports. As it will become an important aquaculture breed, the study of the impact of the salinity has an important significance to the breeding of Starry flounder.

2 Materials and methods

2.1 Origin and domestication of experimental fish

Experimental fish was taken from the Dalian Bay Seafood Aquaculture Company, which produces artificially bred albino juvenile Starry flounder, and its initial weight was 10.60 ± 0.27 g, and the individual test fish was healthy.

The water of experiment was the sand leach sea water at the salinity of 32 while the dilution water was the aerated running water (the aeration time is over 24 hours). Salinity controlling used the proportional method of adding fresh water, and the YSI-63 salinity meter calibration produced by the United States Jinquan Scientific Instruments Company. Excessive salinity domestication uses the stepwise method, which reduced the salinity of 4 once every two days to make the fish fully adapt to the new environment. After the salinity down to 8, the salinity was reduced for 2 every time. Half water in the tank was changed every day.

2.2 Experimental design

Experimental design is divided into a control group whose salinity is 32(natural sea water), four treatment groups whose salinities are 24, 16, 8, and 0 (running water), and each group had three parallels, and random twelve fish were within each flume experiments. At the beginning and ending of experiment, the fish was weighed after 24 hours' hunger respectively. Official experiment lasted forty-two days.

The salinity of the experiment container and the salinity gradient ibid are mentioned see above, and twelve fish which were fed in the sea water of 32 were put into each sink with salinity of 24, 16, 8, and 0. Their living status was observed after 24h, 48h, 72h, and 96h.

2.3 Feeding and management

The juveniles were fed in the white tank (600 mm × 400 mm × 300 mm) of Key Laboratory of Mariculture & Stock Enhancement in North China's Sea by Ministry of Agriculture in Dalian Ocean University, and they were cultured by special feed for turbot, specifications for P1 and P2. Feed them on 7 am and 5 pm every day, siphon out manure before each feeding, suck out residual bait after feeding half an hour, record weighing after drying, control the water temperature 18 ± 0.5 ° c, pH 8 ± 0.5.

2.4 Determination method

Electronic balance (MP200B electronic balance, accurate to 0.01g) was used. The formula is as follows:

Survival rate (%) = survival of fish / total fish ×100

Weight gain rate (%) = $(W_t-W_o) / W_o \times 100$

Specific growth rate (SGR,% / d) = $(\ln W_t-\ln W_0) / t \times 100$

Feeding rate (FR,%) = $F_c / [t \times (W_0 + W_t) / 2] \times 100$

Feed conversion efficiency (FCE,%) = $(W_t-W_0) / F_c \times 100$

W_t = final weight (g); W_0 = initial weight (g); F_c= total feeding amount (g);t = time (d)

2.5 Data processing

SPSS 12.0 statistical software was used for statistical analysis of the experimental data, the single factor analysis of variance (one-way ANOVA), significant differences ($P < 0.05$), multiple comparisons with Duncan for differences between the test group. Chart production used Microsoft Excel 2003 software.

3 Results

3.1 Impact of salinity on the survival of juvenile Starry flounder

The experimental results showed that salinity of 32, 24, 16, 8 and 0 have no effect on the survival in each group. During all of the 42 days, there was no death of the fish and the

survival rate was100%. The acute decline of salinity at 24, 16, 8, and 0 also had no effect on the survival of the fish in 96h, and the survival rate was 100% too.

3.2 Impact of salinity on the feeding and growth of juvenile Starry flounder

3.2.1 Impact of salinity on the weight gain rate of juvenile Starry flounder

As shown in Tab. 1, after the entire cycle of feeding, both the weight gain rate and specific growth rate of juvenile Starry flounder had varying degrees improved, and the weight gain rate of salinity 8 group was significantly higher than that of the other groups, while 24 group had the lowest rate. The variance analysis of differences between groups was not significant ($P > 0.05$).

Tab. 1 Effects of salinity on the weight gain rate of the juvenile Starry flounder (Mean±S.D)

salinity	32	24	16	8	0
Initial weight / g	10.57 ± 0.31	10.47 ± 0.05	10.59 ± 0.36	10.55 ± 0.31	10.82 ± 0.18
Final weight / g	28.40 ± 2.73	27.60 ± 1.41	30.75 ± 4.53	32.33 ± 3.30	32.66 ± 2. 33
Weight gain rate / %	169.11 ± 32.58	163.60 ± 14.70	190.09 ± 39.76	205.91 ± 22.56	202.06 ± 19.16

3.2.2 Impact of salinity on the specific growth rate of juvenile Starry flounder

The specific growth rate in different salinities is shown in Fig. 1. The specific growth rates of the salinity 32, 24, 16, 8 and 0 group were 2.35% / d, 2.34% / d, 2.52% / d ,2.66% / d and 2.63% / d, while the salinities of 0 and 8 treatment group were slightly higher than those of the other groups. The variance analysis of differences between groups was not significant ($P > 0.05$).

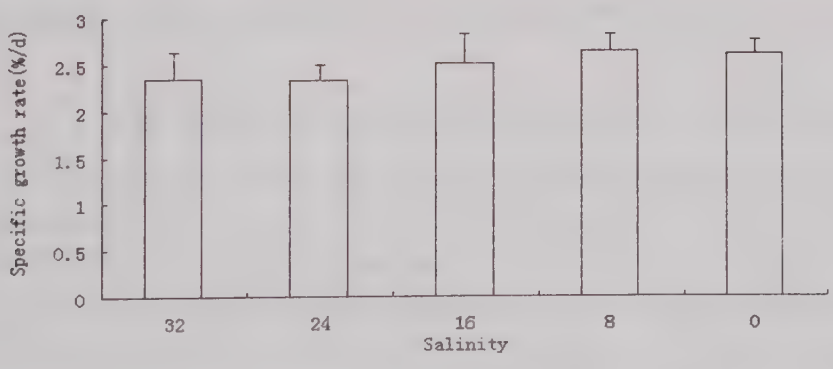

Fig. 1 Effect of salinity on the specific growth rate of the juvenile Starry flounder

3.2.3 Impact of salinity on the feeding rate of juvenile Starry flounder

Feeding rate under different salinity is shown in Fig. 2. In turn, the feeding rates of salinity 32, 24, 16, 8, 0 were 1.97%, 1.77%, 1.63%, 1.69%, 1.79%, while that of the 32 control group was slightly higher than those of the other groups. The variance analysis of differences between groups was not significant (P> 0.05).

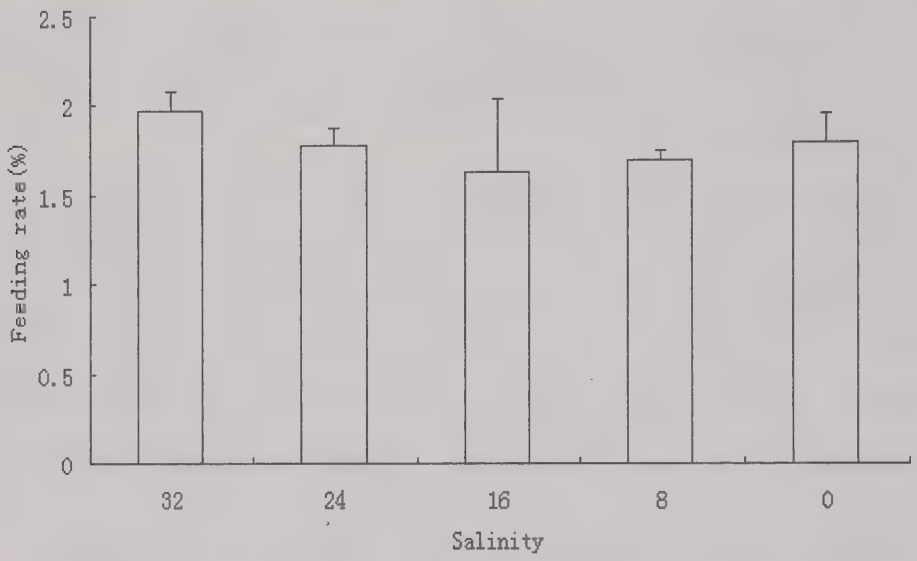

Fig. 2 Effect of salinity on the feeding rate of the juvenile Starry flounder

3.2.4 Impact of salinity on the feed conversion efficiency of juvenile Starry flounder

Starry flounder of the feed conversion efficiency under different salinity is shown in Fig. 3. The feed conversion efficiencies of the salinity 32, 24, 16, 8, 0 group is 124.6%, 102.54%, 171.24%, 146.62%, 134.81%. Salinity of 16 group is the highest, while the salinity of 24 group is the lowest, The variance analysis of differences between groups was not significant (P> 0.05).

3.3 Impact of the salinity the albinism of juvenile Starry flounder

The experiment showed that low salinity was conducive to juvenile Starry flounder albino individuals to recover normal, and a higher proportion of salinity 0 and 8 albino individuals to recover normal, and the higher salinity go ill with the albino recovery. The variance analysis of differences between groups was not significant (P> 0.05).

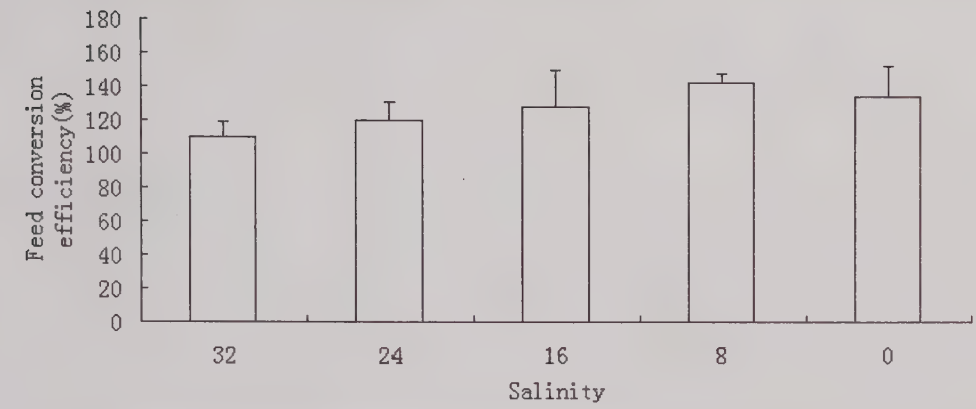

Fig. 3 Effect of salinity on feed conversion efficiency of the juvenile Starry flounder

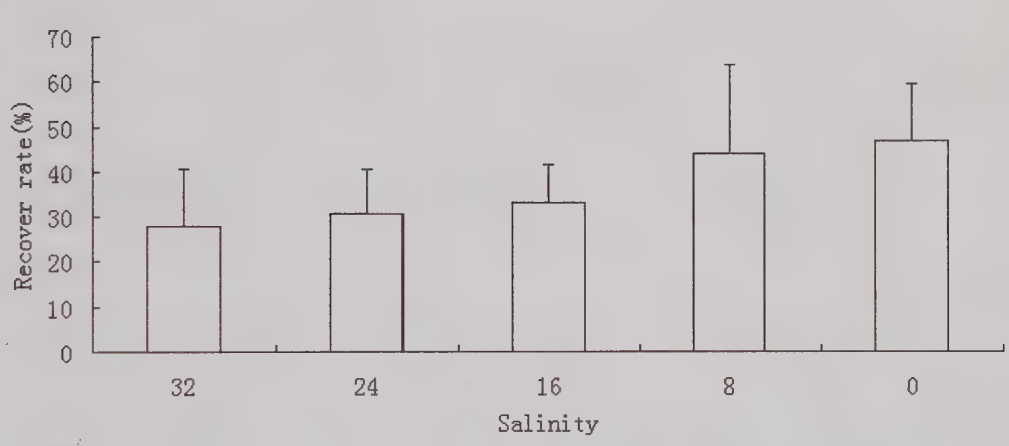

Fig. 4 Effect of salinity on recovering albinism of the juvenile Starry flounder

4 Discussion

4.1 Impact of salinity on the survival rate of juvenile Starry flounder

Euryhaline fish often can survive and have larger feeding rate, absorption rate, conversion efficiency and growth rate in a larger range of salinity [3]. The salinity has a significant effect on the daily growth and transient weight gain rate of the *Oreochromis niloticus*, *Sarotherodon melanotheron* and Israel red tilapia, the same as the survival and growth of *Pseudobagrus vachelli* [4,5], but the best growth salinity of different fish is somewhat different. Mu Yun-lei found that in the experiments on the effect of water temperature and salinity of juvenile turbot survived, the salinity of 28 and 32 reserved the highest survival rates that in 120 hours, the rate were 100% and 92.5%. The salinities of

12 and 40 test group with the lowest survival in 24h survival rate were only 12.5% and 20%, respectively, and all died within 48h [6]. The research result on *Plecoglossus altivelis* larvae of JI Guang-wen showed that except the fry in the freshwater sink the other average survival rate was 53.9% [7].

According to Wang Bo's report [2], the Starry flounder was a euryhaline cold water fish. Its suitable salinity range from 5 to 40, and the best growth salinity was from 10 to 30. The results of this experimental study showed that juvenile Starry flounder in salinity 32, 24, 16, 8, 0 could normally survive , which was consistent with the results of Wang Bo. However, the freshwater group salinity was not in juvenile Starry flounder appropriate range, and the result showed no death. The reasons for this may be related to the size of the fish, the body length of the experimental fish from the beginning to the end did not exceed 15 cm, so all survived in the fresh water, exactly the same as Wang Bo introduced the length of 15.24cm before juveniles can live in the fresh water. Article on the salinity mutations over 20 had no effect on their feeding and growth, in this experiment, the salinity mutation 8,16,24,32 experiment groups of fish can live normally, and the survival rate was up to 100%. This showed no effect on the salinity mutation 32 of their survival rate .Under this situation, we can put into fresh water as soon as possible in the farming to reduce farming costs in the farming production, and 32 salinity fluctuation will not cause too much impact on their survival rate, which was farmed flounder in the inland possibly, enough to fill the vacancies in the west.

4.2 Impact of salinity on the feeding and growth of juvenile Starry flounder

The appetite of the fish have been reported affected by salinity, in accordance with the principle of osmotic adjustment, osmotic pressure is minimum when the fish in the isotonic point, the maximum food intake in the lowest metabolic rate, the maximum efficiency of growth and transformation, many euryhaline fish having such characteristics [8-10]. After salinity exceeds isotonic salinity, fish decreased appetite, and a significant reduction in the absorption rate, conversion efficiency and growth rate, until death. Fish maximum feeding rate, absorption rate, conversion efficiency and growth rate, often appear in salinity between freshwater and loss of appetite [3]. Atlantic cod (*Gadus morhua*) growth rate and food conversion efficiency is closely related to the change of salinity. The Atlantic cod present less food intake and growth rate than the salinity of 28 when the salinity is 7 in summer[11]. Juvenile European flounder (*Platichthys flesus*) in conditions of salinity (5 and 15) than in the 0 and 35 to be fast-growing, Gutt analyse that the low rate of growth of the freshwater group the sake of feeding low, the low growth rate of salinity 35 group is caused by lower food conversion. This significant difference, not lead to changes in the energy component of the food intake change, no change to the form of the relative energy

distribution within the fish body muscle, liver, gonads, and other organs, but the change in the amount of fish biomass, restricted the use of an energy source [12].

The experimental results show that the salinity 8 group specific growth rate and weight gain rates are higher than the other groups, and food conversion efficiency of 16 is the highest, compared with a salinity of 24 weight gain rate, feeding rate, feed conversion efficiency is lower than other groups. Analyze the reasons for the juveniles isotonic point salinity may be between 8-16, used for regulating the osmotic pressure of metabolic energy consumption at least, and more energy for growth. The researchers believe that the isotonic point salinity can save fish energy, when the fish live in the plasma or isotonic medium, metabolism consumes minimal. Fish osmolality and ion concentration with different environmental media, the fish need to devote some energy to meet the consumption of ion and osmoregulation metabolism. Thus, by controlling the external environment to make the fish osmotic pressure adjusted to reduce energy consumption to a minimum, and to some extent can enhance the growth of fish and food utilization. The starry flounder as a euryhaline fish, the effect of salinity on physiological activities is also multifaceted.

4.3 Impact of salinity on the albinism of juvenile Starry flounder

Albinism is a kind of body color anomaly that often encountered in the juvenile Starry flounder. When culturing some other kinds of flounder, this kind of disease also commonly appears. Although the albinos' growth and feeding are the same as the normal ones, but the prices of the adult fish are greatly reduced. There are a lot of studies about the cause of the albino. It is generally believed that it always related to a variety of factors, like the larval stocking density, light, water temperature, water changes, the bait and nutrition [13]. The appropriate control measures have been proposed. However, in the aquaculture production of juvenile Starry flounder, it is unable to prevent the emergence of albino.

Different seawater salinity has influence in the flounder larvae's growth, survival rate and albinism rate. In low salinity, larvae showed higher survival rate and lower albino rate. The salinity between 21 and 26 was a critical salinity stage that produced significantly different results in the flounder larvae's survival rate and albino rate [14]. In addition, the experiment showed that the low salinity would help juvenile flounder albino returned to normal color. In the salinity of 8 and 16, a higher proportion of albino individuals returned to normal body color, and the higher the salinity was, the lesser the low salinity was conducive to the juvenile flounder albino individual returning to normal body color. When Wang Han-sheng [14] conducted the experiment of the salinity's influence on the flounder larvae, he found that the flounder albino rate decreased with the salinity reduction[15]. All

the fish used in this experiment were albino individuals, but after one month feeding in different salinity, the albino rate of each group had greatly changed. In the groups of the salinity of 0 and 8, above 50% of the fish restored to the normal body color while in the salinity of 16,24and 32 groups, it was only about 35%.

In the past, people generally believed that the formation of the flatfish albino was in the period of about 8 mm, a little fish could be gradually restored to normal body color individual in the later stage. However, the experimental results showed that the salinity had significant influence on the juvenile Starry flounder body color. We should further carry out this research in future.

Acknowledgements

This study was supported by the Key Projects of Science and Technology Department of Liaoning province "The Research and Demonstration of the Efficient and Safe Feeding Technology of Seafood" (No. 2008203002).

Reference

[1] YE Fu-liang. Ecology of Fish [M]. Guangzhou: Guangdong Higher Education Press. 2002, 22 - 84.

[2] WANG Bo, WANG Zong-ling, SUN Pi-xi, et al. The Culture Conditions and Development Prospects of *Platichthys stellatus* [J]. Fishery Modernization, 2006(5): 16 - 18.

[3] WANG Yun-feng, ZHU Xinhua. A Review on Impact of Salinity on Patterns of Fish Ecophysiology[J]. Studia Marina Sinica, 2002, 44(5): 151 - 158.

[4] WANG Wu, GAN Lian, ZHANG Dong-sheng, et al. Effects of Salinity on Survival and Growth of *Pseudobagrus vachelli* [J]. Fisheries Science & Technology Information, 2004, 31(3): 121 - 124.

[5] LI Xue-jun, LI Si-fa. Variation of growth,survival rate and condition factor of juvenile *Oreochromis niloticus,Sarotherodon melanotheron* and Israeli red tilapia at different salinities [J]. Journal of Fishery Sciences of China, 2005, 12(3): 245 - 250.

[6] MU Yun-lei, SONG Guang-jun. The Effects of Temperature and Salinity on Survival Rate of Juvenile Turbot Scophthalmus maximus [J]. Fisheries Science, 2005, 24(12): 1 - 3.

[7] JI Guang-wen. The Effects of Salinity on growth and survival rate of *Plecoglossus altivelis* larvae [J]. Freshwater Fisheries, 2003, 33(4): 3 - 5.

[8] Farmer Z J, Beamishf W H. Oxygen consumption of Tilapia nilotica in relation to swimming speed and salinity [J]. J. Fish Res. Board. Can., 1969, 26(4): 2 807 - 2 821.

[9] Kinne O. Growth food intake and food conversion in a enryplasticfish exposed to different temperatures and salinities [J]. Physiol. Zool., 1960, 33: 288 - 311.

[10] Brocksen R W, Cole R E. Physiological response of three species offish to various salinities [J]. J.

fish Res. Bd. Canada, 1972, 29: 399 - 455.

[11] Lambert Y, Dutil J D, Munro J. Effects of intermediate and low salinity conditions on growth rate and food conversion of Atlantic cod(*Gadus morhua*) [J]. Can. J. Fish. Aquat. Sci., 1994, 51: 1 569 - 1 576.

[12] Gutt J. The growth of juvenile flounders (*platichthys flesus L.*) at salinity of 1, 5, 15 and 35‰ [J]. Appl. Ichthyol., 1985, 1: 17 - 26.

[13] WEI Li-ping, CHANG Jian-bo, JIANG Hai-bin, et al. Culture and Processing Technology of Seafood [M]. Jinan: Shandong Science and Technology Press, 1995.

[14] WANG Han-sheng. Effects of Salinity on Growth,Survival Rate and Albinism Rate of The Larvae and Juveniles of *Paralichthys olivaceus* [J]. *Oceanologia Et Limnologia Sinica*，1997, 4: 399 - 405.

[15] JIANG Zhi-qiang, ZHAO Xiang-dong, WANG Guo-zu. The effects of salinity on survival, growth and feeding of *Paralichthys olivaceus juveniles* [J]. Journal of Dalian Fisheries University，2002, 2: 79 - 83.

盐度对星斑川鲽(*Platichthys stellatus*)幼鱼摄食生长的研究

尤宏争[1]，张升利[2]，郭忠宝[3]，姜志强[4*]

(1. 天津市水产技术推广站，天津 300221；2. 北京市水产科学研究所，北京 100068；
3. 广西水产研究所，南宁 530021；4. 大连海洋大学，农业部北方海水增养殖重点实验室，辽宁 大连 116023)

摘 要：在实验室塑料水槽中，观察了不同盐度条件下星斑川鲽（Platichthys stellatus）幼鱼（10.6 ± 0.27 g）的存活率，摄食和生长状况。结果表明：将星斑川鲽幼鱼从盐度为 32 的海水中直接移入低盐水中，在各个盐度下 96 h 后存活率均为100%；经盐度驯化后 42 d 的各组鱼成活率也为100%。盐度0，8，16组的增重率和特定生长率高于 24 和 32 组；摄食率 32 时最高，16 时最低；饵料转化效率 16 时最高 24 时最低，各组间差异不显著（P>0.05）。另外实验表明低盐度有利于星斑川鲽白化病的康复。

关键词：星斑川鲽；盐度；存活率；摄食；生长

Research advances in the biological characteristics of the crustacean spermatozoa

XU Xing-hong[1], YAN Bin-lun[1], ZHENG Jia-sheng[2], XU Jia-tao[1], XU Guo-cheng[1], SHAO Ying-ze[1], WU Jian-xin[1], SHEN Cheng[1]

1. *Jiangsu Key Laboratory of Marine Biotechnology, Huaihai Institute of Technology, Lianyungang* 222005, *Jiangsu province, China;*

2. *College of Marine Life Sciences, Ocean University of China, Qingdao* 266003, *Shandong province, China*

Abstract: The biological characteristics of crustacean spermatozoa is important for the artificial reproduction and genetic breeding. With reference to the latest studies and related materials, this paper reviewed the research progress in the biological characteristics of crustacean spermatozoa, such as morphological structure of sperm, spermatogenesis, sperm viability, preservation in vitro and acrosome reaction et al. The prospects of the research field have also been anticipated.

Keywords: crustacean; spermatozoa; morphological structure; spermatogenesis; viability; preservation in vitro; acrosome reaction

Research on the biological characteristics of spermatozoa is the basis for artificial reproduction and genetic breeding of economic animals. Two types of spermatozoa were found in crustaceans: the sperm of three subclasses of crustaceans has flagellum capable of movement, including the species of Mystacocaride, Cirripedia and Branchiura; while the sperm of the other five subclasses can not move without flagellum, including most crustaceans with economic value [1]. When meting, most male crustaceans bring the spermatophore made up of spermatozoa with spermaductal secretion to the abdomen or seminal female spermatheca, except the Cirripedia species transfer the sperm directly [2]. Special type of sperm and reproduction causes great difficulty in artificial breeding, which attracts increasing attention for a long time. The paper reviewed the research progress in the biological characteristics of crustacean spermatozoa, such as morphological structure of sperm, spermatogenesis, sperm viability, preservation in vitro and acrosome reaction etc, and the prospects of the research field have also been anticipated.

Received on Mar. 6, 2013

Corresponding author: xhxu119@163.com

1 Morpha and structure of spermatozoa

There are a variety of shapes in the spermatozoa of crustacean, such as spherosome (e.g. *Oratosquilla oratoria*), clavate (e.g. *Daphnella brachyuran*), sickle-shaped (e.g. *Moina macrocopa*), thumbtack (e.g. *Fenneropenaeus chinensis* and *Macrobrachium nipponense*), vesicle (e.g. *Panulirus stimpsoni*) and radisal (e.g. *Procambarus clarkia*) et al. [3]. The sperm of decapoda can be divided into two types based on the number of cell spike: single spike type of natantia and multi - spike type of reptantia [4].

1.1 Single spike type of sperm

An unified structural model has been established in the research areas about the sperm of Penaeidae, Natantia [5, 6]. The overall length of the prawn sperm is about 10μm, which consists of three parts: the front spike, the middle cap-shaped body and the main body behind[7]. The spike is about 3μm long, which has thick base and thinner apex containing membranous structure and endoplasm. The cap-shaped body is comprised of acrosomal granule, H-shaped ringlike structure and membrane vesicle. The nucleolus lying in the the main body, which is surrounded with cytoplasm including endoplasmic reticulum, vesica of unequal size and annulate lamellae.

Some difference in characters of the sperm structure was observed between canidea and penaeidae. The sperm of *Exopalaemon modestus* resemble everts umbrellas, which is 11 μm - 13 μm long, and a single 6 μm - 7 μm spike extend from the main body with disk top, and the cap-shaped body contains about twenty radial fibrils converging and extending to the spike [8]. The nucleus of most canidea species are not concentrated, which consist of zona visiculose near the cap-shaped body and zona membraniform close to the disk top[9,10]. Three kinds of vesicles in the zona visiculose can be distinguished based on the contents: vesicle with stroma showing PAS positility inside, vesicle container with granule, and vacuole with no stroma.

Although *Macrobrachium rosenbergii* and *Macrobrachium nipponense* belong to the same category, the sperm nucleus of *Macrobrachium rosenbergii* are homogeneous with no vesicle. This phenomena was supposed to be relevant to the lower evolutional position of *Macrobrachium Bate* [11]. Jiang et al. [12] have documented that the sperm of *Macrobrachium* and *Palaemon* possessed similar morphological characters, but significant difference were noted in the interior structure especially the nucleus between them, exhibiting a species-specific which could provide clues to the deep research of the genesis

and evolution among the class group of canidea. Endoplasmic reticulum and centrosome, et al. were not observed in the cytoplast of mature sperm of canidea[9, 13,14]. The evolution status of canidea and penaeidae requires further research.

As Qiu et al. reported [9], the front spike of sperm was made up of protein fibrillar structures enclosed by cell membrane, and this solid structure could bend when the sperm entered into the ovum. Acid phosphatase activities were detected in the spike and the cap-shaped body of the sperm in *Exopalaemon modestus*, so it was suggested that the spike and the cap-shaped body might play some roles during acrosome reaction [8]. The common opinion at present is that the the spike and the cap-shaped body form the acrosome complex [7, 15-17].

1.2 Multi - spike type of sperm

The common features of the sperm of reptantia species: they have more than three spikes; the spike looks like arms and thorns; membrane complex appears in the degenerative cytoplasm, and the acrosome structure is complicated [1]. The reptantia contains three groups including brachyuran, macrura and anomura, and the sperm of these three groups species has its own characteristics. The sperm of brachyuran species resembles steamed bread, which is comprised of acrosome, membrane complex and radial arms; the spherical acrosome surrounded with nuclear cup is comprised of apical cap, acrosomal vesicle and acrosomal tubule; an conical perforator is in the middle of acrosomal tubule formed with thin tubular structure lengthwise [18,19]. The macrura species have long sperm with irregularly shaped nucleus, and part of nucleus membrane commingles with cell membrane; three spikes extend from nucleus; the acrosome appears cylindrical or like a helmet, protruding from the nucleus with primary acrosome tubule [20]. The sperm of anomura species is shorter than macrura, the back and side karyotheca of the nucleus commingling with ceptantiaell membrane; the ovate-oblong acrosome has short and simple primary arosome tubule [21]. The evolvement direction of reptantia species is: macrura→anomura→brachyuran [22], and the sperm volume is gradually reduced during the evolvement process, and the acrosomal structure evolves from simple to complex, and the acrosome is considered as the traits of reproductive evolution of reptantia.

The radial arms extending from the nucleus may help the sperm contact the egg surface. The number of radial arms is different in different species, and mostly 10 - 20 [18, 19, 22, 23]. There are kinds of protein enzymes in the acrosomal vesicle, playing important role in decompouding egg membrane and helping the sperm enter into the egg [22].

2 Spermatogenesis

The reports about the spermatogenesis of crustaceans were mainly focused on the decapoda, such as *Crangon septemspinosa*[24], *Palaemon serratus* [25], *Parapenaeus congirostris*[26] and *Uca tangeir*[27] et al. Related to other countries, the domestic research started later, and several studies had been carried out on the following species: *Eriocheir sinensis*[28], *Portunus trituberculatus*[23, 29], *Scylla serrata*[30], *Fenneropenaeus chinensis*[31], *Thenus orientalis* [32], *Exopalaemon modestus* [8], *Litopenaeus vannamei* [33] and *Macrobrachium rosenbergii*[34] et al.

The spermatogenesis of crustaceans is the same as other animals, and it would go through five cell stages: spermatogonium, primary spermatocyte, secondary spermatocyte, spermatid and sperm [3, 35]. The early spermatid of crustaceans with the similar structure possesses a nucleus and a big preceding acrosome cavity lying in the cell polar respectively. Development differences happen in the later period: the spermatid of natantia becomes single spike type of sperm for the cytoplasm surrounding the nucleus [8, 25, 26, 31], while the spermatid cytoplasm of reptantia locates between the preceding acrosome cavity and the nucleus, and forms multi - spike type of sperm [23, 28, 29].

2.1 Spermatogenesis of natantia

The cytological variations of the spermatogenesis in *Exopalaemon modestus* have been reported [8]. The diameter of spermatogonium is 13 μm - 14 μm with higher nucleo-cytoplasm ratios, and vesicles in the cytoplasm resulting from the fragment of endoplasmic reticulum enclose the nucleus and arrange in a cord. The diameter of primary spermatocyte increases to the 19 μm - 20 μm, and vesicles from endoplasmic reticulum also increase; the diameter of second spermatocyte decreases to 15 μm - 16 μm. Significant changes occur in the structure of spermatid: cytoplasm reduces in the early stage, and a part of mitochondria and golgi body become disaggregating, and vesicles reduce noticeably; nucleus and cytoplasm poles of spermatid come into being in the middle of this stage, and the bonnet cytoplasm surrounds half of the nucleus; in the later stage, the nucleus of spermatid depress in the middle zone, while the cytoplasm evaginate and centrioles appear, and threadlike structure from annulate lamellae collects to the center and forms the spike. Some organelles such as centriole and mitochondria disappear and abundant vesicles with high electrom density distribute around the cap-shaped body in the sperm stage. Male reproductive cells of each stage in *Fenneropenaeus chinensis* are smaller than those in *Exopalaemon modestus*, and the mature sperm is only bout 3.4 μm long, and the primary spermatocyte has two annulate lamellae [31].

Vesicles around the cap-shaped body are a kind of acrosome granule with acid phosphatase activity [6], while the vesicles in the concave of nucleus are related to the absorbtion and transportion of substance [8]. Kang et al. [31] considered that the annulate lamellae was formed by the amalgamation of vesicles from endoplasm reticulum or the disaggregation of mitochondria, while Shigekawa et al. [36] presumed the annulate lamellae was derived from the nuclear membrane because he observed that the annulate lamellae is closely linked with the endoplasm reticulum and nulear membrane. Zhao et al. [14] did not discover the annulate lamellae in the sperm of *Macrobrachium nipponense*, so he made a conclusion that the spike consisted of the endoplasm reticulum and substance expelling from the nucleus. However, Koehler [37] and Huang et al. [8] had the different opion that the slices from the annulate lamellae collected and extended gradually and formed the spike. Thus differences exist in the structure and origin of the annulate lamellae among species.

2.2 Spermatogenesis of reptantia

The changes of cellularity of reptantia are significantly different with the natantia since the spermatid stage [23, 28-30]. Take *Scylla serrata* [30] for instance, the nucleus in the early spermatid stage are homogeneous and membrane system occupies most of the cytoplasm spape. The karyoplasms appear filamentous in the middle spermatid stage, membrane system and some substrate enter into the cavity from the base of acrosome cavity, and push ahead, join with acrosome cap, and form the spide. In the later spermatid stage, the globular acrosome generates the acrosomal vesicle and acrosomal tubule, and the front of acrosomal tubule is filled with much irregularly tubular and vesicular structure, and the nucleus extent around radially and form the radial arm. The acrosome of mature sperm protrudes forward obviously, and short tubular structure in the acrosomal tubule arrange regularly and form the perforator, and the membrane complex also comes into being.

The membrane complex is similar to the annulate lamellae of natantia, and its formation varies by species. The membrane complex of *Sinopotamon yangtsekiense* is made up of golgi body and mitochondria et al. [38]. Wang et al. [30] reported the membrane system of *Scylla serrata* came from the endoplasmic reticulum. Du et al. [28] and Mcknight et al.[39] both demonstrated nucleonic membrane and mitochondria participated in the form of the membrane complex except for the endoplasmic reticulum. The radial arm, alias nuclear arm for its origin is from the nucleus which contain abundant microfilament inside [29, 38]. However the radial arm of lobster is filled with microtubule, and the breakup of part of nuclear membrane of spermatid creates the conditions for the microtubule immigrating the nucleus [32, 37].

3 Viability of sperm

The viability of sperm would be influenced by temperature, salinity, pH, hormone, and removal of the eyestalk etc. More sperms and lower abnormal sperm rates in the parent prawn of *Litopenaeus vannamei* were detected after 42d of artificial feeding at 26 °C, and the sperm number reduced and the abnormal sperm rates rose with the increase of temperature, and no sperm could not be generated at 32 °C [40]. The viability rates of sperm in *Charybdis japonica* were higher in the environment with lower salinity and alkalescence [41]. Alfaro [42] reported that 17-α-testosterone had the ability of improving significantly the sperm number and the spermatophore weight and decreasing the abnormal sperm in *Litopenaeus vannamei*, but 17-α- progesterone had no effect. It has been also demonstrated for *Panaeus monodon* [43] and *Litopenaeus vannamei* [44] that the removal of single eyestalk could increase the sperm number without the influence on the sperm quality.

The motorial induce is not applicable to estimate the sperm quality of crustacean, because the sperm of crustacean has not the flagellum without motor ability. The evaluation methodology of crustacean sperm may adopt staining, fertility rate in vitro, biochemistry analysis, and acrosome reaction rate of artificial inducing et al. Zhu et al. [46] and Xu et al. [41] both documented that staining in eosin B was apply to estimate the sperm viability for *Portunus trituberculatus* and *Charybdis japonica*, respectively. The sperm of *Fenneropenaeus chinensis* had the fertilization ability after entering into the water for 3h, while the fertility rate of the ovum decreased to 62.7% after entering into the water for 1 min [47]. The fertility rate of the sperm in *Fenneropenaeus chinensis* was 73.6% after refrigeration [48]. Higher fertility rate of the sperm in *Eriocheir sinensis* was measured to 74% - 88% after entering into the water within 20min, and the fertilization ability existed until the sperm in the water for 40 mins [49].

The unfertilized mature eggs of crustacean are hard to obtain, so there is big limitation in estimating the sperm quality by the fertility rate. As observed by Feng et al. [50] for *Fenneropenaeus chinensis*, activities of Na, k^+-ATP enzyme and Mg^{2+}-ATP enzyme of sperm in spring were higher than those in autumn. Jeyalectumie et al. [51] reported the semen and spermatophore contained abundant protein, carbohydrate and fat, and the quantity of these substance in the spermatophore were more than those in the semen, and the energy metabolism of sperm was the process of anaerobic glycolysis, and the organism in the seminal receptacle of female crabs increased after mating, while the carbohydrate content in the seminal receptacle decreased significantly in the course of

sperm reserve. The evaluation system of sperm in biochemical induces for estimating the sperm quality in crustacean has not been established at present.

4 Preservation of sperm in crustacean in vitro

The preservation of sperm in aquatic economicalanimal in vitro is paid more attention with the development of the artificial insemination technique and the demand of protecting the genetic resources. Compared with the research of other aquatic organisms, the reports about the preservation of sperm in crustacean are little [53], only about the *Eriocheir sinensis* [54], *Scylla serratea* [53], *Fenneropenaeus chinensis* [55], and *Charybdis japonica* [56]. The preservation methods of animal sperm include two types: hypothermic preservation in deepfreeze and cryopreservation in liquid nitrogen.

4.1 Hypothermic preservation of sperm

Hypothermic preservation of sperm at 0 °C - 5 °C has the advantage of simple operation and no requirement for the special condition such as liquid nitrogen and nitrogen canister, which play the important role in the practice, although the preservative time is shorter than cryopreservation in liquid nitrogen[57]. It is essential that dilution solutions, cryoprotectants and antibiotics et al. are added to the semen in order to extend the lifetime of the sperm under hypothermic preservation.

Chen et al. [58] compared the effect of six kinds of dilution solutions for the sperm of *Eriocheir sinensis* under 4 °C, and drew a conclusion that Ca^{2+}-FASW (*calcium*-free artificial sea water) II was an excellent solution to preserve *Eriocheir sinensis* sperms, and the surviving rate of sperm was 92.19% after 6 day's preservation, and the formula of Ca^{2+}-FASW II is: NaCl 399.61mmol/L, KCl 9.725mmol/L, Na_2SO_4 27.72 mmol/L, $NaHCO_3$ 2.70 mmol/L, $MgCl_2.6H_2O$ 52.56 mmol/L, the osmotic pressure is 791.0 ± 4.0, pH value is 7.5.

It has been suggested that adding moderate carbohydrate e.g. glucose could maintain the low level of metabolization and extended the lifetime of the sperm from the research of the preserve of the sperm in mammal and fish [59]. However adding glucose and yolk et al. is not suitable for the sperm of crabs, which may be related to the types of the sperm. The sperm of mammal and fish have the ability of movement with a flagella which consume much energy, while the sperm of crabs can not move without flagella and the metabolization is at the lower lever, so it demands less energy substance as carbohydrate. On the other hand, adding glucose influences the osmotic pressure of the dilution solutions and leads to the heavy burden of maintaining the balance of the osmotic

pressure extracellular and intracellular causing the decrease of the sperm vitality.

The cryoprotectants of the sperm are different by animal species, and two common kinds are dimethysulfoxide (DMSO) and glycerin [60]. 5% (V/V) DMSO is suitable for hypothermicly preserving the sperm of *Scylla serrata*. The viability rate of the sperm was 58.7% after 24h preservation at 4 °C, which was higher significantly than 30.2% of the control group [53]. The sperm density is closely related to the preservation effect of the sperm, and appropriate decrease of the sperm density could reduce the metabolization of the sperm and decrease the toxicity damaged by the metabolic product and extend the lifetime of the sperm, while higher sperm density increase the chance of sperm collision leading to induce the acrosome reaction and decreases the viability rates of the sperm [61]. According to the previous report, the optimal preservation density of the sperm in *Eriocheir sinensis* is 10^6 - 10^7 sperm /mL[58].

4.2 Cryopreservation of sperm

The sperm under cryopreservation in liquid nitrogen (-196 °C) is in a thanatosis state that the feitilization ability can be maintained for several years and even several decades, so the technique of cryopreservation is very important for resource protection of economic animals, crop hybridization and the foundation of animal germplasm repository et al. [62].

12.5% glycerin is the optimal cryoprotectants for the cryopreservation of the sperm in *Eriocheir sinensis*, and the viability rate of the sperm is 62.6% after preservation 8h in liquid nitrogen [54]. Ke et al. [55] reported the viability rate of the sperm of *Fenneropenaeus chinensis* was 60% and the fertility rate was 59% under cryopreservation with the cryoprotectants of 10% DMSO and 5% - 10% glycerin. However the effect of 5% DMSO as the cryoprotectants is better for the cryopreservation of the sperm of *Sicyonia ingentis*[63], while 15% DMSO is suitable for the sperm of *Charybdis japonica* [56].

The cooling rate for sperm directly influences the cryopreservation effect: if the cooling rate is too quick that intracellular water can not transmit to the outside, it will cause the ice crystal form, which will destroy the cell membrane and cause the cell death; while if the cooling rate is too slow that the intracellular water freezes later than extracellular water causing the imbalance of salinity, which will injure the cell under higher salinity for a long time [64]. Two-step freezing method is generally adopted in the cryopreservation of the animal sperm: the first precool is putting the samples above the liquid nitrogen away from 5cm for several minutes , and then, putting the samples into the liquid nitrogen for the second precool, finally the samples can be conserved in the nitrogen canister chronically [54, 56, 62].

5 Acrosomal reaction of sperm

Since Binford [65] observed the everting of crabs sperm, the acrosome reaction of sperm in crustaceans has attracted many scientists at home and abroad in the last hundred years, and thoroughly studies have been carried out in this field [65-69]. Wang et al. [70] demonstrated the process of acrosome reaction of the sperm in *Scylla serrata* could be divided into two stages: the acrosomal vesical everting and the acrosomal tubule protraction.However Zhu et al. [69] and Xia et al. [71] reported respectively the processes of acrosome reaction of *Portunus trituberculatus* and *Eriocheir sinensis* consists of four stages：swelling of the apical cap, everting of acrosomal vesical, then protraction of the acrosomal tubule, and form of acrosomal filament.

pH, $Ca^{2+}$and A23187 (one kind of ionophore, as the inducer of the acrosome reaction) are the key factors influencing the acrosome reaction [72]. Wang et al. [70], Xia et al. [71] and Xu et al. [73] analyzed respectively the optimal induced conditions of acrosome reaction in vitro by orthogonal experiments for *Scylla serrata*, *Eriocheir sinensis*, and *Charybdis japonica,* respectively, and concluded that the pH value was 9.0, 6.0, and 8.0; the concentration of $CaCl_2$ was 0.25%, 0.20%, and 0.30%; the concentration of A23187 was 64 μg/mL, 40 μg/mL, and 60 μg/mL. Du et al. [68] obtained 93% of the acrosome reaction rate induced by egg-water of *Eriocheir sinensis*, but Wang et al. [70] documented the acrosome reaction could not be induced by egg-water of *Scylla serrata*. It suggests that the egg-water can not be replaced completely by A23187 for its instable inducing effect.

6 Expectation

6.1 Mechanism of the sperm preservation in female spermatheca

The sperms of crustaceans decapoda would be stored in the female spermatheca for several days to months after mating. Several ultrastructural differences were observed between the sperm from the male seminal receptacle and the sperm from the female spermatheca by Lin et al.[7], Shangguan et al[19]., and Xu et al.[41] for *Fenneropenaeus chinensis*, *Scylla serrata*, and *Charybdis japonica*, furthermore, the sperm in male seminal receptacle formed many spheroidal spermatophore，but the sperm in female spermatheca was dispersed. Xuan et al.[74]reported that the morphostructure of the spermatheca in *Portunus trituberculatus* from the East China Sea changed significantly after mating and the sperm stopper appeared, but the concrete chemical components were not analyzed. Thus it is necessary to carry out the research on the inner environment of the spermatheca

and the mechanism of the sperm preservation in female spermatheca, which will help the study of the preservation in vitro of the sperm in crustaceans and the fertilized mechanisms.

6.2 Acrosin activity in sperm

The acrosin is a special kind of enzymes that play the important role in dissolving the egg membrane, unclosing the routeway of the sperm entering into the egg, and accomplishing the acrosome reaction. The researches about the acrosin are mainly focused on the mammal at present, but seldom about the crustaceans [52, 75]. Many problems in this field are not resolved as yet, such as the difference in the acrosin activity between two source sperms from the female spermatheca and the male seminal receptacle, the effect of the environmental factors on the acrosin, the variety of the acrosin activity of the sperm preservation in vitro and the respiratory metabolism of the sperm et al.

6.3 Preparation method, constitute and induced metabolism of the egg-water

As egg-water has the advantage of easily obtaining and low cost, it is meaningful of the preparation of the egg-water with steady inducing effect to replace expensive A23187 in practice. So it is necessary to make further research on the constitute, preparation method, and induced metabolism of the egg-water.

6.4 Artificial fertilization

Special type of sperm and reproduction of crustaceans cause great difficulty in artificial fertilization, although there are little reports about success experiment, but there is still keeps pace with applying the technique in practice. So it is one of the important directions of researches in the future.

6.5 Function gene of sperm

The research on the molekularer mechanisms of reproduction is mainly focused on the human being, model organisms and critter, and the reports about the crustaceans are seldom. So it will make the breakthrough for the study on the biological characteristics of the sperm in crustaceans to carry out the research of the function gene about the spermatogenesis, maturation and feitilization of the sperm of crustaceans.

Acknowledgments

This work was supported by the Jiangsu Province Science and Technology Development Project (Grant No. BN2010026).

References

[1] Pochon-Masson J. Arthropoda-crustacea in reproductive biology of invertebrates. Vol. II. Spermatogenesis and sperm function [M]. New York: John Wiely & Sons Ltd, 1983, 407 - 449.

[2] Subramoniam T. Spermatophores and sperm transfer in marine crustacean, dvances in marine biology [M]. Madras: Academic Press Limited, 1993, 129 - 215.

[3] Li X. Histology and embryology of aquatic animals [M]. Beijing: Chinese Agricultural Publishing Press. 2006, 217 - 220, 292 - 294.

[4] Talbot P, Summers R G. The structure of sperm from *Panulitus*, the spiny lobster, with special regard to the acrosome. J. Ultrastru. Res., 1978(64): 341-351.

[5] Xi Y L, Tan X K. The morphology and ultrastructure of the sperm in *Macrobrachium nipponense*. Acta Hydrob. Sin., 1997, 1(1): 59-63.

[6] Wang Y F,Du N S, Lai W. Cytological study on the mechanism of fertilization in *Macrobrachium rosenbergii* (Crustacea,Decapoda). Acta Zool. Sin., 1998, 44(2): 195-202.

[7] Lin Q W, Liu R Y, Xiang J H. Studies on the morphological structure and physiological and biochemical functions of the sperm in *Penaeus chinensis*: I. The ultrastructure of the sperm. Oceanl. Et Limnol. Sin., 1991, 22(5): 397-401.

[8] Huang H X, Tan Q K. The morphology and ultrastructure of the sperm of freshwater shrimp *Exopalaemong modestus*. Chinese J. Zool., 2001, 36(4): 2-6.

[9] Qiu G F, Du N S, Lai W. Studies on the male reproductive system of *Macrobrachium nipponense* II. The morphology and ultrastructure of the sperm. Acta Zool. Sin., 1996, 42(4): 349-354.

[10] Felgenhauer B F, Abele L G, Kim W. Reproductive morphology of the anchialine shrimp *Procaris ascensionis*(Decapoda:Procaridae). J. Crust. Bio., 1988, 8(3): 333-339.

[11] Yang W X. The status of the sperm in *Macrobrachium nipponense* during the reproductive evolution of Caride. Donghai Marin. Sci., 1998, 16(4): 14-19.

[12] Jiang Y Q, Han Z P. A review of sperm ultrastructure in Caridea. J Huzhou Teach. Coll., 2001, 23(3): 47-50.

[13] Lynn J W, Clark W H J. The fine structure of the mature sperm of the freshwater prawn,*Macrobrachium rosenbergii*. Biol. Bull., 1983, 164: 459-470.

[14] Zhao Y L, Du N S, Lai W. Studies on the spermatogenesis of *Macrobrachium nipponense*. Acta Zool. Sin., 1997, 43(3): 243-248.

15] Yang W X, Du N S, Lai W. The changes of golgi body in *Macrobrachium nipponense* during the spermatogenesis . Acta Zool. Sin., 1998, 44(4): 377-383.

[16] Hong S G, Chen X f, Zhou S, et al. Studies on the spermatogenesis of *Penaeus penicillatus* I. Morphological structure of the sperm. Acta Zool. Sin., 1993, 39(3): 239-241.

[17] Kang X J, Wang S A. Studies on the changes of morphology and structure of the spermatozoon in

Penaeus chienensis. Donghai Marin. Sci., 2000, 18(3): 40-46.

[18] Wang L, Du N S, Lai W. Ultrastructure of sperm in freshwater crab (Sinopotamon yangtsekiense). Acta Zool. Sin., 2000, 46(2): 227-229.

[19] Shangguang B M, Li S J. Studies on the ultrastructure of sperm in *Scylla serrata*. Acta Zool. Sin.,1994, 40(1): 7-11.

[20] Beach D,Talbot P. Ultrastructural comparison of sperm from the crayfishes *Cherax tenuimanus* and *Cherax albidus*. J. Crust. Biol.,1987., 277: 205-218.

[21] Tudge C C. Comarative ultrastructure of hermit crab spermatozoa (Decapoda, Anomura, Paguroidea) [M]. J. Crust. Biol., 1992, 12(3): 387 - 409.

[22] Du N S, Lai W, Chen L Q, et al. Studies on the comparative ultrastructure of crab spermatozoa (Crustacea, Decapoda, Reptantia, Brachyura).Zool. Res.,1999, 20(5): 372-378.

[23] Li T W. Studies on the spermatogenesis and ultrastructure of the sperm in *Portunus trituberculatus*. Acta Zool. Sin., 1995, 41(5): 41-47.

[24] Arsenault A L. Changes in the nuclear envelope associated with spermtid differentiation in the shrimpm, *Crangon septemspinosa*. J. Ultrastruct. Res., 1984, 8:.294-308.

[25] Papathanassion E, King P E. Ultrastructural studies on gameto-genesis of the prawn *Palaemon serratus*(Pennant) II. Spermiogenesis. Acta. Zool.,1984, 65: 33-40.

[26] Medina A. Spermiogenesis and sperm structure in the shrimp *Parapenaeus congirostris*(Crustacea: Dendro branchiata): comparative aspects among decapods. Mar. Biol.,1994, 119: 449-460.

[27] Medina A, Rodriguez A. Spermiogenesis and sperm structure in the crab *Uca tangeir*(Crustacea, Brachyura), with special reference to the differentiation. Zoomorph., 1992, 111: 161-165.

[28] Du N S, Xue L Z, Lai W. Studies on the sperm of *Eriocheir sinensis* II. Spermiogenesis. Et Limnol. Sin., 1988, 19(1): 71-75.

[29] Guan W B, Xuan F J, Dai X J, et al. Spermatogenesis and spermatophore formation of swimming crab (*Portunus trituberculatus* Miers, 1876) in East China Sea. J. Fish. Sci., 2009, 16(2): 173-182.

[30] Wang Y L, Zhang Z P, Li S J. The ultrastructure of spermiogenesis in *Scylla serrata*. Acta Zool. Sin., 1997, 43(3): 249-254.

[31] Kang X J, Wang S A, Du N S, et al. Study on the endoplasmic reticulum variation during spermatogensis in *Penaeus chinensis*. J. Xiamen Univer. (natural science), 2000, 39(6): 849-855.

[32] Zhu D F, Li S J, Wang G Z. Ultrastructure of spermatogenesis in the squat lobster (*Thenus orientalis*). Acta Zool. Sin., 2002, 48(1): 240-246.

[33] Xu Y H, Liu X D, Zhang L P, et al. Studies on the ultrastructure of spermatogenesis in shrimp, *Litopenaeus vannamei*. J. Tropic. Ocean., 2010, 29(4): 89-93.

[34] Wang Y F, Yang X J, Zhu C B, et al.Ultrastructure of spermatogenesis in freshwater prawn, *Macrobrachium rosenbergii* (Crustacea: Decapoda).J. centr. China norm. uni., 2003, 37(4): 531-537.

[35] Xu X H, Yan B L, Zheng J S, et al. Study on the development of sex gland and reproductive cycle of

Charybdis japonica (A. Milne-Edwards). Trans. Ocean. Limnol., 2010, 2: 29-36

[36] Shigekawa K, Clark W H J. Spermiogenesis in the marine shrimp,*Sicyonia ingentis*[J].Dev Growth Differ,1986,28(2):95-112.

[37] Koehler L D. A unique case of cytodifferentiation:spermiogenesis of the prawn,*Palaemonetes paludosus*. J. Ultrastruct. Res.,1979, 69: 109-120.

[38] Wang L, Du N S, Lai W. Studies on spermiogenesis of a freshwater crab *Sinopotamon yangtsekiense* (Crustacea decapoda). Acta Hydrob. Sin., 1999, 23(1): 29-33.

[39] Mcknight C E, Hinsch G W. Sperm maturation and ultrastructure in *Scyllarus chacei*. Tiss. Cel., 1986, 18(2): 257-266.

[40] Perez-Velazque M, Bray W A, Lawrence A L, *et al*. Effect of temperature on sperm quality of captive *Litopenaeus vannamei* broodstock. Aquac., 2001, 198(34): 209-218.

[41] Xu X H, Yan B L, Xu J T, et al. Spermatozoa morphology and influence of environmental factors on viability rates in crab *Charybdis japonica*. Acta Ocean. Sin., 2010, 32(5): 93-99.

[42] Alfaro J. Effect of 17 alpha-methyltestosterone and 17 alpha-hydroxyprogesterone on the quality of white shrimp *Panaeus vannamei* spermatophroes. J. World Aqua. Soc., 1996, 27(4): 487-495.

[43] Gomes L A O, Honculada-Primavera J. Reproductive quality of male *Panaeus monodon*. Aqua., 1996, 112: 157-164.

[44] Leung-Trujillo J R, Lawrence A J. The effect of eyestalk ablation on spermatophore and sperm quality in *Panaeus vanname*. J. World Aqua. Soc.,1985, 16: 258-266.

[45] GuanW B, Wang G Z, Li S J. Cryopreservation of spermatozoa of mud crab (*Scylla serrata*) and viability assay by biostain method. J. Oceano. Taiwan Stra., 2002(2): 457-463.

[46] Zhu D F, Zhou S. Viability assessment of spermatozoa in the swimming crab *Portunus trituberculatus*. J. Fisher. China, 2008, 32(5): 765-771.

[47] Cai N E, Lin F, Chen B N, et al. Studies on the fertilization biology of *Penaeus chinensis*. Oceanl. Et Limnol. Sin., 1997, 28(3): 271-277.

[48] Wang Q Y, Yang C H, Ma C S, et al. Studies on the applying spermaduct of *Penaeus chinensis* with the artificial insemination. Mar. Fisher. Res., 1989, 10: 69-72.

[49]Chen L Q, Wang Y F, Zhao Y L, et al. Studies on the artificial insemination and cultivation in vitro of *Eriocheir sinensis*. Freshw. Fisher. (supplement), 1996, 26: 143-147.

[50] Feng B Y, Xu M Y, Zhu J Z, et al. Analysis on the relationship between the ATP enzyme activity of sperm and the reproduction in *Penaeus chinenses*. Mar. Sci.,1995, 2: 33-36.

[51] Jeyalectumie C, Subramoniam T. Biochemistry of seminal secretion of the crab *Scylla serrata* with reference to sperm metabolism and storage in the female.Mol. Reprod. Dev.,1991, 30: 44-55.

[52] Liu Q, Yang X Z, Cheng Y X, et al. Comparison of sperm morphology acrosin activity and immune indices between precocious and normal *Eriocheir sinensis*. J. Fish. Sci., 2009, 16(2): 183-191.

[53] Guan W B, Wang G, Li S J. Progress on research of sperm cryopreservation of Decapods, Crustacean. Reser. Fisher., 2002, 32(3): 50-52.

[54] Chen D H, Li Y D, Jia L Z, et al. Cryopreservation of *Eriocheir sinensis* (in vitro) with different cryoprotective solutions and prefreezing time [J]. Acta Hydrob. Sin., 2008, 32(4): 579 - 585.

[55] Ke Y F, Cai N E. Studies on the cryopreservation of the sperm in *Penaeus chinenses* [J]. Oceanl. Et Limnol. Sin., 1996(1): 187 - 193.

[56] Xu X H, Yan B L, Xu J T, et al. Cryopreservation of Spermatozoa in Japanese Swimming Crab *Charybdis japonica* [J]. Fisher. Sci., 2010, 29(10): 601 - 604.

[57] Deng Y S. Cryopreservation of fish sperm [J]. Reser. Fisher., 1996(4): 7 - 8.

[58] Chen D H, Zhou Z L, Fan L J, et al. Viability rates of Eriocheir sinensis sperms in six preservation solutions (in vitro) [J]. J. East China Norm. Univ. (natural science), 2007(4): 86 - 94.

[59] Su D X, Yan A S, Tian Y S. Effects of Na+, K+, Ca2+ and Glucose on Sperm Mobility in Northern Pike, *Esox lucius* [J]. Chinese J. Zool., 2004, 39(1): 16 - 20.

[60] Bhavanishankar S, Subramoniam T. Cryopreservation of spermatozoa of the edible mud crab *Scylla serrata* (Forskal) [J]. J. Exp. Zool., 1997, 277: 326 - 333.

[61] Van D N L, Couturier L R. Flow dialysis as a mean preserving boving semen at roon: temperature [J]. J. Dairy Sci., 1958, 41: 530 - 536.

[62] Yu H R, Zhang X M, Chen C. Prospect of cryopreservation of fish spermatozoa [J]. Trans. Ocean. Limnol., 2004 (2): 66 - 72.

[63] Anchordoguy T J, Crogwe J H, Griffin F J, et al. Cryopreservation of sperm from the marine shrimp *Sicyonia ingentis* [J]. Cryobiology, 1988(25): 238 - 243.

[64] Mazur P. The role of intraceallular freezing in the death of cells cooled at supraoptimal rates. Cryobilogy, 1977, 14: 251-272.

[65] Binford R. The germ cells and the process of fertilization in the crab *Menippe mercenaria* [J]. J. Morphol., 1913, 24: 147 - 202.

[66] Brown G G. Ultrastructural studies of sperm morphology and sperm-egg interaction in the decapod *Callinectes sapidus* [J]. J. Ultrastruct. Res., 1966, 14: 425 - 440.

[67] Goudeau M. Fertilization in a crab. I. Early events in the ovary and cytological aspects of the acrosome reaction and gamete contacts [J]. Tissue and Cell, 1982, 14: 97 - 111.

[68] Dan N S, Lai W, Xue L Z. Studies on the arosome reaction of the sperm in *Eriocheir sinensis* [J]. Acta Zool. Sin., 1987, 33(1): 8 - 13.

[69] Zhu D F, Wang C L, Yu H W, et al. Morphological and structural changes of sperm during the acrosome reaction in the swimming crab *Portunus trituberculatus* [J]. Acta Zool. Sin., 2004, 50(5): 800 - 807.

[70] Wang Y L, Zhang Z P, Xie Y J. Acrosome reaction in sperm from mud crab (*Scylla serrata*) [J]. Acta Zool. Sin., 2001, 47(3): 310 - 316.

[71] Xia A J, Ding S Y, Pan J L, et al. Morphological characteristics and acrosome reaction in the sperm of Chinese mitten crab (*Eriocheir sinensis*) [J]. J. Nanjing Uni. (natural science), 2007, 43(2): 139 - 144.

[72] Bhavanishankar S, Subramoniam T. Cryopreservation of spermatozoa of the edible mud crab *Scylla serrata* (Forskal) [J]. J. Exp. Zool., 1997, 277: 326 - 336.

[73] Xu X H, Yan B L, Xu J T, et al. Morphological changes and induced conditions of acrosome reaction in vitro induction of sperm from marine crab (*Charybdis japonica*). J. Fisher. China, 2010, 34(12): 1821-1828.

[74] Xuan F J, Guan W B, Dai X j, et al. Structure and Content of Spermathecae of *Portunus trituberculatus* from East China Sea [J]. Chinese J. Zool., 2009, 44(2): 1 - 11.

[75] Guan W B, Wang G Z, Li S J, et al. Acrosin activity of spermatozoa in spermathecae of *Scylla serrata* [J]. Mar. Sci. Bul., 2005, 24(6): 87 - 91.

甲壳动物精子生物学的研究进展

许星鸿[1]，阎斌伦[1]，郑家声[2]，徐加涛[1]，徐国成[1]，
邵营泽[1]，吴建新[1]，沈 城[1]

（1. 淮海工学院 江苏省海洋生物技术重点建设实验室，江苏 连云港 222005；
2. 中国海洋大学海洋生命学院，山东 青岛 266003）

摘 要：甲壳动物精子生物学的研究对于甲壳动物的人工繁育及遗传育种等工作有重要意义。本文归纳了甲壳动物精子生物学的最新研究进展，包括精子的形态结构、发生、活力、体外保存及顶体反应等方面，并对该领域今后的研究方向提出了展望。

关键词：甲壳动物；精子；形态结构；发生；活力；体外保存；顶体反应

To establish CMOC China as an important component of marine data and service international cooperation in China

DU Qiong-wei, LIN Shao-hua, WANG Feng

National marine date and information service, Tianjin 300171, China

Abstract: JCOMM has strategy to establish the network of WMO-IOC Centres for Marine-meteorological and Oceanographic Climate Data (CMOCs) under the new Marine Climate Data System (MCDS) in 2012 for improving the quality and timeliness of the marine-meteorological and oceanographic data, metadata and products available to end users. China as a candidate of CMOC China has been approved to run on a trial basis after the 4th Meeting of the Joint IOC/WMO Technical Commission for Oceanography and Marine Meteorology (JCOMM). This article states the developing intention of CMOC China in the next few years through the brief introduction to critical marine data, products and service system and cooperation projects in the world.

Keywords: marine; data and service; international cooperation; future development

Since from 1970's, China has participated into various marine international cooperation projects and affairs under the UNESCO. Marine Data as fundamental element for all the marine activities plays an important role in the marine international cooperation. To meet the requirements of Global Climate Observing System (GCOS), Global Framework for Climate Services (GFCS) and Global Ocean Observing System (GOOS), JCOMM has decided to establish a new Marine Climate Data System (MCDS). The core of the system is the network of WMO-IOC Centres for Marine-meteorological and Oceanographic Climate Data (CMOCs). CMOCs will rescue, collect, process, conduct quality control, archive, share, distribute, and mirror worldwide historical, real-time, delayed mode marine-meteorological and oceanographic data, metadata and products of MCDS component data centres, and appropriate WMO and IOC projects and programs, in accordance with the agreed protocols and formats. It will make data sets, and corresponding metadata, maintained as part of its scope available, and discoverable through the WMO Information System (WIS) and/or the IOC/IODE Ocean Data Portal (ODP). China (NMDIS) and Germany has been approved running CMOCs on a trial basis

Received on Oct. 18, 2012

Corresponding author: duqw@mail.nmdis.gov.cn

on the 4th session of JCOMM in May 2012. This will greatly raise quality and efficiency of the marine-meteorological and oceanographic data, metadata and products available to users, and enhance the cooperation with JCOMM. This paper states the intention plan of China in the next few years within the new Marine Climate Data System.

1 The latest development of marine data and service systems in the world

1.1 WMO information system (WMO/WIS)

The 14th World Meteorology Congress（Cg-XIV,2003）approved to establish the WIS , which as a general, integrated and high efficient information service platform, supports the data and information exchange under the WMO projects and related Data Centers, international organizations and programmes, and provides service for some other institutions.

WMO Information system (WIS) is the single coordinated global infrastructure responsible for the telecommunications and data management functions. It provides an integrated approach suitable for all WMO Programmes to meet the requirements for routine collection and automated dissemination of observed data and products, as well as data discovery, access and retrieval services for all weather, climate, water and related data produced by centres and Member countries in the framework of any WMO Programme. (http://www.wmo.int/pages/prog/www/WIS/)

1.2 Ocean Data Portal (IOC/IODE/ODP)

IODE established the Ocean Data Portal (ODP) in 2009 under the IODE which aims to facilitate and promote the exchange and dissemination of marine data and services, through the network of national oceanographic data centres (NODCs). It provides seamless access to collections and inventories of marine data from the NODCs in the IODE network and allows for the discovery, evaluation (through visualization and metadata review) and access to data via web services.

IODE is working closely with JCOMM that ensure ODP could provide marine meteorological and oceanographic data and information requirements, also ODP supports the data access requirements of all IOC programmes and areas as well. (http://www.oceandataportal.org/)

1.3 Sea data net

Sea data net (2006 - 2011) is an EU funded project aiming to create and operate a pan-European, marine data management infrastructure, accessible online through a unique portal. Its primary goal is the development of a system which provides transparent access to marine data sets and data products from 36 countries in and around Europe. It will construct a standardised, distributed system for managing the large and diverse data sets collected by oceanographic fleets and the new automatic observation systems. There are 49 major European instates and marine data centers participated into the SeaDataNet in the first phrase. Second phase of SeaDataNet (SeaDataNet 2 project, from Oct. 1, 2011 to Oct. 1, 2015) aims to upgrade the present SeaDataNet infrastructure into an operationally robust and state-of-the-art Pan-European infrastructure for providing up-to-date and high quality access to ocean and marine metadata, data and data products. (http://www.seadatanet.org)

1.4 Marine climate data system (JCOMM/MCDS)

For the purpose to meet the requirements of long term climate monitoring (Global Climate Observing System – GCOS), seasonal to inter-annual climate forecasts for the Global Framework for Climate Services (GFCS), and ocean climate requirements of the Global Ocean Observing System (GOOS), MCDS was established under the JCOMM which is expected to improve timescales for met-ocean climate data availability, and facilitate the exchange of historical met-ocean climate data sets between countries, and thereby increase the amount of ocean observations eventually made available to the relevant end user applications.

The Vision for a Marine Climate Data System (MCDS) is to formalize and coordinate the activities of existing systems, and address gaps to produce a dedicated WMO-IOC data system operational by 2020 in the view to have compiled coherent met-ocean climate datasets of known quality, extending beyond the GCOS Essential Climate Variables (ECVs). (http://www.jcomm.info/)

1.5 Global ocean data assimilation experiment (GODEA ocean view)

GODAE was set up in 1997 and sponsored by Met Office, UNESCO, IOC, NASA, NOAA, Mercator Ocean, Ifremer et al. Initially, it started as an experiment, with the aim of demonstrating the feasibility and utility of global ocean monitoring and forecasting and to assist in building the infrastructure for global operational oceanography (Smith and Lefebvre, 1997; GODAE Strategic Plan, 2001). Until 2008, GODEA Ocean view has

transited into an operational project of ocean modeling, data assimilation, observation, analysis and forecast products, and provides service and support for public marine environment monitoring, weather forecasting, seasonal & climate prediction, ocean research, maritime safety and pollution forecasting, national security, the oil & gas industry, fisheries management and coastal and shelf-sea forecasting. (https://www.godae-oceanview.org/)

Above regional and global cooperative projects and service systems had been developed successfully and rapidly. CMOC as the new developing marine data and service operational center under JCOMM, the key part of developing strategy of the new MCDS, need to be mirrored with other CMOCs by WIS and IODE/ODP to obtain and exchange the real-time, near real-time and delayed model data and information.

2 Developing intention of CMOC China in the next few years

Expert Team on Marine Climatology of The Joint IOC/WMO Technical Commission for Oceanography and Marine Meteorology (JCOMM) proposed to establish WMO-IOC Centres for Marine-meteorological and Oceanographic Climate data (CMOCs) on the Third session of JCOMM in February 2009. It provides the capability to develop standardized international data management system, to assist WMO and IOC member states rescue, exchange, process and storage marine meteorology and climatology data and relative metadata, and integrate all the marine investigation data and products, and supports service effectively to all the member states through CMOCs. China has made an offer to host a CMOC at National Marine Data and Information Service (NMDIS) during the workshop for a new Marine Climate Data System (MCDS) which was held at the Deutscher Wetterdienst in Hamburg, Germany, from Nov. 28 to Dec. 2, 2011. For fulfilling the responsibility and duty of IOC member state, China has submitted the Statement of Compliance and Commitment to Voluntarily Host a Centre for Marine-Meteorological and Climate Data (CMOC) to IOC and WMO in February 2012.

NMDIS, China, is a public service institution under the State Oceanic Administration (SOA). It is responsible for centralized management of national marine resources; providing information, technical support and services to marine economy, marine integration management, and marine environment protection. It also coordinates and guides the tasks of national marine data and information in China. As a candidate of CMOC, it will be responsible for the collection, rescue, processing, quality control, archival, management and sharing of historical, real-time, delayed mode marine-meteorological and oceanographic climate data and metadata from relevant accomplished, on-going, and

future WMO and IOC projects/programs and all the data-flow sources in the framework of MCDS. In the meantime, it will actively participate in the research and development of data and metadata products and provide corresponding services. CMOC China will undertake the following four tasks:

a) Integrating JCOMM/ODAS Metadata Service hosted by the National Marine Data and Information Service (NMDIS/China) into the management of CMOC China to strengthen and stream the management of the ODAS data and metadata from all cooperative programs/projects in the framework of JCOMM and develop associated metadata products.

b) Undertaking the standardized processing and quality control of CMOCs data. Through the MCDS data flow, CMOC China will collect the real time, delayed mode and historical marine-meteorological and oceanographic climate data and associated metadata including marine meteorology, up-air meteorology, air-sea flux, ship measurements, CTD, BT, XBT, XCTD, ADCP, land-based radar, oceanographic stations, to the best of its abilities, and then conduct associated quality control to produce standardized datasets of high quality, including quality control procedures recommended by the WMO and IOC as part of the MCDS.

c) Developing marine meteorological and oceanographic climate data products and providing related services. CMOC China will develop statistical products to meet the various requirements for marine meteorological and ocean data. It will actively participate in the international cooperation projects/programs such as JCOMM/OCEANView in multi-source ocean data assimilation and ocean reanalysis technologies, and provides free access service to the end users of WMO and IOC through CMOCs mirrored network.

d) Providing capacity building support and technical training for the region. Providing capacity building support and technical training for the region, CMOC China also will contribute to funding MCDS related technical training courses to be held in China. Moreover, CMOC China will send technicians to study abroad and invite foreign experts to conduct training in China so as to strengthen the technical exchange and training with other CMOCs.

The successful operational running of CMOC China will enlarge the catalog, scale and efficiency of marine meteorological and climate data and products information, also could enhance the capability of integrating, collecting, rescuing, quality controlling, formatting, archiving, exchanging, and accessing marine-meteorological and oceanographic real-time and delayed-mode data and associated metadata in China by cooperation with other CMOC members.

References

[1] JCOMM-4/Doc.11 [Final] Relationship of the Commission with Programmes and Bodies of WMO and IOC, and with External Organizations. http://www.jcomm.info/JCOMM4, 2012.

[2] The IODE Ocean Data Portal-current status and future http://www.jcomm.info/JCOMM4, 2012.

[3] JCOMM-4/Doc.7.3 [Final] JCOMM Data Management Practices: Achievements and Future Priorities. http://www.jcomm.info/JCOMM4, 2012.

[4] JCOMM-4/Doc.12.1 [Final] WMO and IOC Strategic Planning and the JCOMM Strategy http://www.jcomm.info/JCOMM4, 2012.

[5] JCOMM-4/Doc.12.2 [Final] Future Work Programme and Operating Plan http://www.jcomm.info /JCOMM4, 2012.

[6] JCOMM-4/Doc.7.4 [Final] WMO Information System (WIS) and Designation of Data Collection and Production Centres (DCPCS) http://www.jcomm.info/JCOMM4, 2012

[7] JCOMM-4/Doc. 13 [Final] The Science and Technology Workshop Summary http://www.jcomm.info/ JCOMM4, 2012.

承建海洋气候和气象资料中心是中国在海洋资料和服务领域参与国际合作的重要部分

杜琼玮，林绍花，王 丰

（国家海洋信息中心，天津 300171）

摘 要：2012 年 WMO-IOC 海洋学和海洋气象学联合技术委员会（JCOMM）提出了在新的海洋气象资料系统（MCDS）下建立海洋气候和海洋气象资料中心（CMOCs）的发展策略。在 2012 年 5 月召开的第四届 JCOMM 大会上，中国被批准候选成为 CMOC 中国中心，并开展试运行工作。本论文通过介绍目前国际上重点发展的海洋资料和服务系统和合作项目，分析了未来几年我国在 CMOC 中国中心的建设和发展设想。

关键词：海洋；资料和服务；国际合作；未来发展

海 洋 通 报（英文版）

HAIYANG TONGBAO

2013 年 5 月 第 15 卷 第 1 期

目 次

基于 FVCOM 的廉州湾及周边海域三维潮汐潮流数值模拟…… 宋德海 等 (15)

运用 SWAN 数值模拟对渤海波浪极值参数的研究…… 孙晓娟 等 (26)

浙南沿岸海表面温度分布特征 …… 韩小燕 等 (38)

一株生防细菌 LHB02 的筛选、鉴定及其发酵条件优化 …… 徐长安 等 (50)

大治河河口无齿螳臂相手蟹生长和成熟的研究 …… 韩 莎 等 (65)

不同盐度对星斑川鲽（*Platichthys stellatus*）幼鱼摄食生长的研究

…… 尤宏争 等 (75)

甲壳动物精子生物学的研究进展 …… 许星鸿 等 (90)

承建海洋气候和气象资料中心是中国在海洋资料和服务领域参与国际合作的重要部分

…… 杜琼玮 等 (96)

Marine Science Bulletin

Marine Science Bulletin publishes papers on marine science and technology including physical oceanography, chemical oceanography, marine biology, marine geology, environmental oceanography, estuarine & coastal sciences, marine technology, digital ocean, coastal zone management, ocean engineering, marine economics, etc., and aims to promote international academic exchange.

Editor-in-Chief: XU Sheng (徐　胜)
Associate Editor-in-Chief: LI Dong-xu (李东旭)　XUE Hui-feng (薛惠芬)
Executive Editor: QIU Wen-jing (邱文静)　LI Xue (李　雪)　YANG Rui (杨　瑞)
LI Xiao-guang (李晓光)　DONG Yi (董　艺)　YUAN Ze-yi (袁泽轶)
English proofed by: WANG Qi (王　琦)

Semi-annually (started in 1999, sum 29)
Publication date: May 15th and Oct. 15th

Marine Science Bulletin **(Vol. 15, No. 1, May 2013)**

Responsible Institution:
State Oceanic Administration of China
Sponsored by:
National Marine Data and Information Service
Edited by:
Office of Marine Science Bulletin (English edition)
Printed by:
Printery of National Marine Date and Information Service

Published by:
Office of Marine Science Bulletin (English edition)
E-mail: msb@mail.nmdis.gov.cn
Tel: (022) 24011287
Address: 93 Liuwei Rd., Hedong District, Tianjin 300171, China

---

ISSN1000-9620
CN12-1271/N

Price: $ 30.00 / ￥40.00 Per year

ISSN 1000-9620

9 771000 962001